Analysis of Oil Flow Mechanisms in Internal Combustion Engines via High Speed Laser Induced Fluorescence (LIF) Spectroscopy

By

Eric Zanghi

B.S. Mechanical and Aerospace Engineering
Rutgers University, 2012

Submitted to the Department of Mechanical Engineering on May 9th, 2014
in Partial Fulfillment of the Requirements for the Degree of

Master of Science in Mechanical Engineering

at the

MASSACHUSETTS INSTITUTE OF TECHNOLOGY

May 2014
[June 2014]

Signature redacted

Signature of Author_____
Department of Mechanical Engineering
May 9, 2014

Signature redacted

Certified by_____
Tian Tian
Principle Research Engineer, Department of Mechanical Engineering
Thesis Supervisor

Signature redacted

Accepted by_____
David E. Hardt
Chairman, Department Committee on Graduate Studies

(This page was intentionally left blank)

Analysis of Oil Flow Mechanisms in Internal Combustion Engines via High Speed Laser Induced Fluorescence (LIF) Spectroscopy

By

Eric Zanghi

Submitted to the Department of Mechanical Engineering in May, 2014 in Partial Fulfillment of the Requirements for the Degree of Master of Science in Mechanical Engineering

Abstract

Automotive manufacturers have a significant challenge ahead of them with new more stringent regulations for exhaust emissions and fuel economy being implemented in the coming future. To make an impact on current emissions and fuel economy, new advanced analytical methods, such as high speed Laser Induced Fluorescence (LIF), must be employed when studying an internal combustion engine. With lubrication in the piston-ring pack assembly being one of the most significant contributors of oil consumption, it directly impacts exhaust emissions as well as indirectly affect fuel economy. High speed LIF spectroscopy has the ability to observe any oil flow mechanisms inside the cylinder which may be directly correlated to performance or oil consumption.

This study intended to be a development process of taking a slower sampling LIF system and creating the high speed LIF for more advanced diagnostic purposes. Significant flaws were observed in the original LIF system, such as extremely low temporal resolution and error caused by temperature dependence in the dyes used for LIF spectroscopy. To develop this system, new lasers, optics, and cameras had to be tested to find which gave the best possible images. The implementation of the high speed camera fundamentally changed the observations and allowed for precise analysis of any and all oil flow mechanisms present in an internal combustion engine.

While testing the system, old phenomena that had been previously documented allowed for a pseudo-calibration in which confirmation could be made that the system is working in a similar manner to the original system. Slow and fast cavitation effects were clearer than previous videos as well as the bridging effects which can be so detrimental to oil consumption. Even new phenomena were documented which provided much more work to be done in the future to truly understand and analyze these new oil mechanisms.

This research is very much a diagnostic proof of concept such that others may be able to build such an analytical tool to understand oil flow mechanisms inside and internal combustion engine to better the fuel economy or exhaust emissions. Future experiments will truly determine the limit of what the system can do and how it can impact future engine designs.

Thesis Supervisor: Dr. Tian Tian
Principle Research Scientist, Department of Mechanical Engineering

(This page was intentionally left blank)

Acknowledgments

First and foremost, I'd like to thank my advisor Dr. Tian Tian for giving me this opportunity. It truly has been an unbelievable experience working with him and learning from his experiences in the field of automotive engineering. His ability to be more than just an advisor and more like a colleague has taught me things not found in textbooks that I will not soon forget. Secondly, I cannot go further without mentioning the friendship I developed with Eric Senzer, a man of wisdom unlike any I have seen before. He always had advice for all my problems, whether they were academic in nature or of life itself, even if sometimes it was not wanted it is always helpful to hear problems from another perspective.

Projects are nothing without the sponsors who support them and this project was no different. These sponsors are members of the Consortium on Lubrication in Internal Combustion Engines at MIT and with their determination and dedication to understanding oil flow mechanisms and oil consumption finding motivation for this project was not difficult. The consortium's current members continue to grow with the list now including: Daimler, Mahle, MTU, Renault, PSA Peugeot Citroen, Shell, Toyota, Volkswagen, and Volvo, with additional outside help from Argonne National Lab and the US Department of Energy, all of which provide a diverse background of expertise to help push through any challenge in this project. I'd like to thank specifically Dr. Rolf-Gerhard Fiedler of Mahle for providing us with pistons to test, as well as Dr. Hans-Jürgen Fuesser, Matthias Matin of Daimler for their friendship and expertise in the optics field. A special thank goes to a friend and fellow student working on a similar project for his PhD thesis, Stefan Wigger, who provided significant insight to any problems I had.

I cannot say thanks without including the wonderful environment with which I do my work at; the Sloan Automotive Lab. Apart from my advisor Dr. Tian, Professor Wai K. Cheng can always be counted on to give constructive criticism of your work. Countless hours have been spent in my office or down in the lab with always a friendly face to be found. I'd like to thank Pasquale Totaro, Mark Molewyk, Tim Murray, Mike Plumley, Dr. Justin Ketterer, Dr. Kevin Cedrone, Tomas Vianna Martins, Camille Baelden, Mathieu Picard, Yang Liu, Tianshi Fang, Qing Zhao, Thane Dewitt, Raymond Phan, and Janet Maslow for providing friendship, advice, or expertise. I would also like to thank all the MIT faculty who have helped me thus far especially Professor Doug P. Hart for his enthusiasm and guidance early on in this project.

Last, but obviously not least, I need to thank my family and friends (who must be struggling without me back in Jersey) because without them I would not be anywhere close to the man I am today. Thanks to both my mother and father, Brenda and Tony, who have taught me things more valuable than any lesson from any class, and of course my sister, Danielle, for listening to me complain about how crazy our parents are. I hope you all know I will never forget where I come from.

Table of Contents

List of Figures

List of Tables

Chapter 1: Introduction

1.1 Lubrication, Oil Consumption, and their Link to Efficiency and Emissions

The main focus of automotive research today comes in two broad forms; emissions control and fuel economy. These two aspects cover a wide majority of concerns that may plague the public at large when it comes to automotive industries and where these companies stand on certain pragmatic issues. Consumers thoughts tend to be more centered on the fuel economy of their car whereas many environmentalists and scientists tend to question the control of emissions being produced by many cars and their respective engines. Rightfully so, both concerns warrant merit and are being researched in any lab that decides to call itself an automotive laboratory. The key aspects to both emissions and fuel economy are lubrication and oil consumption. Lubrication itself is such a large component of engine dynamics as it can directly impact any engines performance. While oil consumption itself can decrease overall engine performance it can also poison and disrupt exhaust after-treatment systems on most commercial vehicles. Keeping up with strict emissions standards and the demand of the consumer public requires advanced designs of engine mechanics as well as improvements in the chemistry of the lubricating oil.

Lubrication has a primary and secondary function in an internal combustion engine. The primary function is to reduce the friction between all components in the power cylinder, the piston and the ring pack, and the liner itself. The secondary function of lubrication is to provide an avenue for heat transfer along with the original cooling method. These two functions serve to improve engine performance when executed correctly. Most automotive engine research focuses on the friction reduction aspect of lubrication due to friction accounting for the majority of mechanical energy lost during any range of operation [2, 12]. As shown in *Figure 1-1*, friction experienced in the power cylinder (or the piston-crank assembly as described in *Figure1-1*) is not a large factor only in Spark Ignition (SI) engines, but is even more prominent in Compression Ignition (CI) engines as well. To understand why the piston/ring pack assembly causes such large amounts of friction, one must understand the roles of each component in this assembly. The ring pack in most SI internal combustion engines is composed of three rings; the Top Ring, the Second Ring, and the Oil Control Ring (OCR). These three rings have their own respective partners on the piston geometry itself. The

Top/Crown Land of the piston is controlled by the top ring, the Second Land is controlled by the second ring, and the Third Land is controlled by the OCR.

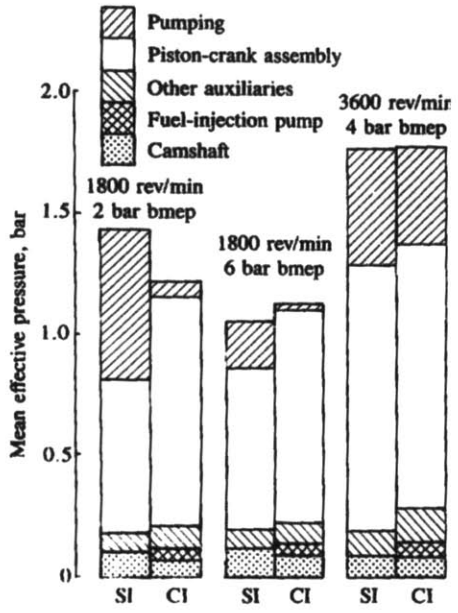

Figure 1-1 – This figure [Heywood] shows the relative losses in an internal combustion engine expressed as mean effective pressure across a range of operating conditions.

The top ring's main purpose is to seal the crank case from the combustion occuring above as to attempt to extract as much work out of said combustion as it can. The job of the OCR is quite self-explanatory, it controls the oil flow and transport in the ring-liner interface through a variety of means due to a variety of different configurations. Due to the chaotic nature of how oil is supplied to the piston-liner interface initial the OCR has the job of accumulating as much oil as it can and distributing it in a consistent manner to the three piston lands above it to provide lubrication for the piston. Finally the job of the second ring can be viewed to have a hybrid functionality of the top ring and the OCR; it has to further seal the crank case from the combustion gases as well as control oil transport by scraping oil off the liner after it was applied by the OCR to prevent oil consumption; this will be discussed further later on in this section. The main mechanisms used to allow these rings to accomplish their respective duties is the ring's tension and in case of the OCR, the spring's tension. This tension is the main cause of friction in the ring pack area and the skirt of the piston is the main source of friction for the entire piston due to its large surface area. The breakdown of friction in the piston/ring pack assembly is that the rings themselves account for 50% of the frictional losses in an engine [1].

One can postulate that if 50% of the piston-ring pack assembly friction is caused by the rings themselves, then the other 50% is caused by the piston itself. The piston can be broken up into four

sections; the three lands previously discussed (top land, second land, and third land) and the piston skirt. The piston skirt is such a large contributor to friction due to its main function which is to brace the piston from the harsh secondary motion caused by combustion during the expansion stroke. Due to the violent "slap" of the piston against the liner, high amounts of oil are delivered to that piston-liner interface via an oil jet fired from the crank shaft in an attempt to circumvent high friction that would normally occur. The design of the piston skirt is centered around gathering a substantial amount of oil to reduce as much solid-to-solid contact as possible. A key feature of the piston skirt is the chamfer feature located at the top of the piston skirt right before the OCR groove. *Figure 1-2* shows how the piston-ring pack assembly looks via a cross-sectional drawing.

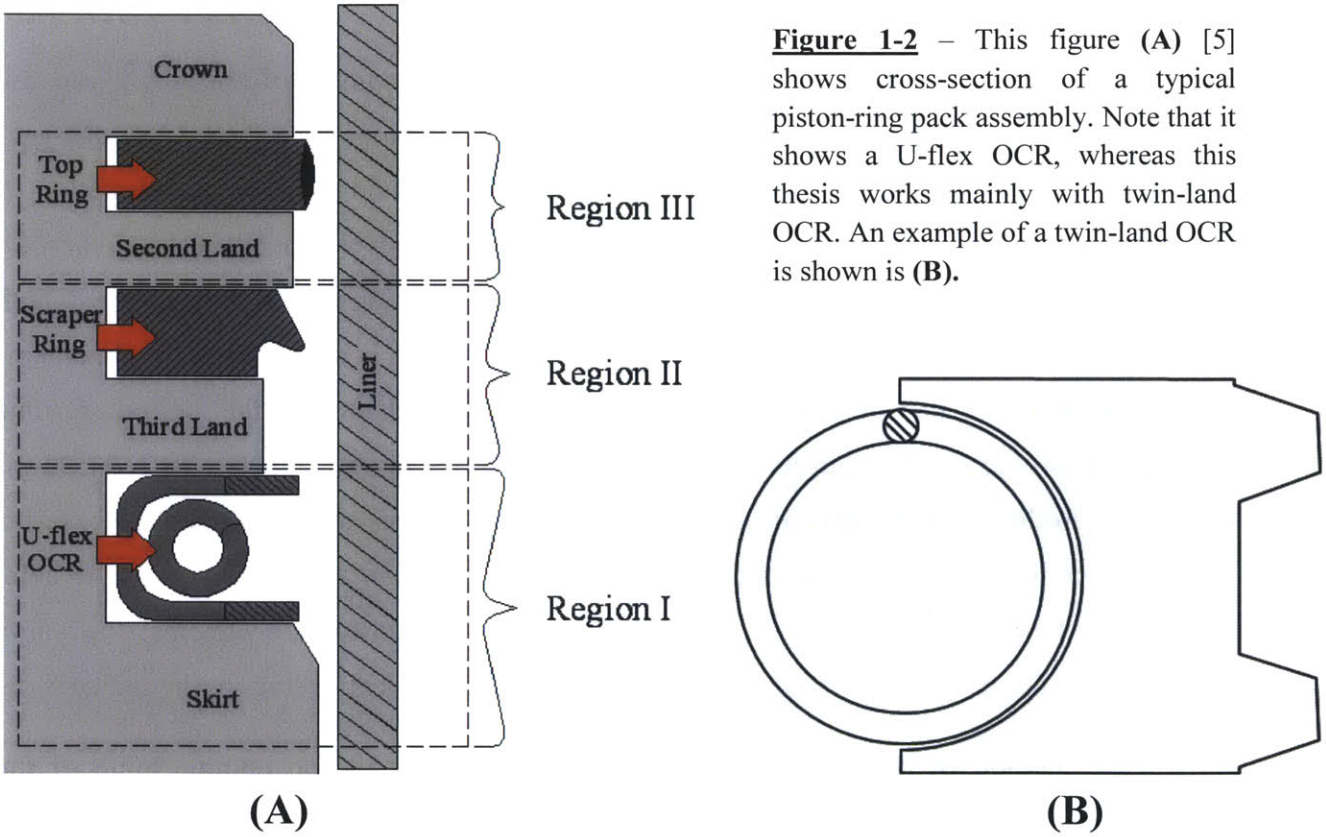

Figure 1-2 – This figure **(A)** [5] shows cross-section of a typical piston-ring pack assembly. Note that it shows a U-flex OCR, whereas this thesis works mainly with twin-land OCR. An example of a twin-land OCR is shown is **(B).**

This thesis will mainly focus on developing an understanding of the oil mechanisms that exist in the piston skirt region for lubrication as well as make parallels between mechanisms that may overlap in the ring pack region. Any improvement made in lubrication of these key areas translates into a direct improvement in the performance of the engine. With an increase in improvement, all things held constant, an increase in fuel economy can be expected, thus creating motive to further study the piston-ring pack assembly.

As important as lubrication, if not more important due to strict government regulations coming in the near future, is the research being done in emissions controls. Emissions of any IC engine are highly dependent on two key components; the fuel used in combustion and the oil used for lubrication. The scope of this thesis will mainly discuss the lubrication side of engine emissions and how to analyze oil transport mechanisms in an IC engine to better understand oil consumption. First to be discussed will be how oil is consumed during an average engine cycle and how oil is being supplied to the piston and its various components. Oil mechanisms that contribute to and explain the behavior of oil and why it is in a position to be consumed will be discussed in *Section 1.2*.

Oil consumption in any IC engine is detrimental for a number of reasons; it can cause performance problems which in turn cause fuel economy to drop and it can cause damage to exhaust after-treatment systems. A recently new understanding of oil consumption has contributed to the belief that combustion of oil may lead to adverse health effects caused by particulate matter emissions [13-17]. A large factor in the reasoning behind why oil consumption can cause such an array of problems is it chemistry. Engine oil is a composite, an amalgam of different compounds in contrast with what its simple nomenclature would suggest. A simple engine oil has evolved far from its original format and in its purest form is now referred to as base stock. Additives with many different properties and purposes are mixed with the base stock in an attempt to have the oil last in this harsh environment of an engine. Oils must be able to survive; in the heat of combustion, the high speeds of the piston movements, the varying climates of different global environments, dilution via fuel, transient operation, the list goes on.

The method of oil production to ensure that specific oil can endure some of these rigorous environments is to introduce additives into the base stock to augment some of the properties of the oil. These additives themselves vary substantially in chemistry as well as functionality. Examples of some of the types of oil additives includes; detergents, corrosion inhibitors, antioxidants, viscosity modifiers, friction modifiers, anti-wear additives, etc. With such a substantial amount of components that vary greatly in chemical composition and functionality, consumption of oil through the combustion chamber can cause serious health care and performance problems. An overview of the effects on performance due to oil consumption can be made very clear when analyzing the effects of different oil additives have on Diesel

Particulate Filters (DPFs); a key component in the exhaust after-treatment system of diesel vehicles. DPFs are, in short, filters that oxidize any excess hydrocarbons that may exist in the exhaust after a combustion event. Due to engine oil's complicated composition, materials such as Calcium, Zinc, and Magnesium cannot be oxidized in combustion or in the DPF and therefore leave behind this layer of ash which can greatly reduce the DPF's performance in way of a larger pressure drop across the DPF itself [8,9]. With a higher pressure drop across the DPF, the more pumping work is needed therefore reducing overall efficiency of the engine. Another side effect of this high pressure drop across the DPF is that with high exhaust gas pressures, draining the combustion chamber during the exhaust stroke will be more difficult allowing for residual gases to stay possibly contaminating intake gas mixtures. Diesel engines are not the sole victims of oil consumption; SI engines have performance problems caused by oil consumption as well. If the unburnt compounds found in engine oil were to make its way to the three-way catalyst in modern SI engines, it can poison and degrade the precious metals found in the component. Specific compounds like sulfur or phosphorous can significantly cause three-way catalytic converts to lose efficiency if not properly accounted for [10, 11].

Performance hindrances caused by oil consumption are only one reason to be concerned and interested in the behavior of oil flow and transport; another major side effect of oil consumption is particulate matter emissions. Anyone who has ever taken apart an engine to change out a piston has seen the large amounts of carbon deposits left stained on the top of the piston. These deposits are caused partly by the normal combustion of fuel, but the majority of deposits are caused by engine oil being burnt during combustion. Engine oil in its base form has a larger count of carbon atoms than that of typical fuel, whether it is gasoline or diesel. This higher concentration of carbon has a difficult, if not impossible, time oxidizing correctly during combustion as typically it is optimized to oxidize the lower carbon species of the fuel. There is not enough oxygen during combustion to oxidize the oil and therefore leaves behind excess carbon species which form the deposits on pistons. These deposits do not cause significant issues mechanically, but can cause problems for emissions controls. As oil is consumed and combusted, these deposits build and can then be exhausted. As discussed earlier exhaust after-treatment systems are very sensitive to variations caused by oil being consumed. Instead of different chemical compounds causing performance problems, the larger hydrocarbons of oil cannot be addressed with average exhaust systems and allow those particulates to be released into the

atmosphere. To truly understand and develop methods for reducing oil consumption to improve emissions and performance, an understanding of the sources of oil consumption is needed. *Figure 1-3* show multiple avenues which oil can take to be consumed during combustion.

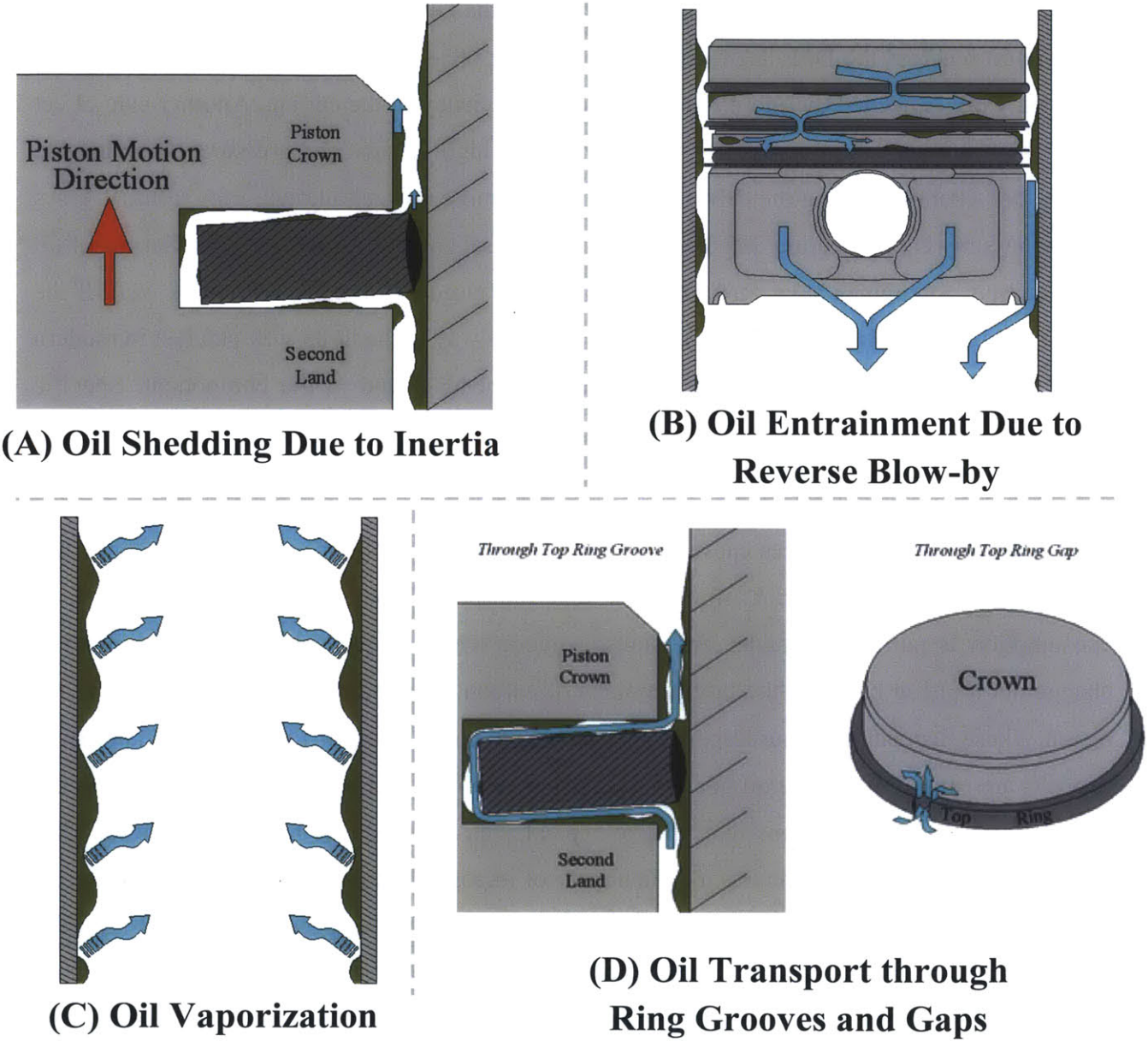

Figure 1-3: Various methods of oil consumption that can contribute to an overall engine's oil consumption leading to performance and emissions issues. Images reproduced and updated from Senzer [5].

Oil on the liner is a necessary feature which contributes to oil consumption, but an engine cannot run without oil, so methods were developed to scrape the oil off the liner by the rings in an attempt to reduce how much was consumed during combustion. This leads to problems such as in *Figure 1-3A*, where the top ring, which is not built specifically for scraping, drags oil from the liner and during the shift from upstroke to downstroke flings or sheds droplets of oil into the combustion chamber. Similarly as oil underneath the top ring is scraped by it, the pressure builds and forces the oil to travel into the lower flank of the ring groove while inertia is keeping the ring in contact with the upper flank of the groove as shown in *Figure 1-3D*. Not only can the oil flow through the ring groove and make its way to the crown land, but fundamentally all rings must have a gap otherwise sealing, replacement and assembly would be difficult and this gap creates zero resistance for the oil to flow through. As the piston and rings begin to move downward, any oil that is near the gap cannot be scraped by the ring and therefore stays on the liner unmolested. These behaviors are applicable to all rings and if some rings were to ever align, significant amounts of oil can be consumed in a cycle.

Although oil can make its way through the ring gaps and grooves on its own through means of pressure build and inertia, it can be assisted by what can be broadly called reverse blow-by. Blow-by itself is the result of high combustion pressure forcing gases downward through the ring gaps and into the crankcase. Normally the direction of this flow is self-explanatory as combustion occurs at TDC and therefore forces gases toward BDC; this is not always the case. Toward the end of the expansion stroke high pressure has been built up in the regions between the lands and the liner while the pressure above the piston is decreasing due to the volume increasing as the piston descends. If the pressure has built up to be high enough to where it exceeds the cylinder pressure above the piston, there is a driving force for the oil to flow upwards towards the crown land; this is reverse blow-by. This is not the only possibility for reverse blow-by to occur; much less likely, but still possible is the even in which the crankcase develops a pressure which exceeds the cylinder pressure creating a potential for oil to be forced upward again. This usually occurs during the intake stroke; while the piston moves downward to draw in the charge, it's possible that the volume of charge is not equal to the volume change in the cylinder as the piston descends, creating a lower pressure in the cylinder.

1.2 Observing Oil Mechanisms through Laser Induced Fluorescence (LIF)

With the knowledge of the sources of oil consumption discussed in the previous section, only a small piece of the puzzle that is oil consumption is understood. One must understand how oil transports itself throughout the entire engine environment and what the mechanisms that allow such transportation are. Oil has to travel through the piston-liner interface and the ring pack in order to be consumed, so developing an understanding of that control volume encompassing that region can better engine development. The method used to observe these oil mechanisms is Laser Induced Fluorescence (LIF) and will be discussed in more depth in *Chapter 2: Experimental Setup*. The basis behind LIF technology is that some chemical species when dissolved in certain solvent have the abilities to absorb and then emit certain wavelengths of light. With this principle, it is possible for oil to be doped with a dye that absorbs and emits light which allows the observation of particular oil mechanisms and phenomena.

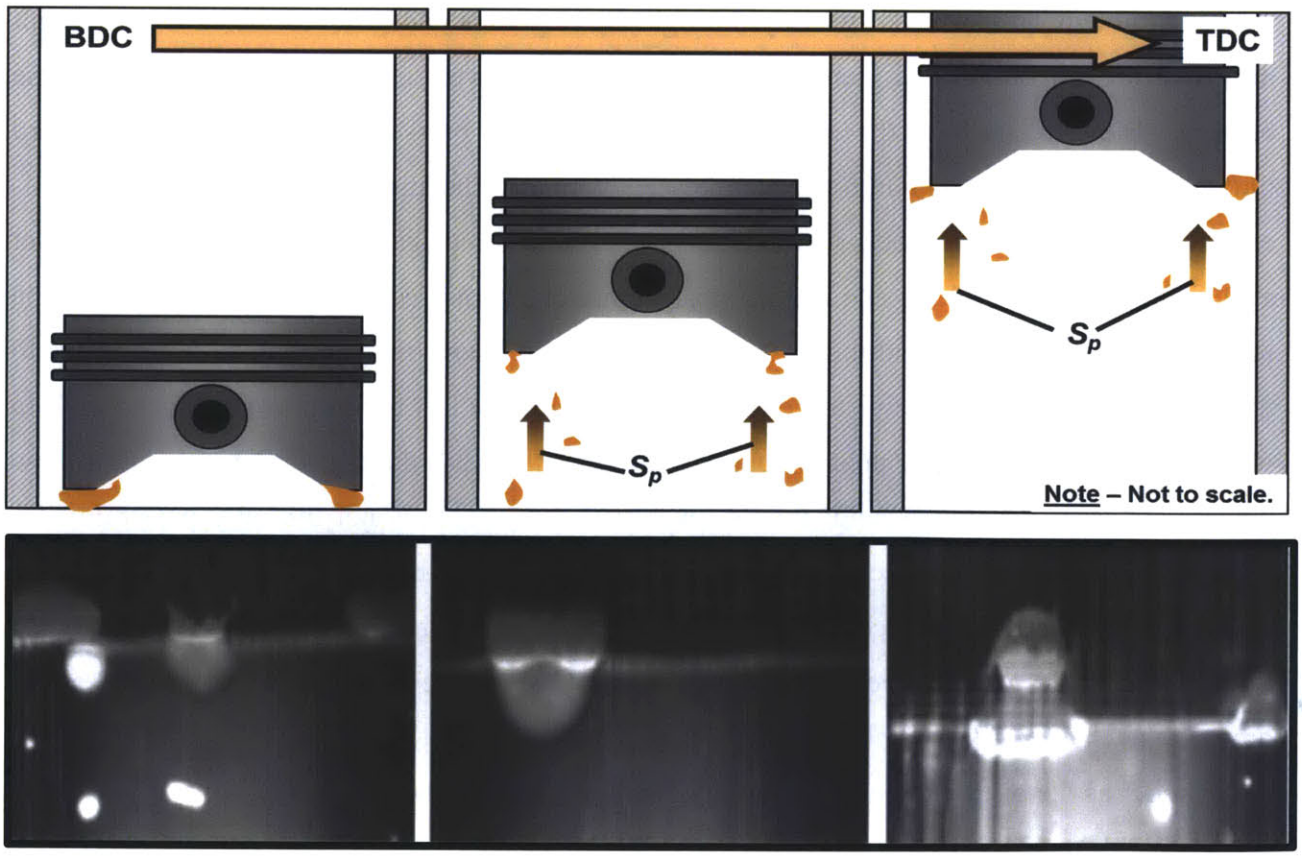

Figure 1-4: Example drawings and images of oil droplet shedding. Images provided through Laser Induced Fluorescence (LIF) measurements taken by E. Senzer [5].

The piston itself drives quite a number of oil mechanisms, specifically with the secondary motion it experiences and its intricate design geometry. Secondary motion is defined as any motion which is not along the axial direction of the cylinder; this includes: horizontal translation and piston rotation along the pin and connecting rod. Piston geometry itself can cause interesting phenomena to occur among the oil. A key feature of piston geometry is the skirt chamfer located right above the skirt and underneath the OCR. This chamfer is to act as a repository of oil which the OCR can use to distribute oil amongst the liner and rest of the rings. Key oil mechanisms found throughout an internal combustion engine are as follows; oil droplet shedding, OCR scraping, oil bridging, oil shearing/streaking, and oil cavitation/separation.

The first oil mechanism to be discussed will be oil droplet shedding. Oil droplet shedding is a phenomena that has been theorized and understood existed for quite some time, but only recently with the LIF setup could actual qualitative observations be made. The initial motivation behind the theory was there must be oil supplied to the skirt from sources other than the primary oil jet. The pictures that were taken using the LIF setup, shown in *Figure 1-4,* show that oil can be supplied to the skirt-liner interface from an outside source. The diagram in *Figure 1-4* gives an explanation of how these droplets can shed from the piston and re-enter the skirt liner interface as a new oil source. As the piston travels during an upstroke the primary and secondary oil jet deliver oil to the piston and a significant amount of oil impacts the underside of the piston. As oil adheres to the piston, it begins to accelerate with the piston gaining inertia, but around mid-stroke where the piston's velocity is greatest the oil cannot stay attached to the piston and therefore sheds. While shedding, the oil still retains a significant fraction of the piston's velocity so as the piston begins to decelerate as it approaches TDC, the droplets begin to catch up and inevitably strike the piston. Some of these droplets have enough force and inertia to enter the low clearance of the skirt liner interface. This phenomenon is more prevalent during early expansion on the anti-thrust side as there is a larger clearance due to combustion slamming the piston toward the thrust side.

Second oil mechanism to be discussed will be OCR scraping. As discussed in the previous section and shown in *Figure 1-3*, OCR scraping is very similar to any of the other rings scraping oil off the liner. The difference between the top two rings and the OCR is that the skirt's chamfer is one of the largest clearances on the piston, allowing for a large amount of oil

accumulation to occur. While the oil accumulates oil pressure begins to rise causing the OCR itself to move upwards allowing oil to flow to the back of the OCR groove. As the piston's inertia and velocity change throughout the cycle, the oil will travel past the upper flank of the OCR and reemerge on the 3rd land where it can repeat this process once again with the second ring. *Figure 1-5* show how oil accumulates in the OCR groove as the piston travels from TDC to BDC in a typical downstroke.

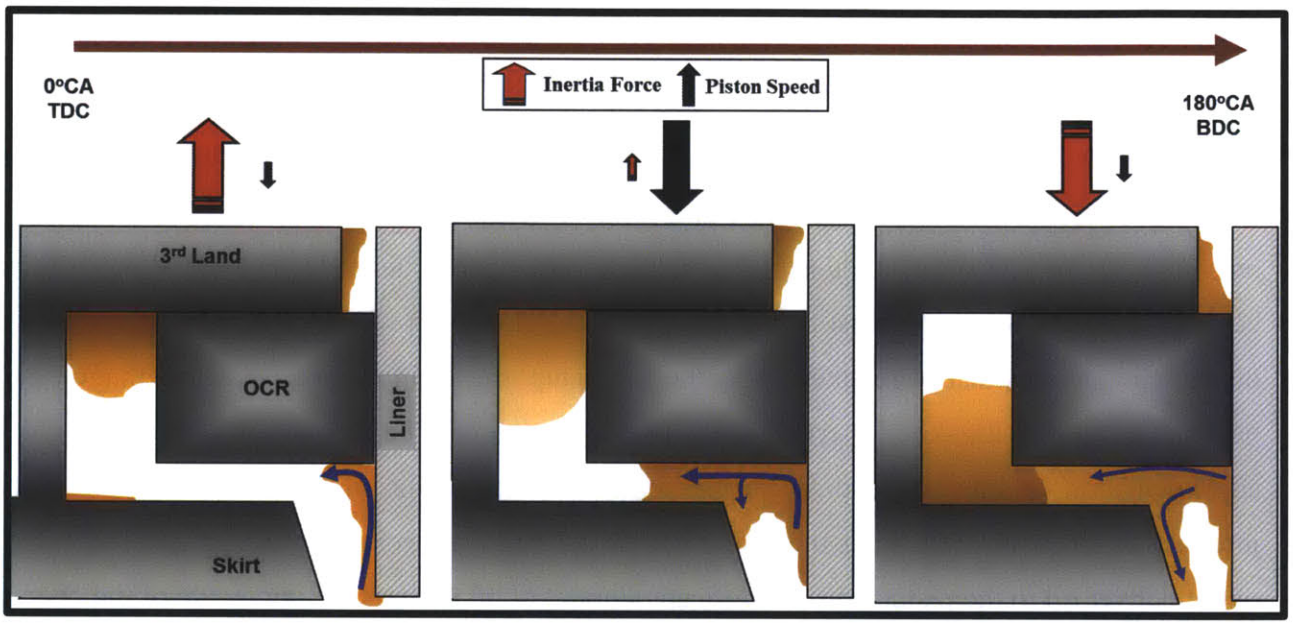

Figure 1-5: Diagram showing the path accumulated oil can take to enter the OCR groove during various points within a sample downstroke [5]. Another mechanism can be seen at BDC in the figure; oil is bridging from the liner to the skirt chamfer.

One large mechanism which is prominent in almost all cycles is oil bridging between the liner and the piston surface. Oil can bridge this gap in a number ways, but it will always occur during a sequence where the inertia of the oil and the piston are of opposite signs. An example would be such that if the piston is slowing down toward BDC, any oil that is in the clearance between the skirt-liner interface will have more inertia moving downwards which will inherently force the oil to move relative to the piston itself. Once the oil has begun to move relative to the piston the oil will reach a point where the clearance between the liner and the skirt is to small and thus force the oil to flow upward onto the liner as shown in *Figure 1-6*. This mechanism can be seen at TDC as well and the flow can be in the reverse direction once inertia forces are balanced again.

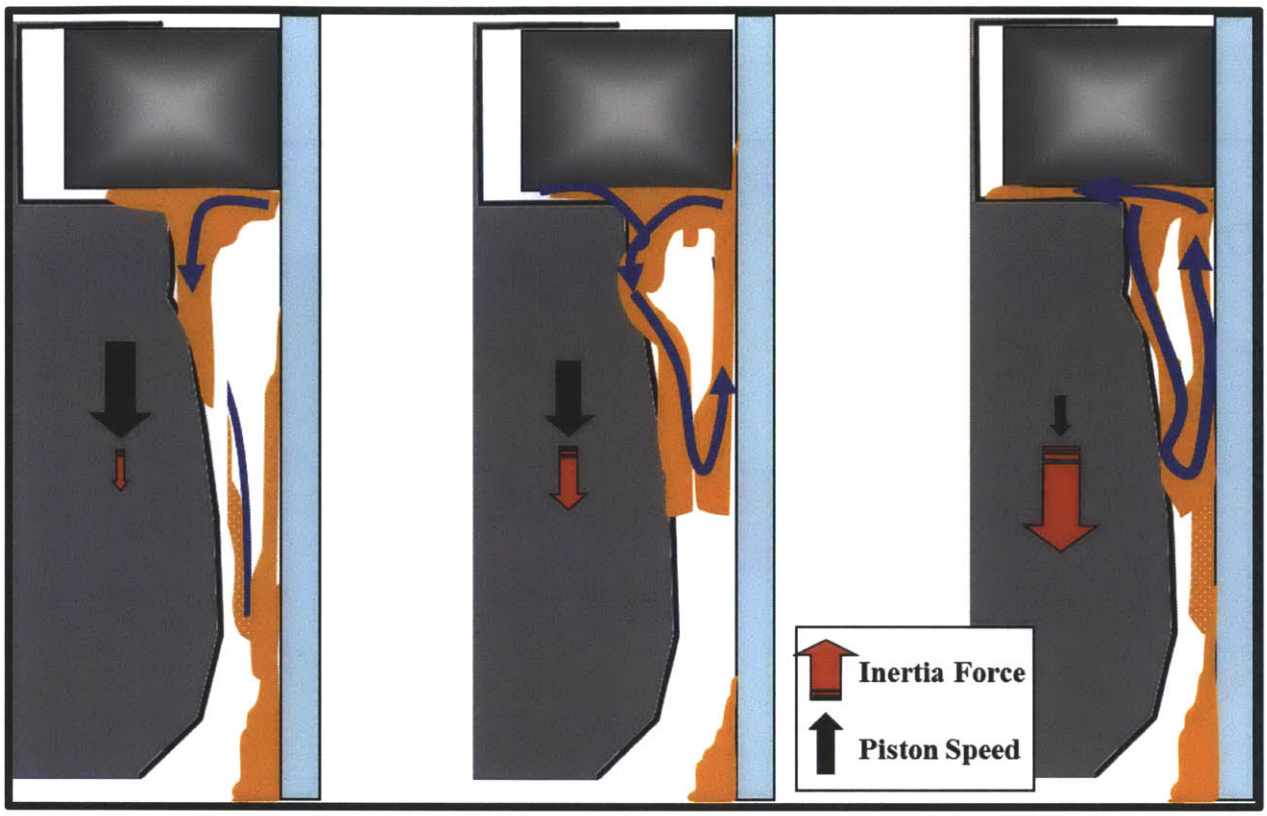

Figure 1-6: Diagram showing the mechanism of how accumulated oil in the skirt chamfer can bridge between the piston skirt and the liner [5].

All mechanisms discussed so far are mainly caused by inertia forces and piston movement along the axial direction which is primary piston motion. The next couple of mechanisms will be explained by secondary piston motion. Secondary motion is defined as the piston either translating in the horizontal direction, perpendicular to the axial direction depending on engine configuration, or if the piston itself begins to rotate towards the thrust or anti-thrust side. When the piston begins to translate or rotate away from the liner any oil that occupies the space between the liner and the piston begins to undergo cavitation/separation. Cavitation can occur at any point during the cycle due to the nature of the piston to rotate back and forth repeatedly throughout the cycle. While severe cases of cavitation happen during the expansion stroke where the large side forces due to combustion make it difficult for the oil to travel as it normally would. As shown in *Figure 1-7*, the separation of the piston and liner causes the oil to create a unique pattern allowing quick identification of engine or piston designs which may prompt cavitation or prevent it. Surface tension is a key factor in creating these cavitation

patterns, which suggests that different forumlae and different additives in the oil may contribute to how these patterns form.

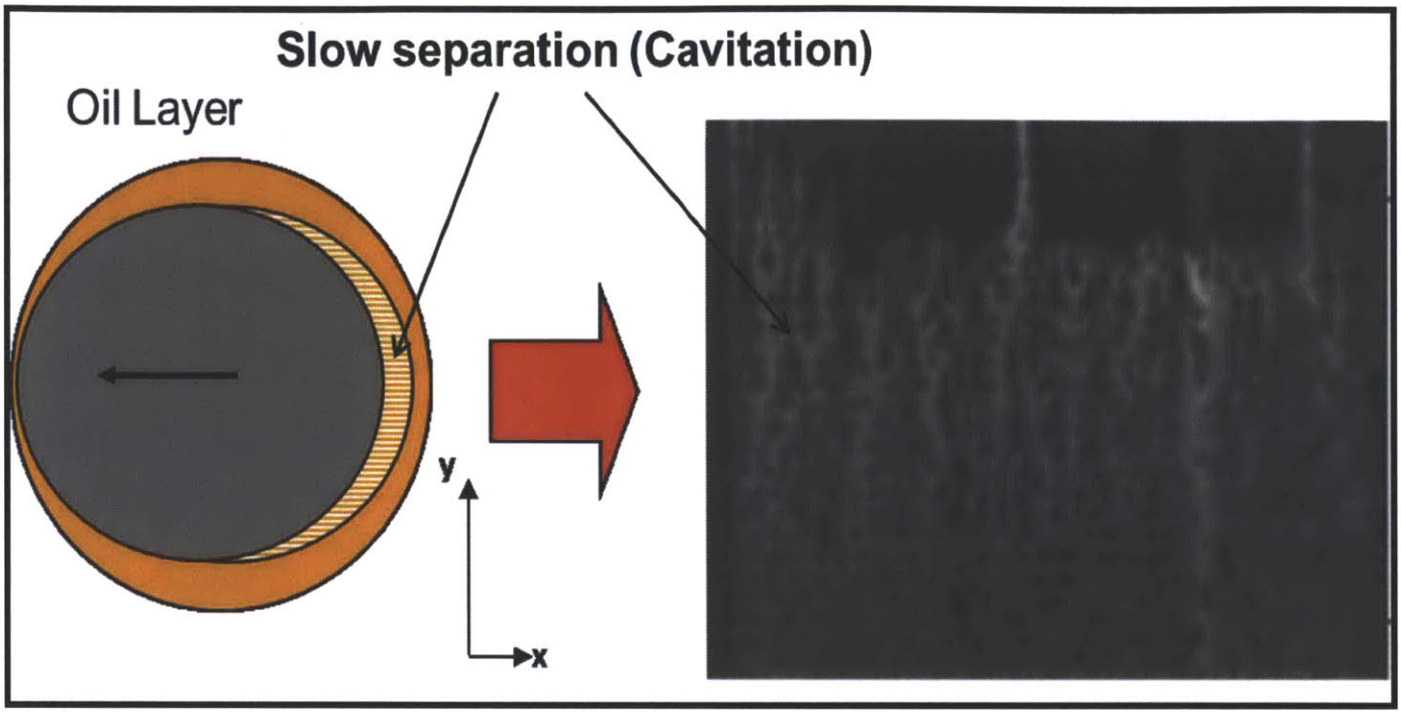

Figure 1-7: Diagram showing the mechanism of slow cavitation/separation and how it can lead to distinct oil transport patterns. Cavitation patterns created by separation due to combustion are far more pronounced than those caused by piston tilt. LIF image produced by E. Senzer [5].

The final oil mechanism that has been observed and will be further discussed later in this thesis is oil shearing/streaking which is a form of cavitation which occurs at faster piston speeds. As the piston gains speed during mid-stroke oil that accumulates at the bottom edge of the piston skirt does not have enough viscosity/surface tension to keep up with the piston. These streaks are to be the lowest surface energy when the oil film can no longer support a full film and therefore must cavitate [30, 31]. This creates the droplet shedding oil mechanism previously discussed, but also leads to distinct patterns slightly similar in fashion to the cavitation patterns. *Figure 1-8* shows that when the speed of the piston reaches a critical maximum the oil begins to thin into an array of streaks. These patterns along with the cavitation ones create problems for the piston, specifically lubrication problems. Ideal cases for lubrication would use full films of whatever compound being used as a lubricant, but during these scenarios there exist partial films where there may be no lubricant or a small enough amount allowing for metal-to-metal contact to occur.

This is an undesirable effect; pistons need full films of lubrication so that enough hydrodynamic pressure can be built up to push the piston away from the liner to prevent any harsh contact.

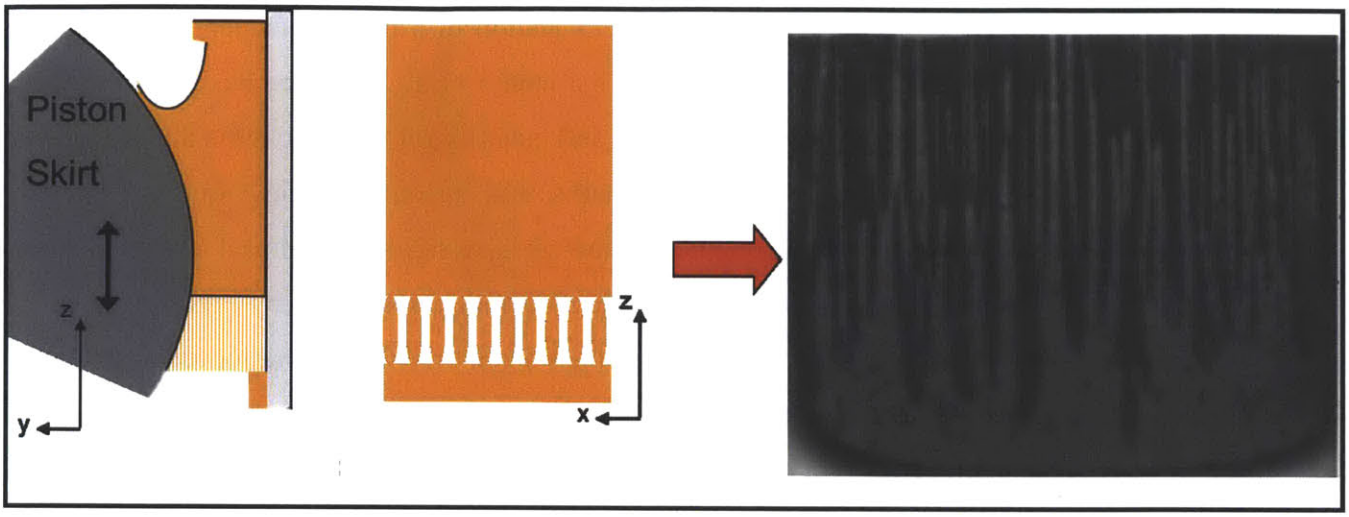

Figure 1-8: Diagram showing how piston primary motion can lead to the oil mechanism of oil shearing/streaking. As the piston speed increases as does the severity and frequency of the streaking. LIF image produced by E. Senzer [5].

The final oil transport mechanism worthy of observation is the piston impacting the thrust side during combustion or also known as the piston "slap". This piston slap causes significant oil transport in an extremely short amount of time due to the high forces caused by combustion. Rough estimates of the piston side force during combustion can be on the order of a thousand newtons. As this large force presses against the oil film in between the piston skirt and the liner the oil rapidly thins out and even breaks to where there is solid-to-solid contact. Any soli-to-solid contact is something engineers try to avoid as much as possible in an internal combustion engine so studying this with the high speed LIF setup is absolutely warranted.

1.3 Previous Research on LIF in Internal Combustion Engines

Laser Induced Fluorescence techniques have been employed before to analyze oil accumulation and transport in internal combustion engines, the only caveat was that only a single point measurement could be taken. This technique was successful at quantifying oil film thickness between the rings and liner [17, 18], but could not measure film thickness for large areas of the piston. Further evolution of the system would bring about a successful attempt at two-dimensional visualization allowing for more sophisticated observation of oil transport

phenomena [19]. The system developed in [19] used a flash lamp as a light source, which did not allow for the greatest fluorescence intensity, thus leading the way for lasers to be introduced into the LIF systems. Successful application and implementation of a two-dimensional LIF system occurred in 2001 by Thirouard [20]. This was the first work to truly show the benefits of having a system which can visualize oil flow mechanisms and quantify oil film thickness albeit with its share of error. Having a system that could visualize and quantify oil flow opened up new research possibilities to pinpoint which engine parameters have significant impact of oil transport. Oil flow mechanisms had not been studied in transient operation until 2008 by Przesmitzki [21]. Oil consumption was shown to be worse in some situations in transient operation than in steady state, once again proving that two-dimensional LIF has great analytical capabilities. As oil consumption become more prominent in the world of automotive engineers with such strict regulations, the two-dimensional LIF system was vital to understanding what aspects of an IC engine can be manipulated to improve oil consumption and fuel economy. Observations found by Senzer in 2012 [5], showed that oil consumption is largely influenced by oil accumulation in the piston skirt chamfer which leads to oil transport into and out of the OCR groove. Experiments such as these have allowed substantial improvements to lubrication models as well as oil consumption models, further allowing automotive manufactures more options in analyzing their respective engine components to better understand where improvements can be made.

1.4 Thesis Objective and Direction

To better solve the problems faced by oil consumption and lubrication, better diagnostic tools must be developed. By using the foundation set by previous work, significant steps toward a diagnostic tool that can measure oil film thickness more accurately at higher rates of speeds can be made. The largest obstacle to date to oppose the development of a high speed LIF setup is the temperature dependence of the oil emission which will be discussed in *Chapter 2*. LIF setups have already proved their effectiveness in describing and evaluating oil flow mechanisms [5, 20, 21] and therefore provided valuable information on lubrication and oil consumption. Accordingly, the primary objectives of this thesis are to:

1. Develop new understanding of how old oil mechanisms truly work and compare to original notions as well as discover new phenomena not previously theorized.

2. Study the effect of engine operating conditions and piston skirt designs on oil film accumulation and transport mechanisms.
3. Help bolster and provide new information and data to current lubrication, oil consumption, and secondary motion models.
4. Create real-time crank angle resolution diagnostic LIF system to further study oil transport in an IC engine.

In this work, a high speed two-dimensional LIF visualization system was developed to conduct real-time observation of oil accumulation and transport mechanisms. Previous systems had to rely on taking an image once every cycle allowing for significant discontinuities in the data. Development was limited solely to a spark ignition single cylinder engine. In conjunction, models for lubrication of the skirt and oil transport in the lands were given data from this setup to better model each activity. Initially, using the original setup, experiments were conducted to view the effects of different piston skirt patterns on oil transport mechanisms. Finally, the process began to develop the new LIF system to achieve higher sampling rates in an attempt to create a more in depth framework for understanding oil transportation in an IC engine.

Chapter 2: Experimental Setup

2.1 Experimental Objectives

The main purpose of these experiments was to create a new robust diagnostic system that built upon the original foundation and fixed some of the problems presented in the original design. As stated earlier, two large concerns in the automotive industry are fuel economy and emissions controls; these two concerns are directly related to lubrication and oil consumption albeit are not the solely caused by them. To better understand oil consumption and lubrication, the LIF system was introduced, but still had its own flaws as well as merits, hence the interest in upgrading the system. This section will discuss the methodology and principles behind the LIF system and its diagnostic value to oil consumption and lubrication.

To create and develop a new diagnostic tool for analyzing oil accumulation and transport mechanisms, every component of the original system had to be evaluated for its relevance and if it could be upgraded for any significant improvement to results. Alongside the analysis of the original setup's components; oil transport mechanisms were also being studied to gather data and new information to observe what changes to the system were accomplishing, if anything at all. The single largest hindrance of the original system was the temporal resolution of the images captured. Each image captured by the camera using LIF, was one image every cycle at a specific crank angle. One objective was to upgrade the sampling rate of the system so that multiple images could be taken per cycle allowing for a much more real-time continuous video to be made; to be discussed further in Section *2.2.2*.

To create such a system with these capabilities multiple setups had to be tested thoroughly. Different lasers had to be used; varying in power as well as operating modes. Different cameras had to be used such as different speeds of exposure as well as sensor types. Optics themselves had to be evaluated and switched out; the original setup had not been changed for quite a long time allowing for artifacts and aberrations to develop in the optics. Ultimately as more of the original setup changed a new calibration method had to be created as well.

2.2 Experimental Equipment

2.2.1 Engine Setup

The most important piece of equipment of this experimental setup, without which there would be a standstill, was the test engine. The engine was a modified production Peugeot (PSA) 2.0L engine, Model XU10J4R. The engine itself was essentially identical to the actual production version with the same cylinder head, connecting rod, crankshaft and other parts as well allowing for ease of replacement if anything were to break. The key modification was that the four cylinder head was modified so that only one cylinder would fire allowing for fewer fluctuations in running conditions. The engine is quite an old design which means that it does not have some modern features such as variable valve timing or cam phasing, but does have 4 valves per cylinder and has the possibility to be run turbocharged. In the future it is more likely that it will be converted from port fuel injection to direct injection. More general characteristics can be found in *Table 2.1*.

Engine Manufacturer	Peugeot Société Anonyme (PSA)
Production Year	1997
Engine Code & Type	Code: XU10J4R/L; Type: RFV
Fuel Delivery	Port Fuel Injection
Ignition Type	Spark Ignition
Boost Type	Naturally Aspirated
Number of Operating Valves	4
Displacement	0.511L
Bore	86.6mm
Stroke	88.8mm
Maximum Specific Power	37.3kW / Liter @ 5500RPM *
Maximum Specific Torque	180N-m / Liter @ 4200RPM *

Table 2-1 - Test engine characteristics courtesy of Peugeot Société Anonyme (PSA). (* Torque and Power numbers are for the 4-cylinder engine from which the research engine is derived from). Ref. [5, 20, 21, 22]

To make the engine run just as efficiently as a single cylinder engine rather than a four cylinder as it was intended; the bucket tappets were removed from the other three cylinders so that when the engine was running there would be no extraneous movement generated by the other valve systems. Additionally, the cooling jacket needed its own modification to allow for the unique optical window access needed for the LIF system. With this engine being modified to be a single cylinder engine the cooling jacket was able to be constructed more freely since the other cylinders did not need cooling, making manufacture slightly easier. Due to the harmonic fluctuations associated with single cylinder operation, the crankshaft and balance shaft had to be

modified. The crankshaft was designed to only use one crank pin which makes it unlike that of a production crankshaft. The balance shaft needed to have its counterweights redesigned so that it could cancel out the harmonic oscillations created by running single cylinder. With the tuning that went into this engine maximum operating peaks at speeds of 6,000RPM although the maximum speed recorded was 3,500 RPM.

2.2.2 Optical Access to the Power Cylinder

During the period when the original setup was created optical windows in engines were not unheard of albeit these engines were not run at high speeds or full loads. Even today with more sophisticated technology there still are not many engines with well-built optical access points such as the current engine. Previous studies have shown large optical access windows using square pistons and liners which for specific reasons do not necessarily translate to production engines when talking about lubrication or oil consumption and even more so when discussing fuel economy and emissions. Developing the optical window for this engine had its difficulties specifically in the heat transfer field. Cooling the liner now became a discontinuous problem where there is a secondary material creating havoc with thermal expansion. Without correct cooling of the liner and window; observation of any oil transport mechanisms will be skewed. To aid in the cooling of the liner the cooling system was split into two separate sub-systems; one for the cylinder head and one for the cylinder liner.

Thermal mechanical stresses were not the only problems experienced when placing a window of different materials into the liner. Oil transportation mechanisms are very sensitive to any changes in engine operation, piston geometry, ring dynamics, and liner distortion and finish, making designing the optical window quite difficult. To diminish any of these negative effects the obvious choice would be to try and make the window as small as possible, but there is still a desire to observe these oil mechanisms in a way they haven't been seen before. Ultimately the size chosen that appears in *Figure 2-1* creates as little experimental fluctuations as possible while providing a significant view into the IC engine. As shown in *Figure 2-1* and *2-2*, the window itself, cannot possibly show all points in a single stroke. At Top Dead Center (TDC), the piston crown land, the top ring, and the 2nd land are obscured from view while at Bottom Dead Center (BDC), the piston skirt is out of view of the camera.

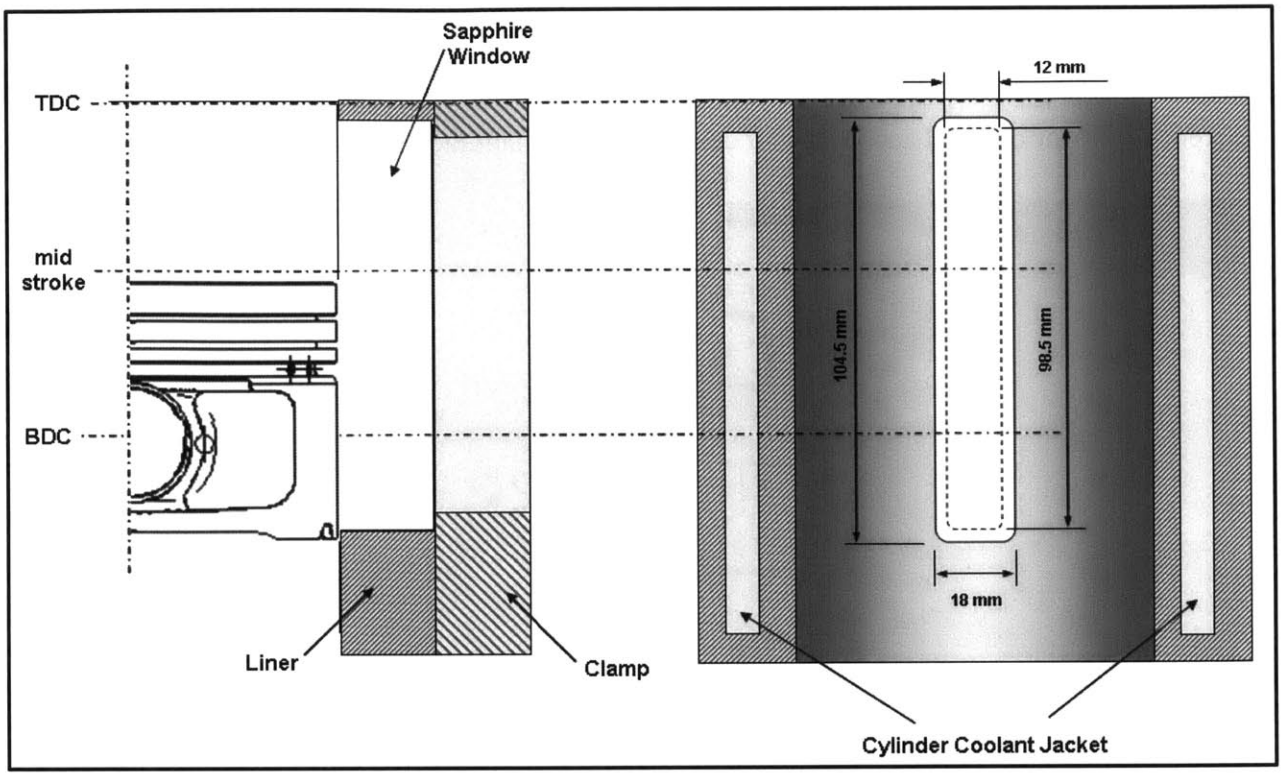

Figure 2-1: The schematic for the sapphire window providing optical access to the power cylinder as well as the coolant jackets specifically designed to cool the modified liner. Provided by and updated from [5, 20, 21].

The criteria for choosing the material for the optical window was straight forward in that the material needed to have a similar thermal expansion coefficient and thermal conductivity to the cast iron liner as well as be transparent in the visible spectrum. The best candidate that was found for the window was sapphire, due to it having a similar thermal expansion coefficient to that of cast iron; 25-40 and 15 K^{-1}, respectively [5]. Not only does sapphire have a similar thermal expansion coefficient to cast iron, but it is harder than it as well meaning that the sapphire will not scratch due to regular engine operation. To get the sapphire window to adhere to the liner, the window and fitting were tapered and a high temperature resistant (up to 230 °C) and high thermal conductivity (1.4 W/m-K) epoxy (ECCOBOND 276) was applied [5]. Due to the hardness of sapphire being that much greater than cast iron, honing the liner became an issue wherein the liner would start to become an oval shape due to the sapphire not honing at the same rate as the cast iron. What was used to solve this problem was a center-less diamond tool which would create a flush interface between the sapphire and the liner. The roughness of the liner was

measured to have an Ra approximately between 0.23 μm and 0.37 μm for the cast iron. The roughness measured for the sapphire window was approximately between 0.58 μm and 0.80 μm [21]. All assembly of engine and optical window was done prior to this thesis, please see reference [20] for original accounts and descriptions of manufacturing and design choices.

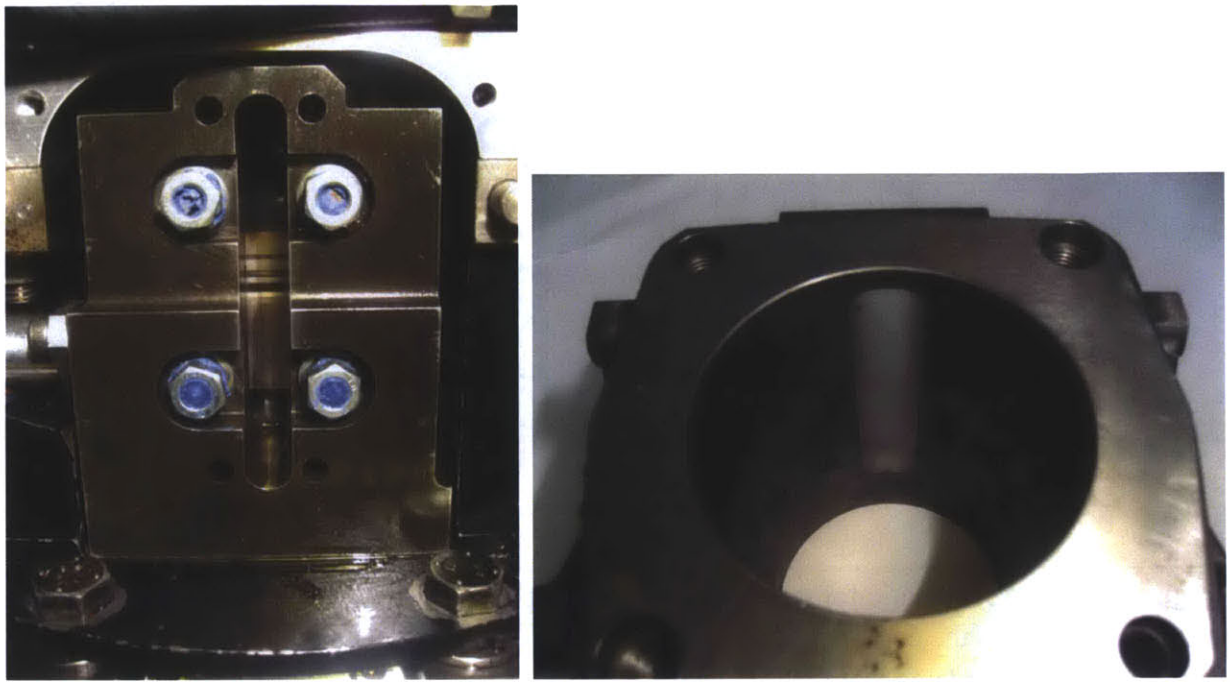

(A) **(B)**

Figure 2-2: Pictures showing the optical window from the outside with piston and ring pack in view **(A)** and from the inside with the liner removed showing the side of the sapphire exposed to combustion and piston-ring dynamics **(B)**. Provided by [5, 21].

2.2.3 Engine Coolant Jacket and Lubrication System

One of the most important pieces of equipment to be manufactured was the coolant jacket. It needed to be precisely designed for optimal cooling of the liner and sapphire such that the window would not overheat. Shown in *Figure 2-3* and *2-4* are an image of the separate pieces of the coolant jacket and the schematic for the coolant passages respectively. A similar cooling system to that of other typical research engines was used; a series of external pumps drive the coolant from a temperature-controlled reservoir through the six coolant passageways shown in *Figure 2-3*. The arrangement of the six passageways are precisely placed such that there are four arranged rather closely together toward the top of the cylinder due to the necessity of cooling the top from the heat of combustion. These six passageways allow for uniform cooling of the liner

and window because without uniform cooling liner distortion *and* window distortion may render the setup inoperable if not correctly tended to. *Figure 2-4* shows how the coolant flows around the cylinder and exits to be recycled in the temperature-controlled reservoir. The temperature-controlled reservoir was held at a constant temperature of 50 °C with fluctuations of only 1 °C maintained by the external pumps and heat exchangers that would exchange heat with the city water system.

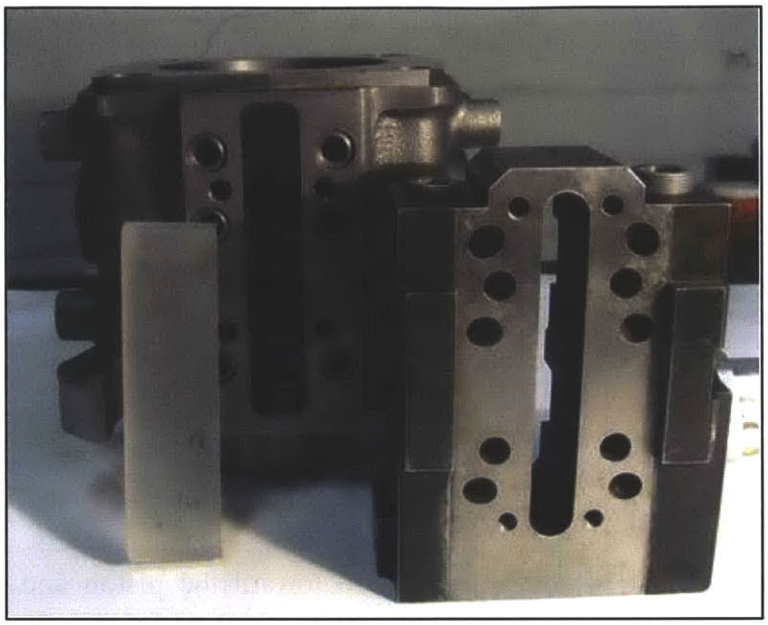

Figure 2-3 – Image showing the disassembled coolant jacket along with sapphire window. As mentioned, there are four coolant passageways closer to the top for better cooling the parts exposed to the much hotter combustion gases [5, 21].

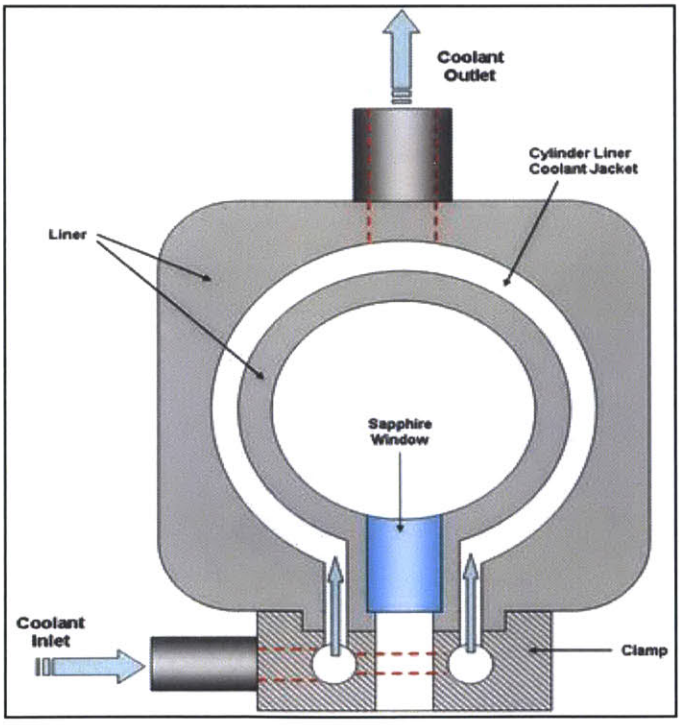

Figure 2-4 – Schematic drawing of how the coolant flows through the jacket and cools the liner and window setup. Everything before and after the coolant jacket are nearly identical to any ordinary research engine setup [5, 20, 21].

The lubrication system of the PSA research engine is similar to the coolant system in which it is controlled by external pumps and circulates from a temperature-controlled reservoir. Each system was designed to behave similarly to any production engine's oil and coolant systems. To create as few variations in the oil parameters as possible the temperature and pressure had to be regularly controlled. Any significant changes in pressure or temperature can change crucial parameters of the oil such as viscosity and density. To achieve this consistent operation the external sump (engine has a dry sump configuration so an external sump was necessary) used for storage of the oil had its own heat exchanger for cooling and electric heater. The set temperature of the oil sump was 50 °C with fluctuations of +1 °C to +3 °C with extreme cases occurring of +9 °C during continuous running at high speeds and loads (i.e. 3500 RPM, 700 mbar).

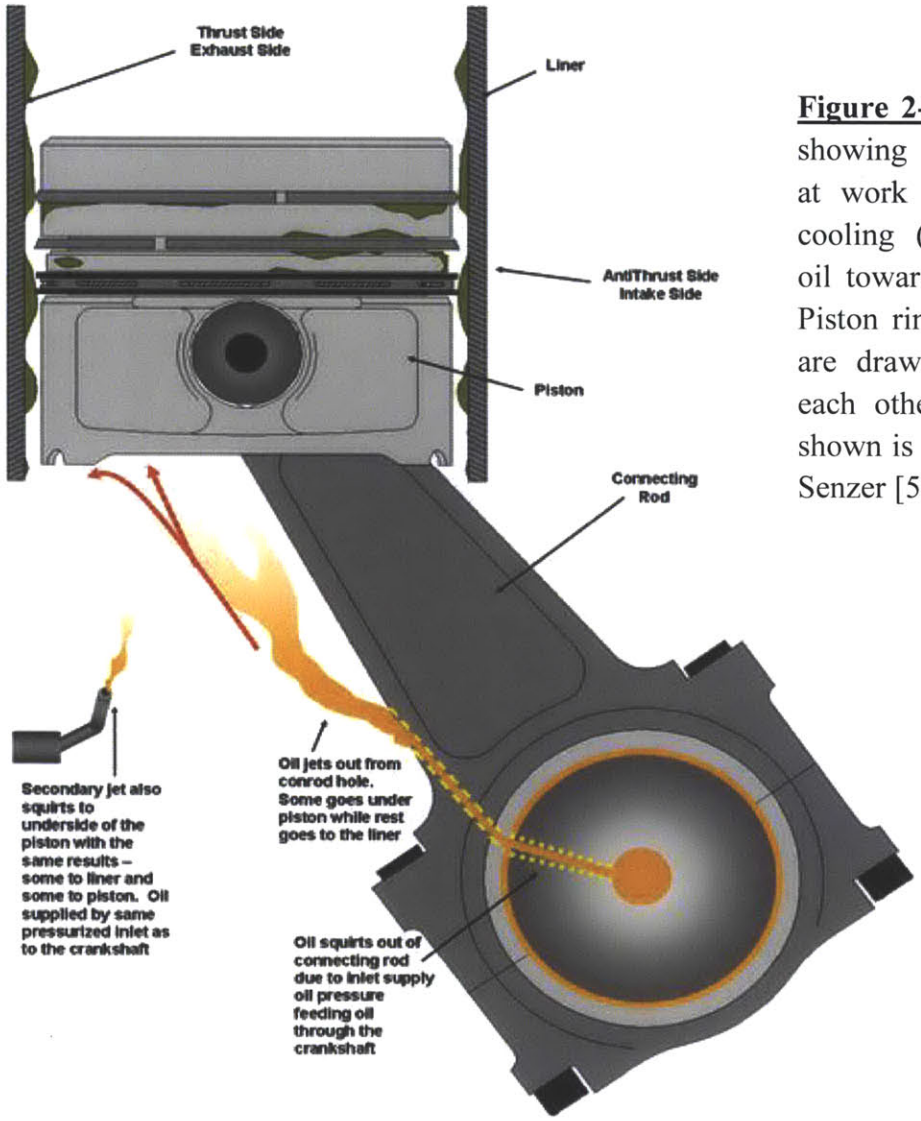

Figure 2-5 – Technical drawing showing the lubrication system at work with crank shaft and cooling (secondary) jets firing oil toward the piston and liner. Piston rings and connecting rod are drawn to scale relative to each other. The amount of oil shown is not. Image provided by Senzer [5].

The current lubrication system of this engine has two oil jets to lubricate the piston and liner; the crank shaft oil jet and the cooling jet shown in *Figure 2-5*. Manufacturers designed the system to take advantage of the high oil pressure that occurs in the crank shaft. This specific design called for two small holes, approximately 2.5 mm in diameter, to be drilled into the connecting rod as well as the crank shaft. This allows for the high pressure oil to flow through both holes whenever the cranks shaft aligns with the connecting rod, which is designed to be at the same specific moment in the cycle. The position is roughly around mid-stroke while the piston is moving toward TDC, this allows for proper lubrication to occur during the expansion stroke, when it is needed most. Although the pressure in the crank shaft may be constant, the fact that the engine speed is not constant can cause problems such as the oil jet becoming a spray rather than a laminar stream. Having a spray rather than a stream is a sub-optimal method for lubricating a system. The reason for this constant pressure is because the engine is a research one with external pumps controlling temperature rather than pressure. On normal production vehicles, the pumps are chain driven meaning that the pressure will increase along with engine speed allowing for a stream to flow even at higher speeds. The crank shaft jet's purpose is mainly for lubrication, but also allows for some cooling of the piston to occur. The cooling jet's main purpose is to cool the piston further; its lubrication role is limited. Control of the cooling jet is possible, but most experiments were run with it at a constant pressure for convenience.

2.2.4 Engine Operation Control and Data Acquisition

Original control system created by Thirouard [20] and updated, due to the limitations of the system while being used in transient engine conditions, by Przesmitzki [21]. All control of engine and data acquisition was initially controlled via LabView; the graphical programming language software by National Instruments. Once the original setup was upgraded, data acquisition was handled via proprietary software that will be further explained in the coming sections. The engine control itself was split into two separate computers to allow more efficient control due to outdated hardware. Data acquisition initially had the camera feed directly to one of the computers labview program such that one could control any related parameters of the camera from one of the computers while operating the engine. The second computer had the assignment of monitoring a significant number of engine parameters to ensure nothing catastrophic would happen. Some of the engine's parameters monitored are: cylinder pressure, RPM, intake pressure,

blowby gases, etc. The engine computer was not just there to monitor parameters, but also control the fuel, spark timing, and intake pressure via the throttle. To accomplish all this, the two computers would communicate with each other via a single Ethernet cable and the engine computer would communicate with the engine via a Field Programmable Gate Array (FPGA) card.

To control the engine and simulate a realistic production vehicle, the controlling program is in a closed loop system to allow for more natural transient operation. Utilization of tables filled with information about how the fuel injector pulse should be at specific speeds and intake manifold pressures were necessary for the more realistic operation of the engine. One crucial parameter of an engine that must be maintained very precisely is the air-to-fuel ratio. This ratio is important to engine operation because it controls the quality of combustion which depending on the ratio can lead to poor fuel economy and/or poor emissions. This ratio is maintained by using an ECM Universal Exhaust Gas Oxygen (UEGO) sensor, which measures the air-to-fuel ratio in the exhaust gas with a range from 7:1 to 20:1. The sensor itself would alter fuel timing and amounts based off of what was being read continuously during engine operation. Most operations completed automatically by the computer can also be altered manually by the operator if needed.

2.2.5 Previous Laser Induced Fluorescence (LIF) Imaging System

2.2.5.1 Principle, Theory, and Application of LIF

Basic fluorescence is a phenomenon which occurs in specific compounds called fluorophores (i.e. fluorescent dyes), wherein a specific wavelength of electromagnetic radiation is absorbed and then re-emitted at a different, but equally specific wavelength [23]. This phenomenon occurs in approximately three stages: Excitation, Excited-State Lifetime, and Fluorescence Emission [20]. Initially a chemical compound is exposed to a photon on energy of specific wavelength from an external source such as a flash lamp or, in case of this thesis, a laser. The chemical compound then absorbs this photon to be forced into an excited state, hence the excitation stage. During the excited-state lifetime stage the molecule that absorbed the photon can only stay in this excited state for a finite amount of time on the order of nanoseconds. This stage gives rise to the parameter know as quantum yield (or the quantum yield efficiency) which

is a parameter that describes how many photons are emitted due to fluorescence versus how many are absorbed by the compound. The reason for this ratio never being 1:1, (i.e. one photon emitted for one photon absorbed) is because a molecule in an excited state has a plethora of ways to disperse its energy. Molecular collisions is just one way for an atom to discharge any energy it has and with that it most likely will not have enough energy to emit another photon. If the molecule does have enough energy though, it enters the third stage fluorescence emission. In this stage, the process is self-explanatory where the excited molecule now emits a photon at lower energy than the initial excitation photon due to the dissipation that occurred while in the second stage. Due to the lower energy of the emitted photon, its wavelength is larger than the excitation photon; this difference in wavelength is called the Stokes Shift. The Stokes Shift is the reason fluorescence spectroscopy exists and allows the excitation and emitted photons to be distinguishable.

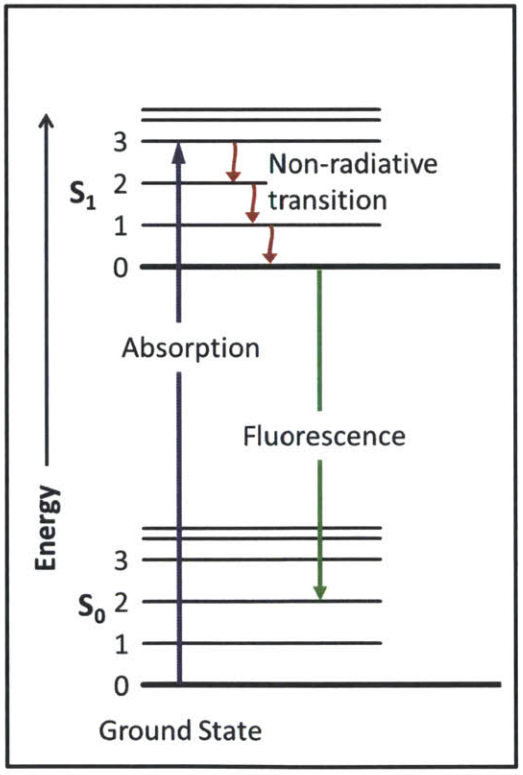

Figure 2-6: Jablonski diagram showing the three stages of induced fluorescence; excited, excited-state lifetime, and fluorescence emission. Provided by Wikipedia commons.

When measuring the fluorescence of a particular compound there exist two types of spectra that are valuable to any researcher; the fluorescence excitation spectrum and the fluorescence emission spectrum. When viewing the spectra of compounds, like polyatomic molecules, in solutions, the spectra become broader when compared to their discrete energy

levels. Example excitation and emission spectra can be found in *Figure 2-7*. Emission spectra of different compounds are only dependent on the excitation wavelength; therefore this allows multiple fluorescent dyes to be used together in the same solvent which was the case for this setup.

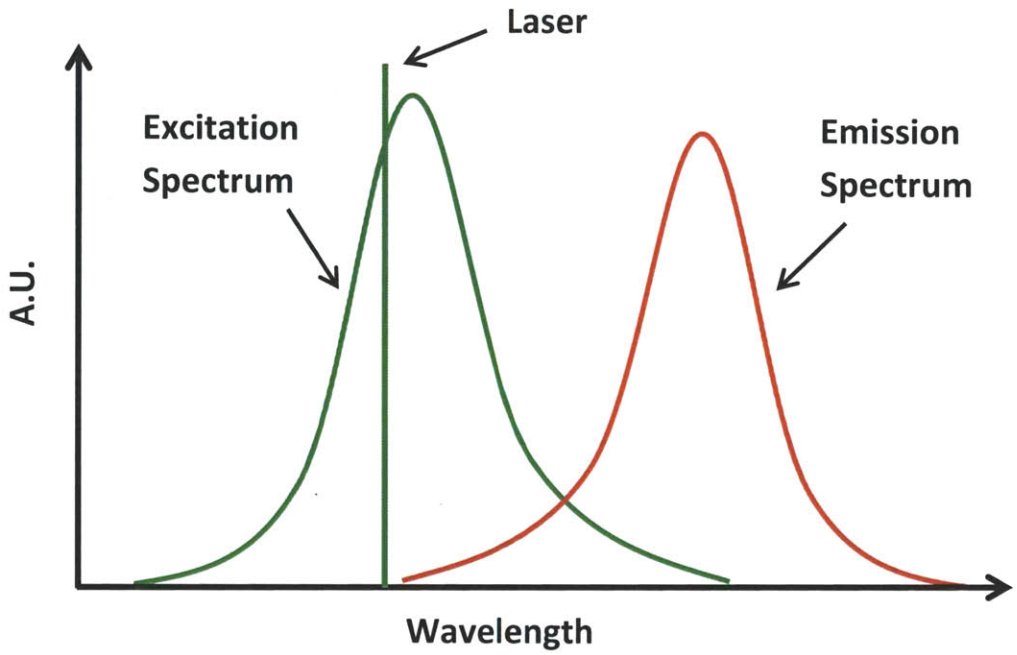

Figure 2-7: Example excitation and emission spectra for arbitrary fluorophore.

In order for this principle to be applied to observing the oil transport mechanisms in an IC engine, the Beer-Lambert law is used. This law states that the intensity of light transmitted through an absorbing medium is inversely proportional to the exponential of the medium's absorption coefficient and the thickness of the medium [24, 25]:

$$\frac{I_{tr}}{I_0}(h) = e^{(-\alpha h)} \tag{2.1}$$

Where:

I_{tr}: Transmitted light intensity (arbitrary units)

I_0: Excitation intensity (arbitrary units)

α: Medium's absorption coefficient (m^{-1})

h: Medium's thickness (m)

The medium's absorption coefficient is dependent of the wavelength of the excitation, but in this thesis only one wavelength is used. The same equation can relate molar concentration and molar absorptivity to the relative intensity if there happens to be an absorbing compound in a solution:

$$\frac{I_{tr}}{I_0}(h) = e^{(-\varepsilon C h)} \tag{2.2}$$

Where: C: Absorbing compound's concentration (mol/m^3)

ε: Absorbing compound's molar absorptivity (m^2/mol)

To be able to relate oil film thickness to emitted light intensity, the relationship between absorbed intensity and film thickness needs to be found first. The absorbed intensity is just the excitation intensity minus the transmitted intensity, which therefore gives:

$$I_{abs} = I_0\left(1 - e^{(-\alpha \cdot h)}\right) \tag{2.3}$$

This setup uses the Beer-Lambert law to measure film thickness of oil in IC engines by doping the oil with multiple fluorescent dyes. The following equations and derivations are an attempt to derive an equation for this specific system.

$$dI_{abs} = I(x) \cdot C_{dye}\varepsilon_{dye}dx \tag{2.4}$$

Where: C_{dye}: Dye molar concentration (mol/m^3)

ε_{dye}: Dye molar absorptivity (m^2/mol)

I(x): Transmitted light intensity incident on layer dx

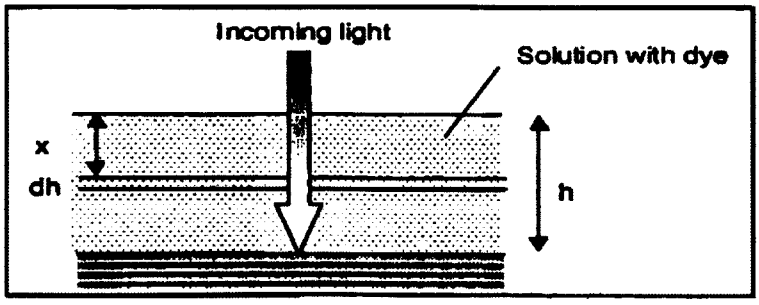

Figure 2-8: Example of the thinking behind the differential equation in (2.4) to understand how incoming light travels through a solution with dye [20]. The datum for x is at the top of the solution.

The light intensity that is incident on any arbitrary layer dx is dependent not only on the properties of the fluorescent dyes diffused in the oil, but also on the properties of the oil as well. This is taken into account when deriving I(x) shown in Equation 2.5.

$$I(x) = I_0 \cdot e^{(-(C_{dye}\varepsilon_{dye}+\alpha_{oil})x)} \tag{2.5}$$

Where: α_{oil}: Oil absorption coefficient (m^{-1})

To arrive at Equation 2.5, an assumption was made that the absorption coefficient of the entire solution is simply the summation of the dye's and the solvent's respective absorption coefficients. This was experimentally verified by S. Saeki et al [26].

Substituting Equation (2.5) into (2.4) gives:

$$dI_{abs} = I_0 \cdot e^{(-(C_{dye}\varepsilon_{dye}+\alpha_{oil})x)} C_{dye}\varepsilon_{dye}dx \tag{2.6}$$

Recall that the emission intensity of a fluorescent compound is related to the quantum yield efficiency, ϕ, which is the ratio of number of fluoresced photons emitted to the number of excitation photons absorbed. Multiplying the absorbed intensity by the quantum yield efficiency gives the fluorescence intensity given by:

$$dI_{fluo} = \phi I_0 \cdot e^{(-(C_{dye}\varepsilon_{dye}+\alpha_{oil})x)} C_{dye}\varepsilon_{dye}dx \tag{2.7}$$

Fluorescence emission is not a unidirectional phenomenon, emission occurs in all direction. This results in not all photons that are emitted to hit the camera and be recorded. As photons travel through the oil they are being absorbed strictly because of the nature of a medium. A scaling term must be used to account for the amount of emitted photons that are actually directed at the camera as well as those being absorbed by the oil itself. For a more in depth explanation on this scaling factor please see B. Thirouard [20]. With this scaling factor the equation becomes:

$$dI_{fluo\ det} = \frac{\theta_s}{4\pi} S_p e^{(-\alpha_{oil} \cdot x)} \phi I_0 \cdot e^{(-(C_{dye}\varepsilon_{dye}+\alpha_{oil})x)} C_{dye}\varepsilon_{dye}dx \tag{2.8}$$

Where: $dI_{fluo\ det}$: Differential of the detectable fluorescence intensity

θ_s: The solid angle created by the camera lens shown in *Figure 2-8*

S_p: The area of the oil layer that corresponds to a single pixel on the sensor

Upon integration of Equation 2.8 from 0 to h; obtained is the total amount of fluorescent photons emitted by the dye that hits a single pixel:

$$I_{fluo\ detectable} = \frac{\theta_s}{4\pi} \cdot \frac{S_p \phi I_0 C_{dye} \varepsilon_{dye}}{C_{dye}\varepsilon_{dye}+2\alpha_{oil}} \cdot \left[1 - e^{(-(C_{dye}\varepsilon_{dye}+2\alpha_{oil})h)}\right] \quad (2.9)$$

This equation alone assumes the fact that the system is isolated enough that only the correct wavelength of light is being received by the camera. In reality as the excitation photons hit the sapphire window, they can reflect as well and if the photons were to hit the CCD camera they would not be differentiated from the emission photons. To resolve this problem a band pass filter is used to only receive the emission wavelengths and reject all others. This means an extra term should be added to account for the filter and since the quantum yield efficiency is also a function of emission wavelength; these two terms can be combined.

$$I_{fluo\ det} = \frac{\theta_s}{4\pi} \cdot \frac{S_p I_0 C_{dye} \varepsilon_{dye}}{C_{dye}\varepsilon_{dye}+2\alpha_{oil}} \cdot \left[1 - e^{(-(C_{dye}\cdot\varepsilon_{dye}+2\alpha_{oil})h)}\right] \cdot \int_{\nu_1}^{\nu_2} f(\lambda)\phi(\lambda)d\lambda \quad (2.10)$$

Where: f(λ): Filter Transmittance at wavelength λ

ν_1: Minimum wavelength transmitted by filter

ν_2: Maximum wavelength transmitted by filter

The environment inside an internal combustion engine allows the simplification of Equation 2.10 due to the fact that the oil will be a very thin film on the order from 10 microns to 200 microns. When $(C_{dye} \cdot \varepsilon_{dye} + 2\alpha_{oil})h \ll 1$, Equation 2.10 becomes:

$$I_{fluo\ det} \approx \frac{\theta_s}{4\pi} S_p I_0 C_{dye} \varepsilon_{dye} h \cdot \int_{\nu_1}^{\nu_2} f(\lambda)\phi(\lambda)d\lambda \quad (2.11)$$

This linearity occurs at extremely thin films, but can also occur at very low concentrations of dye. This comes at a cost though because as the concentration of dye diminishes so the does intensity therefore decreasing the signal-to-noise ratio.

Equation 2.11 still allows one to treat this equation in the form of:

$$I_{fluo\ \det}(T, h) \approx \mathrm{A}(T) \cdot h \quad (2.12)$$

Where A(T) is a variable that is only dependent on temperature. All other variables are fixed once the engine is operating. The solid angle and area of the oil translate onto the CCD sensor are constants; as are the absorptivity, and concentration of the dye. The oil does degrade over time, but the engine is not running long enough for these changes to create error. As long as proper calibration is done, A(T) would be measured for various temperatures before each test allowing for simple oil film thickness measurement. The quantum yield efficiency and filter transmittance are constant if the filter never changes and I_0 as well should never change with the correct laser light source.

Corrections: In Thirouard [20], the author either assumes that the oil layer absorbs all incoming light or that the surface of the piston behind the oil layer has zero reflectivity. This is not the case as the nature of the Beer-Lambert law is exponential suggesting there is always transmission and the surface of the piston being aluminum will surely have some reflectivity. Due to the reflection of the piston the total incident light intensity on the oil film is equal to the initial laser intensity and the reflected laser intensity. The reflected laser intensity is just the transmitted intensity multiplied by reflectivity. The following equations will derive a revised version of the fluorescent emission intensity using similar approaches from previous equations:

$$I(x) = (I_0 + \rho I_{tr})e^{(-\alpha_g x)} \tag{2.13}$$

Where:

$$\alpha_g = C_{dye}\varepsilon_{dye} + \alpha_{oil}$$

$$I_{tr} = I_0 e^{(-\alpha_g h)}$$

ρ: Reflectivity of piston surface

$$dI_{abs} = (I_0 + \rho I_{tr})e^{(-\alpha_g \cdot x)} C_{dye}\varepsilon_{dye}dx \tag{2.14}$$

$$dI_{fluo\ det} = \frac{\theta_s}{4\pi}\phi S_p e^{(-\alpha_{oil} \cdot x)}(I_0 + \rho I_{tr})e^{(-\alpha_g \cdot x)} C_{dye}\varepsilon_{dye}dx \tag{2.15}$$

$$I_{fluo\ det} = \frac{\theta_s}{4\pi} \cdot \frac{S_p(I_0+\rho I_{tr})C_{dye}\varepsilon_{dye}}{\alpha_g+\alpha_{oil}} \cdot \left[1 - e^{(-(\alpha_g+\alpha_{oil})h)}\right] \cdot \int_{\nu_1}^{\nu_2} f(\lambda)\phi(\lambda)d\lambda \tag{2.16}$$

$$I_{fluo\ det} \approx (\Theta C_{dye} \varepsilon_{dye} I_{TI} \Lambda)\mathrm{h} \tag{2.17}$$

Where:

$$\Theta = \frac{\theta_s S_p}{4\pi}$$

$$I_{TI} = I_0 + \rho I_{tr}$$

$$\Lambda = \int_{\nu_1}^{\nu_2} f(\lambda)\phi(\lambda)d\lambda$$

Note that Equation 2.17 is the same equation as 2.11, but I_0 is replaced with I_{TI} to account for the reflectance of the piston surface.

In this thesis multiple applications of these principles will be discussed. Initial experimental setups took advantage of the fluorescence phenomenon by doping the oil with a combination of two dyes that were excited by a 3 W average power, 15-25 mJ per 6 ns pulse, Nd:YAG laser at an excitation wavelength of 532 nm. As the dyes in the oil fluoresced, a narrow band-pass filter would isolate the fluorescent light from the laser light so the high-intensity CCD camera could collect it. In the newly developed setup the fluorescent dyes are excited by different lasers for optimization purposes; the new lasers are a Continuous Wave (CW) Ti:Sapphire laser and a pulsed Nd:YVO_4 laser. The reasons behind these changes will be discussed in detail in Section 2.2.6. An example of the old setup is shown in *Figure 2-10*.

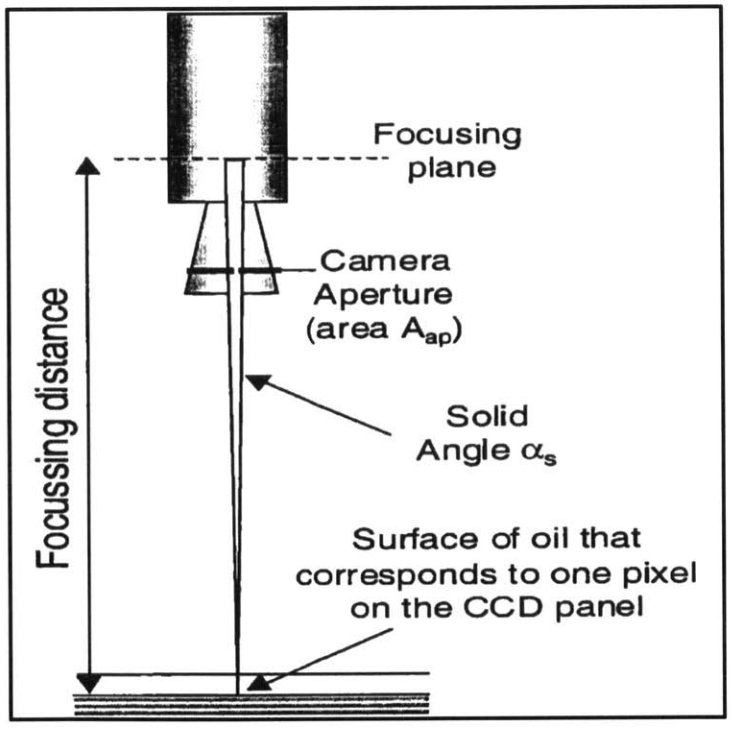

Figure 2-9: Diagram showing the solid angle created by the aperture in the camera [20].

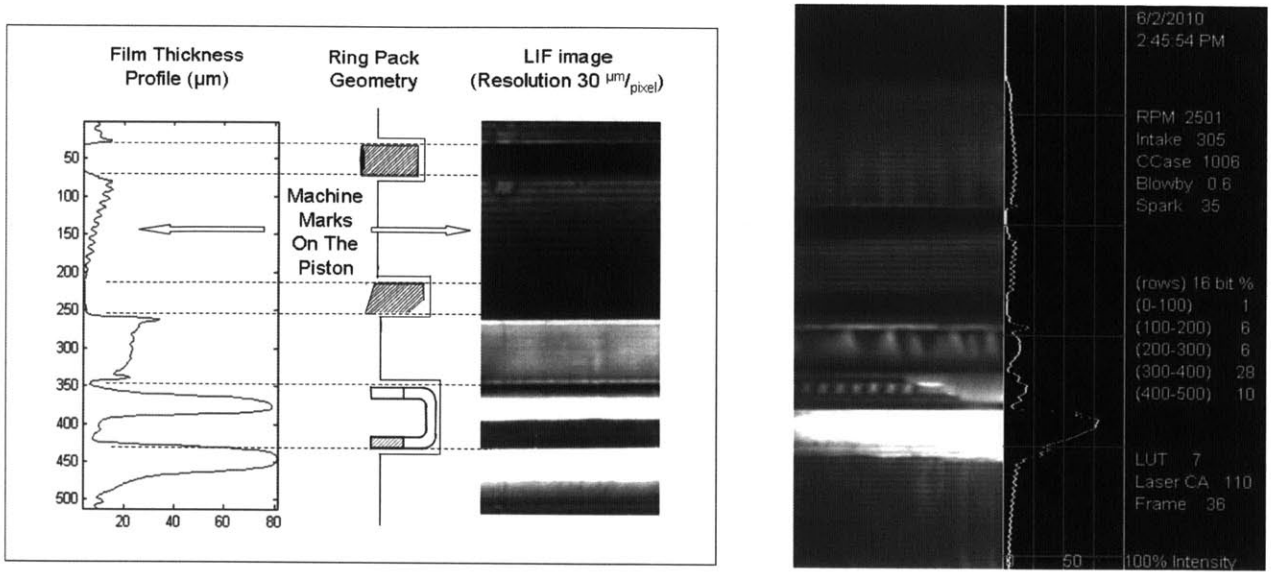

(A) **(B)**

Figure 2-10: (A) Sample image of the original 2D LIF system with intensity profile showing geometric features of the piston. (B) Single frame from a video taken using the 2D LIF system with engine parameters shown on the side [5].

2.2.5.2 Calibration of the LIF Signal

Calibrating the LIF system is necessary if any quantitative data is to be obtained. For this thesis the old setup was not calibrated extensively due to the development of the newer system which will be explained in Section 2.2.6. One major reasoning behind the necessity to calibrate the system before every experiment is that the fluorescence of the dyes is strongly affected by temperature. Temperature can ultimately permanently distort the chemical compound being used for fluorescence possibly rendering it unable to fluoresce; this is called thermal bleaching. To avoid this extensive work was done by B. Thirouard [20] to research which dyes could withstand the high combustion temperatures experienced in an IC engine. Apart from thermal bleaching, temperature can cause variations in the absorptivity, the quantum yield efficiency, and the excitation and emission spectra of a dye. As shown by F.P. Shafer [27], the absorptivity decreases as temperature increases as well as the quantum yield efficiency. These effects are best described in more detail in the literature: [20, 24, 27]. In significantly simpler terms the higher temperatures cause a higher probability of molecular vibrations and collisions which facilitates more energy dissipation allowing changes to the fluoresced photons. Viscosity of the solvent can also play a role in the altering of the fluorescent properties of a dye and due to engine oil having

a temperature dependent viscosity; this worsens the temperature effect on the dye. Although as long as the chemical structure of the dye stays intact during the experiment all these effects are reversed as the oil regains its original temperature.

The main problem with the temperature in an IC engine is not that the temperature varies so greatly throughout the cycle; it's that it can vary drastically across the piston itself. The piston temperature can vary anywhere from 250 °C at the top surface of the crown land to around 80 °C on the piston skirt. Most fluorescent dyes have a large change in quantum yield efficiency over this large of a temperature range. *Figure 2-11* shows just how varied the temperatures can vary on a piston as well as among different ignition types.

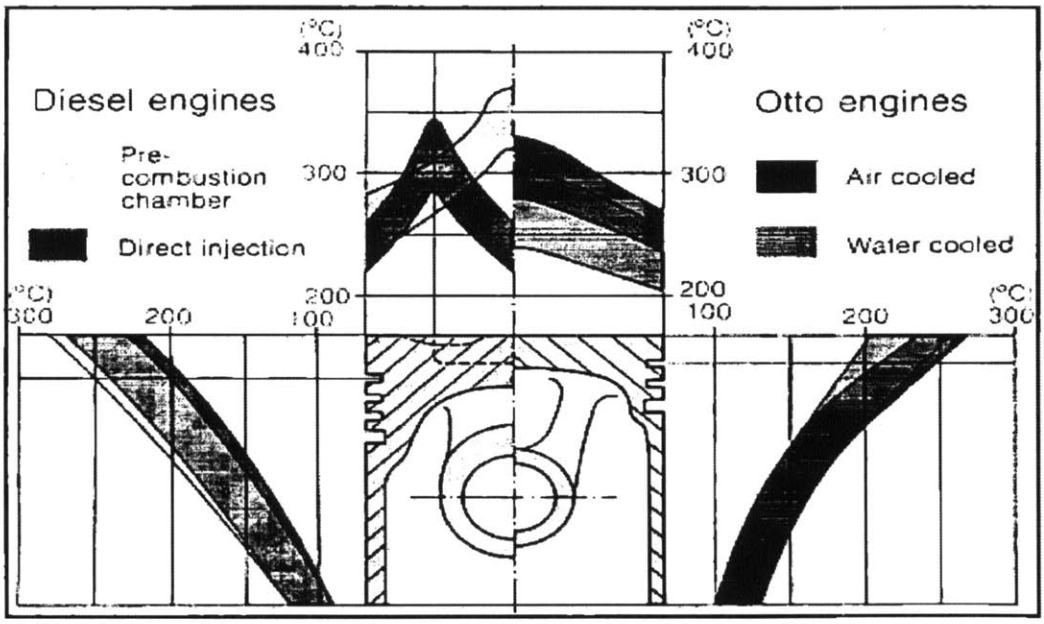

Figure 2-11: Piston operating temperatures at full load mapped to piston geometry [20, 28].

The original method for calibrating this system was to find a certain geometric feature on the piston, something that was clearly visible in the intensity profile, and use that as a reference point for the rest of the piston. This assumes that the section chosen is fully flooded with oil such that there are no gaps between the oil and either surface. With this one can measure the difference in intensities of two points, one point is the feature and the other is the feature-less section, and this difference in intensities is essentially the intensity of a volume of oil the exact same size as the feature. An example of this method is shown in *Figure 2-12*. This allows for the

A(T) term to be calculated, but this is assuming quite a lot and therefore has some uncertainty to it. Temperature cannot be assumed as uniform across the piston nor can one assume that the features are fully flooded when measurements are taken.

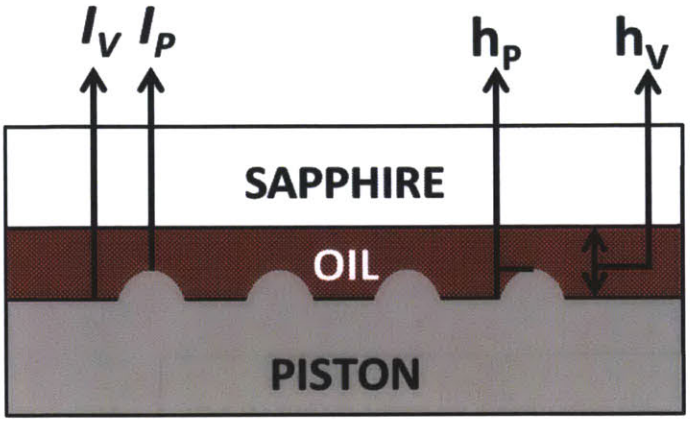

$$I_{emission} \approx Ah$$

$$A = \frac{I_V - I_P}{h_V - h_P} = \frac{I_V - I_P}{tooling\ mark\ depth}$$

Figure 2-12: Diagram showing the calibration method initially used to measure oil film thickness.

$$I_{fluo\ det} \approx \frac{\theta_s}{4\pi} \cdot S_p \cdot I_0 \cdot C_{dye} \cdot \varepsilon_{dye} \cdot h \cdot \int_{\nu_1}^{\nu_2} f(\lambda)\phi(\lambda)d\lambda \qquad (2.11)$$

In order to have the most accurate calibration method, each variable in Equation 2.11 must be accounted for in some way. Many of these parameters are difficult to measure at the exact same conditions that are experienced inside an IC engine. Some parameters like θ_s, S_p, C_{dye}, and $f(\lambda)$ can all be externally measured and kept identical throughout multiple experiments.

The initial intensity of the incident beam, however, is much more difficult to measure directly. The issue is that the intensity profiles of all lasers follow a Gaussian distribution in the radial direction causing non-uniform excitation of the dye in any given area of oil. Lasers themselves also have variations in time not just in space, especially pulsed lasers. As each pulse is fired, each one has a different special profile and how these pulses vary is dependent of laser type and construction. An early proposition was made to have a secondary setup capture the beam profile to then use against the images captured in the engine, but this would have required a second camera which was not considered an option.

Another difficult parameter to control is the oil absorption coefficient, α_{oil}. During normal operation of the IC engine the oil itself can degrade by being oxidized; this is why one of the

additives added to oils is an anti-oxidant. As oil oxidizes the absorption coefficient increases. It can increase with the addition of combustion soot as well [20]. As Thirouard discusses, oil oxidation does not occur until temperature reaches above 140 °C. This temperature is usually exceeded in all IC engines except with extremely low load operation. At the top of the crown land and the top of the liner are where the temperature is most likely to exceed 140 °C. The residence time with which the oil is in contact with either of these spots is quite low therefore allowing for little oxidation to occur if the tests are quite short. For new oil with the same dye concentration, the oil absorption can account for 15% of the total absorption of the solution [19, 26]. After a cumulative total of 20 hours of running the oil can account for more than half of the total absorption [20]. This makes it clear that the oil must be changed consistently to ensure the lowest oxidation of oil during experiments.

As stated earlier the absorptivity and the quantum yield efficiency of the dyes has a strong temperature dependence which can cause problems with the previous calibration method shown in *Figure 2-12*. Both the absorptivity and the quantum yield efficiency can be measured using a spectrofluorometer, but the temperature of the oil would still be an unknown. To counteract the effect of temperature, two combinations of dyes were used to manipulate the temperature effect into being as limited as possible. Theories for measuring the temperature simultaneously with the fluorescence was also proposed, but were too complicated for the original setup. For a more detailed explanation of this method refer to B. Thirouard [20]. Taking all these into consideration, selecting a dye was very strict. Dyes needed to: be soluble in the engine oil, have high melting points (>200 °C), have high quantum yield efficiencies, and not oxidize in the engine. There were initially 18 different dyes that were chosen because they were excited by the Nd:YAG laser at 532 nm, after the initial requirements were set only six dyes were chosen for experimental tests. Out of these six dyes three of them were from the Rhodamine family and the other three were of the Pyrromethene family. One from each family was chosen for the combination that was believed to be necessary to reduce the temperature dependent nature of the dye. Using a two dye solution also made it possible to setup the dual emission calibration which was not applied to this specific engine setup. After all tests were conducted, the dyes chosen were Pyrro 567 and Rhd 640 due to the different temperature dependencies shown in *Figure 2-13* and *Figure 2-14*.

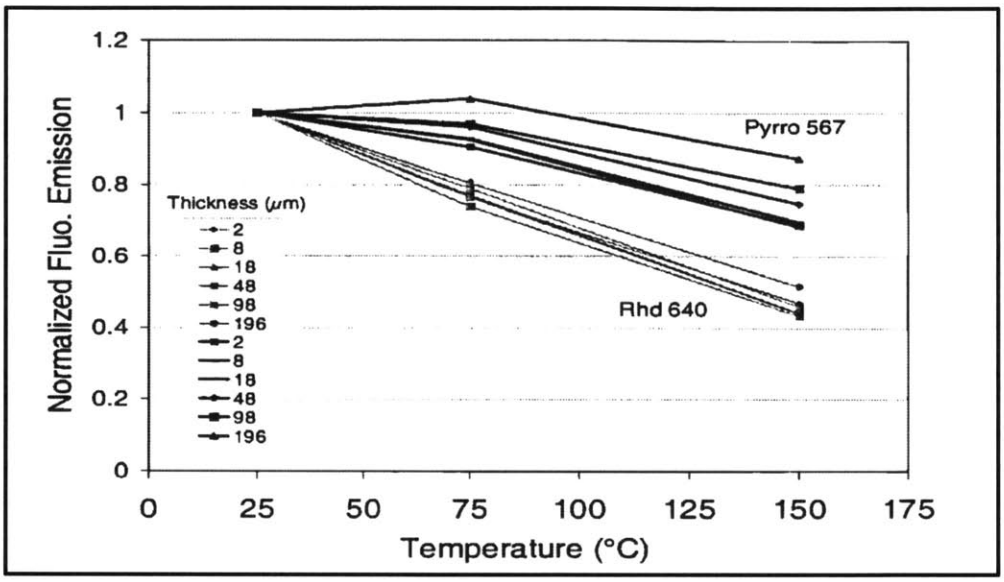

Figure 2-13: Normalized fluorescence emission intensity versus temperature for combination Pyrro 567 and Rhd 640. Emission of Pyrro 567 measured at 570 nm with 10 nm narrow-band filter, emission of Rhd 640 measured at 650 nm with 10 nm narrow-band filter [20].

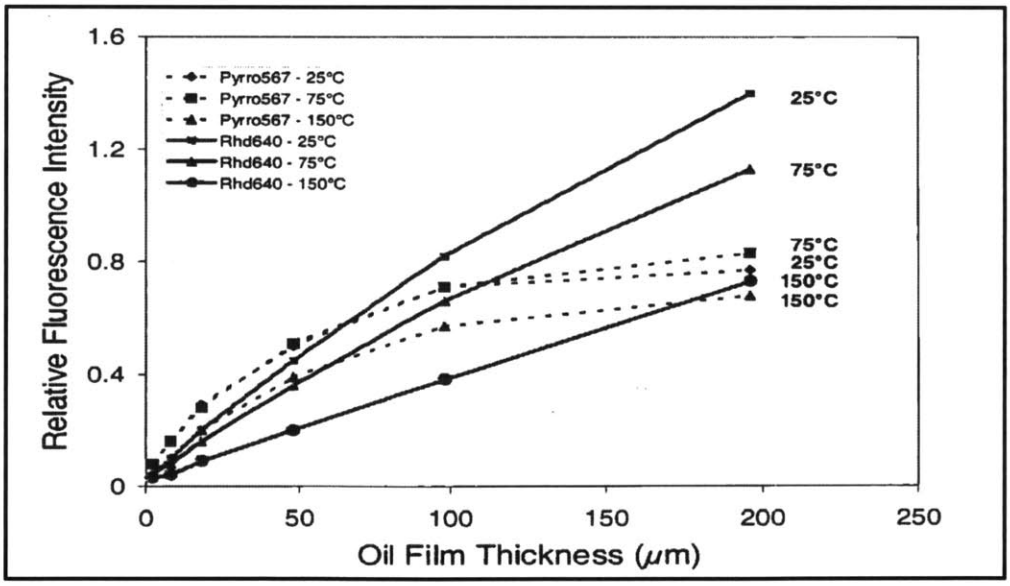

Figure 2-14: Relative fluorescence intensity versus oil film thickness for combination Pyrro 567 and Rhd 640. Emission of Pyrro 567 measured at 570 nm with 10 nm narrow-band filter, emission of Rhd 640 measured at 650 nm with 10 nm narrow-band filter [20].

2.2.5.3 Previous Laser System

The laser chosen for the initial setup was a second harmonic Nd:YAG laser pulsed at 532 nm wavelength to excite the fluorescent dye. The ideal candidate for LIF studies would be a laser with the wavelength in the ultraviolet region of the electromagnetic spectrum since it has a wide variety of dyes that can be fluoresced by that wavelength range. The 532 nm wavelength was a limiting factor in choosing the dye. In order to capture sharp images at speeds as high as 6,000 RPM (testing never passed 3,500 for this thesis) the laser had to have a pulse width that was less than 1 μs. To make sure exposure time was on this order of magnitude a laser with a very short pulse width of 6 nanoseconds was used.

The power output of the laser was 3 W average power and the laser specifications says it can output 100 mJ per 6 ns pulse at 532 nm wavelength. This would translate to about 16.7 W peak power, but the maximum energy per pulsed used in the experiments was only about 25 mJ allowing for a peak power of about 4.2 W. The laser has the ability to run at a repetition rate of 30 Hz, although operation occurred at 20 Hz.

The optical setup used in conjunction with the laser contained a beam expander, a collimator, a polarizer, and a cube beamsplitter. The laser had a beam size of 2.5 mm, so in order to properly illuminate the ring pack and piston skirt regions, the beam needed to be expanded by a factor of 10. The cube beamsplitter had to be used due to spatial constraints with the geometry. The disadvantage of using a cube beamsplitter is that a significant amount of light will be wasted once it is reflected by the beamsplitter. This was a 50/50 beamsplitter so 50% was reflected and transmitted, the alternative was a dichroic beamsplitter which uses reflective coatings, but when this setup was being created, dichroic beamsplitters would create ghost images and that was unwanted. Ultimately 52% of the laser intensity was wasted as a result of using the cube beamsplitter. The complete optical setup can be seen in a diagram in *Figure 2-15*.

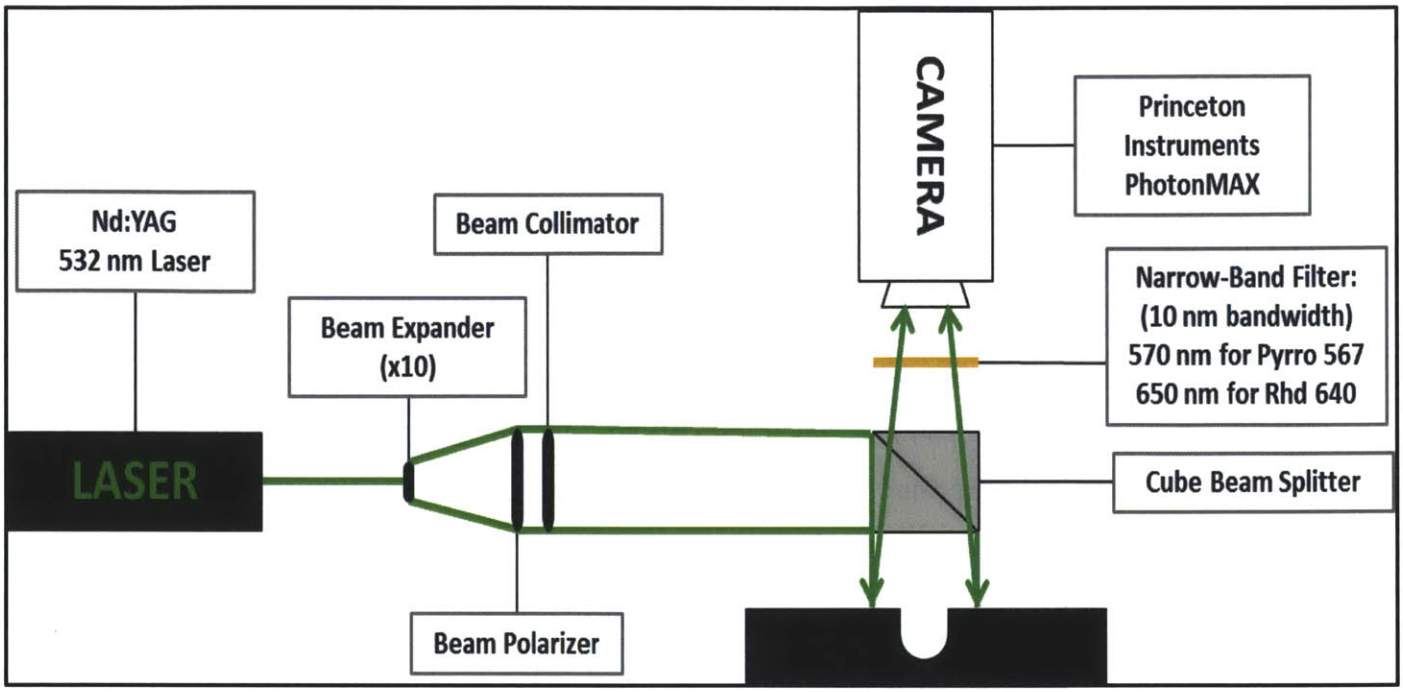

Figure 2-15: Diagram of complete optical setup of original LIF system.

2.2.5.4 System Limitations

The original system had a significant limitation with observing oil transport mechanism; only one image could be taken per cycle. This means that an entire cycle of intake, compression, expansion, and exhaust occurs before another image is captured.. Broad steady-state conclusions can be drawn such as how much oil on average can be seen moving through the OCR gap, or how much oil has accumulated in the skirt chamfer after intake. All of these results were made using videos comprised of these images at different crank angles, which would give the impression that the videos were continuous, but that is far from the case. *Figure 2-16* shows the disparity between two frames of these videos which are supposed to represent the same exact moment in a cycle. Although this system cannot show continuous effects, it can show effects that persist over large periods of times. An example of these longer lasting phenomena is that if the ring gap is not in a position to be observed by the camera through the optical window, then the oil films in the piston lands tend to move very slowly. These effects are better seen using the original system and not the high speed LIF system.

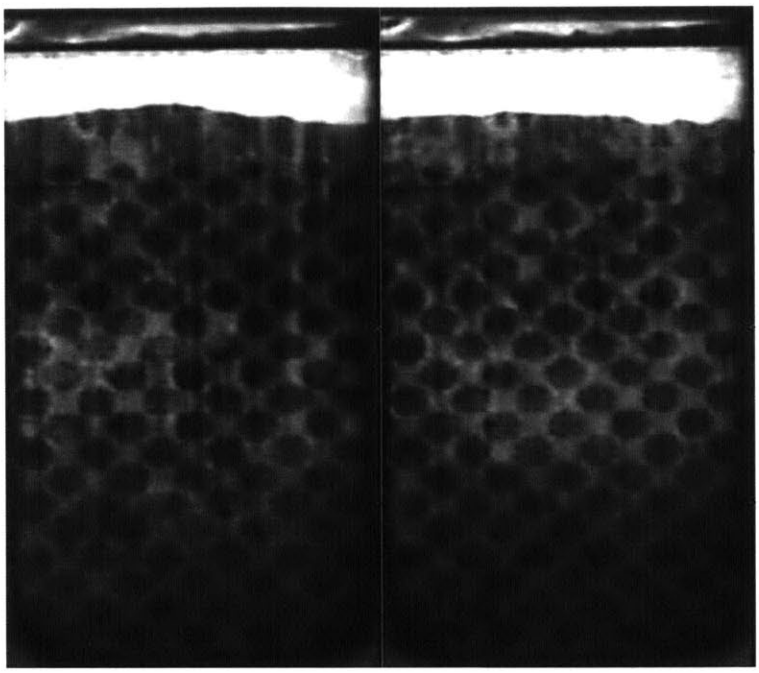

Figure 2-16: Two images taken at 466 Crank Angle (CA) degrees near BDC during the expansion stroke. The original laser could only operate at a maximum repetition rate of 30 Hz and the camera itself could only operate at 15 Frames Per Second (FPS).

2.2.6 Development of High Speed LIF System

The main focus of this thesis is to show the results of creating a new diagnostic LIF system using the integration of high speed imaging. The initial setup as stated before had limitations of only having a camera that could run at 15 FPS and a laser that could only operate at 30 Hz. To truly observe the oil mechanism phenomena described earlier, an upgrade had to be made. In this section, the selection and testing of multiple components for the new setup will be discussed along with possible future additions for more quantitative results. The engine itself has not changed along with the optical access of the engine. The only components to be changed were: the camera, the laser, and the optics used to alter the laser profile.

2.2.6.1 High Speed Camera Selection

The initial system used a high intensity camera, a Princeton Instruments PhotonMAX 512B. This camera was acquired during Przesmitzki's studies [21] and was an improvement over the one used by Thirouard [20]. It was able to provide high quantum efficiency and a high signal-to-noise ratio in the output signal. In Table 2-1, the details and specifications of the camera are shown.

Quantum Efficiency	~95%
Intensifier Required	No
CCD Format	512 x 1024, with 512 x 512 imaging
Pixel Size	16 microns
System Read Noise	< 1 e- rms 10 MHz effective
CCD Cooling	80 °C
Bit Depth	16 Bits
Frame Readout	10, 5, or 1 MHz
Frames per Second (FPS)	15 (max 30)
Video Output	Digital Only

Table 2-2: A summary of important specifications of the PhotonMAX camera that was used during this study.

The PhotonMAX has a quantum efficiency of about 95% in the wavelength range that is of interest to this project (550-650 nm), the highest possible quantum efficiency at the time for that wavelength range. The camera uses a back illuminated CCD sensor which gets rid of the need for an intensifier, which was used for the old camera and caused a delay in image capturing. This camera was not fast enough to capture the fine details of oil transport mechanisms so the thought of using high speed cameras was proposed.

It was initially decided that the speed necessary to capture the images that were desired had to give a time resolution of roughly one crank angle per frame. This varies with speed; for 800 RPM the camera speed would have to be 2,400 FPS and for 3,500 RPM the speed would have to be 21,000 FPS. So the initial tests were to see if high speed camera were even capable of sensing the high intensity fluorescence of the dye. Once that was tested and came back with satisfying results, the benchmark was made to find a camera that could reach 21,000 FPS at a decent resolution. The first high speed camera tested was the Phantom V4.2. This camera was able to record at 2,100 FPS at a resolution of 512 x 512 and a maximum of 90,000 FPS at a severely reduced resolution of 32 x 32. The recording bit depth however was only 8 bits which would not be able to record the emission intensity without saturating at the laser power currently being used.

This camera was controlled via Ethernet connection to a computer which used proprietary software provided by the manufacturer. With the current model there was only 256 megabytes of on-board memory available for recording. This would cause the videos to be quite short, which

can be about 0.5 seconds of recording which may not capture many cycles at lower speeds such as 800 RPM. This camera was not tested directly with a laser due to there not being a laser available for this project that could synchronize at such high frequencies. There needs to be at least one pulse per frame, so in place of a laser, a high intensity fiber light was used. Actual tests run had the camera operating at 3,000 FPS at a resolution of 512 x 128. The videos produced were adequate for a discontinued product, but there were better cameras on the market.

The second camera to be tested was a much more modern camera, recently developed; the Photron Fastcam SA-5 provided by Tech Imaging Inc. as well as by Professor James Bales of the Edergton Center at MIT. This camera was a substantial jump in performance allowing for 7,500 FPS at a resolution of 1,024 x 1,000 and a maximum frame rate of 775,000 FPS at 128 x 24. The sensor for this camera was a monochromatic (black and white) CMOS sensor instead of a CCD allowing for better photo-sensitivity. Maximum shutter speed is 1 μs, but normally it operates and a shutter speed of 1/(FPS). The bit depth also increased to viewing videos at 12-bit, but being able to separately download the images as 16-bit TIF files. On-board memory also received an upgrade from as low as 8 gigabytes to as high as 64 gigabytes. The camera was controlled through optional keypad with integrated viewfinder and Gigabit Ethernet or RS-422. In this project instead of a keypad being used to control the camera, it was hooked up to a computer while using more software created by the manufacturer. The frame rate chosen for this project was 30,000 FPS at a resolution of 896 x 192. This camera was operated using the fiber light source as well as a synchronized laser source. It has the ability to send and receive TTL pulses through the I/O port using BNC cables.

Tests were conducted using the SA-5 while using multiple lasers, such as a continuous wave (CW) laser and a pulsed one to see which would provide the best imaging system possible. The specifications of each laser will be discussed in the following section. Initially while using the CW laser motion blurring would occur suggesting that CW might be the wrong choice or that the camera needs to operate at a faster shutter rate or possibly at a higher frame rate. Once all tests were conducted on the SA-5, a new model was subjected to tests. The new camera was the Photron SA-X2 (monochromatic as well). At the time of testing this was the top of the line product that Tech Imaging could provide.

The maximum frame rate was not faster than the SA-5, but the resolution at the same speeds were higher allowing for much better quality videos. And due to the thin nature of the optical window, it was impossible to fit the entire window in the image without making observation of the oil flow near impossible. So the window was broken up into three sections and this allowed for the maximum vertical pixel length to decrease and if the resolution decreases then frame rate can increase. The tests with the SA-X2 were able to achieve 72,000 FPS at a resolution of 656 X 256. The simple time resolution stated earlier of one crank angle per frame was actually not enough to view the higher speed of 3,500 FPS without some discontinuities at mid-stroke, where the speed is greatest. With such a high frame rate that is relatively excessive, there is a significant amount of freedom to change the resolution where need be if there is a certain area of interest that may need more pixels at the cost of frame rate and still operate at fast speeds. Tests have been conducted with a pulsed laser of high repetition rates and the synchronization between the camera and laser work well.

2.2.6.2 Laser Selection

The original laser that was used in the setups of Thirouard, Przesmitzki, and Senzer [20, 21, 5] was a New Wave Research MiniLase II-20, 532 nm, Nd:YAG pulsed laser with an average power of 3 W. The quality of the fluorescence when used for the old system was good, but once a high speed camera was proposed to replace the original camera, more power was going to be needed. High speed imaging requires a significant amount of light and the higher the frame rate the more light is necessary. Initially the procedure was to test a CW and a pulsed laser to decide which can give the best quality images at relatively the same power.

The first laser to be tested was, the Verdi G18 CW laser made by Coherent Inc., a Ti:Sapphire laser capable of running at a maximum power of 18.5 W at 532 nm. The laser had the ability to run at an output power between a range of 0.5 W and 18.5 W. It was controlled via a large benchtop power supply with a built-in computer as well as being able to receive external inputs. For full specifications see *Appendix A.3*. The positive side of a CW laser is that there is no need to synchronize the camera's shutter speed with the laser pulses such as with a pulsed laser. This does however cause some problems if the exposure time is not small enough or the camera is not operating at high enough frame rates. Motion blur begins to occur if the frame rate is not high enough which creates images that a difficult to study for oil transport mechanisms. To

counter act the motion blurring effect, test were conducted to see if changing the exposure time via manipulating the shutter speed would have any beneficial effect. Other testing included a significant amount of optimization tests, specifically testing different optical components such as lenses, beam expanders, collimators, beamsplitters, etc.

The second laser to be tested was, the Matrix 532-7-30 pulsed laser manufactured by Coherent Inc., a Nd:YVO4 (Neodymium:Yttrium Vanadate) laser capable of running at a maximum average power of 7 W at a repetition rate of 30 kHz. The pulsed width was a maximum of 20 nanoseconds with a recommended repetition range of 5-60 kHz. To see full specifications, see *Appendix A-4*. This laser was controlled via a software GUI provided by the manufacturer through the use of a USB-to-miniUSB or an RS-232 connection as well as having the triggering system be connected via a BNC to 25-pin connector adapter. The high speed camera is connected to the laser via a BNC cable and whenever the recording has been initiated the camera sends a TTL pules to the laser to begin burst mode operation where it is continually fires pulses at the designated repetition rate. Similar tests to the ones conducted with the CW laser were conducted with the pulsed laser as well. Further discussion on the optics used in the new setup will occur in the next section.

2.2.6.3 Optical Components

The optical equipment used in the previous setups, [5, 20, 21] had to be upgraded for the integration of the high speed camera to be most effective. Some components had worn and been distorted over the year. An engine laboratory is not a typical optical environment and therefore may cause damages to some optics. The original 10x beam expander selected by Thirouard had developed artifacts that could be seen whenever images were captured either with the original camera or the high speed cameras. Replacing the old beam expander was a top priority when deciding what optics needed to be upgraded or if they can be removed altogether. Due to the varying beam sizes of the lasers that were tested, two 10x beam expander systems were purchases. The beam size of the Matrix 532-7-30 was approximately 0.23 mm whereas the beam size of the Verdi G18 was 2.25 mm. To achieve necessary beam diameter of approximately 20-25 mm the Verdi laser needed only a single beam expander instead of the two necessary for the Matrix laser.

Along the lines of beam profile manipulation, a diffuser was purchased to attempt to create a more uniform beam profile as opposed to the typical Gaussian distribution. Previous setups would create a normalized average beam intensity profile which was used to divide out the laser profile in the images capture by the LIF system. This however becomes difficult if the divergence of the beam is significant enough to change the beam profile from where you take the normalized profile image to where you take the LIF images. The diffuser was used to possibly make this method obsolete when calibrating the system.

The old collimator was deemed unnecessary due to the beam expanders being assemble as a system of expander and collimator permanently fixed, effectively reducing alignment problems. Along with the collimator, the polarizer was of no use at this stage in the optimization of the optical components. The polarizer was initially used to polarize light in a way such that it would create less constructive thin film interference as it passed through the sapphire window. In the current setup the need for a polarizer is redundant while using a dichroic beamsplitter. As the high speed cameras were being tested, the amount of light intensity that was needed began to increase significantly as frame rates increased and this called for a new beamsplitter that did not waste over 50% of the laser energy. As Thirouard [20] mentions the cube beamsplitter was chosen due to it having no ghost images even while it wasted a significant amount of the laser energy, which was tolerable due to the high energy pulses (~25 mJ). The Matrix pulsed laser only pulses with approximately 0.233 mJ of energy thus energy could not be spared. The new beamsplitter was a single-edge laser dichroic beamsplitter with a >94% transmission band of 541.6 nm to 1200.0 nm. This dichroic beamsplitter allows for almost all the laser light to be reflected toward the sapphire window and transmit all emitted light in the direction of the camera's sensor. The reason for the polarizer being redundant was because a long-pass filter was used in conjunction with the dichroic beamsplitter effectively reducing any unwanted reflections or interference. The same could have been achieved without the filter and just the polarizer and is just a matter of preference.

An interesting problem occurred when the very first tests were conducted with the high speed camera and the original filter. The images captured by the high speed camera were completely black, with no discernible features being seen. This was quite a problem and fellow colleagues in Germany at Daimler were able to conduct spectroscopic analysis of the doped oil used in the

tests discussed in this thesis; the results are shown in *Figure 2-17.* Initial thoughts were that the wrong filter was being used so instead of using the original band-pass filter of 570 nm ± 10 nm, a long pass filter with a 50% transmission at approximately 540 nm was used instead. This ended up working significantly better than the original filter than the one Thirouard had chosen. The initial understanding is that the original filter was actually at an incorrect wavelength for the emission spectra, but the original laser had such a high energy pulse that it was able to penetrate through the high optical density filter at that wavelength.

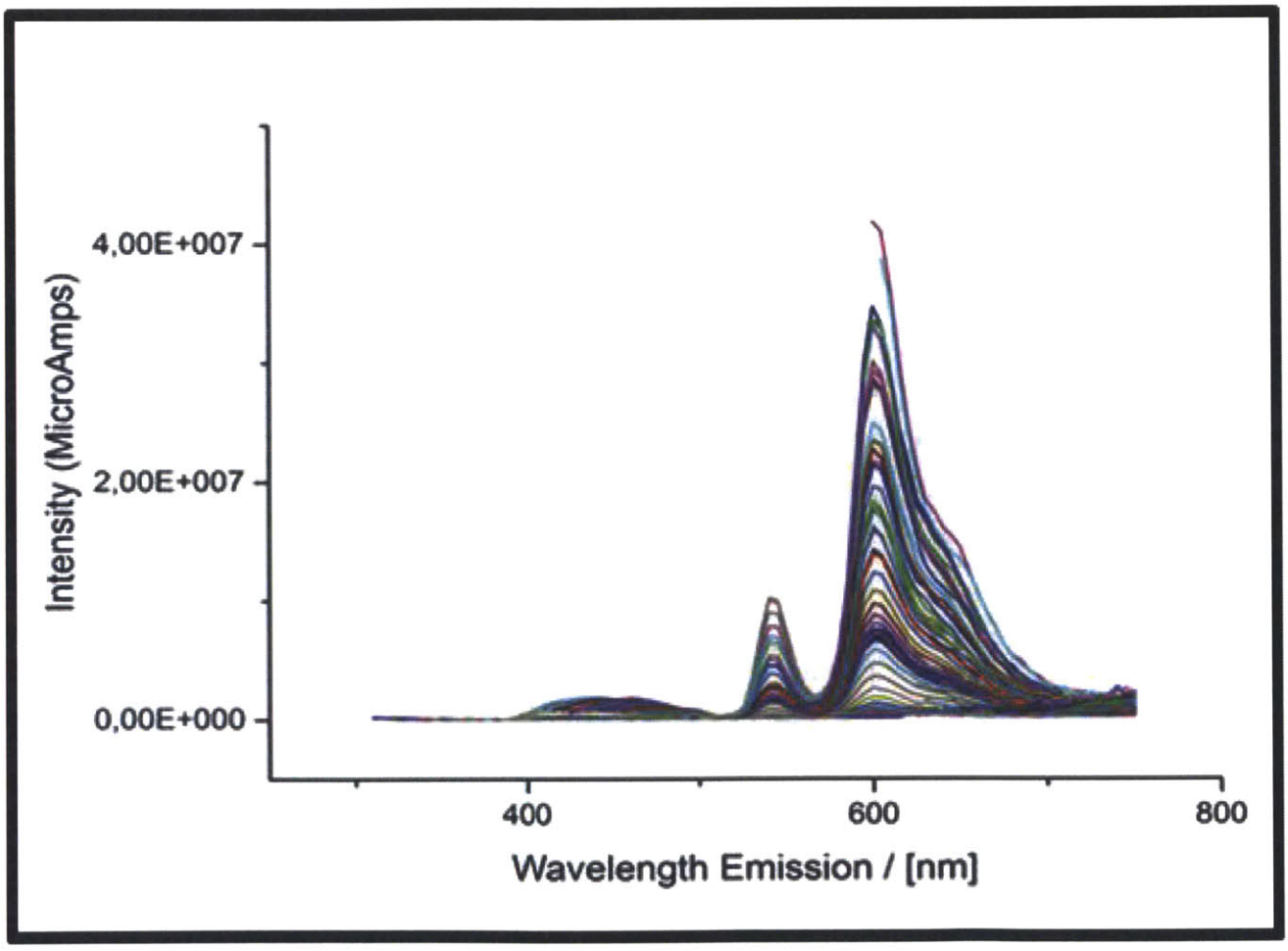

Figure 2-17: Measurement of spectral information of selected dyes, Pyrro 567 and Rhd 640 provided by Daniel Fuhrmann, Institute for Combustion and Gas Dynamics, University of Duisburg-Essen, Germany.

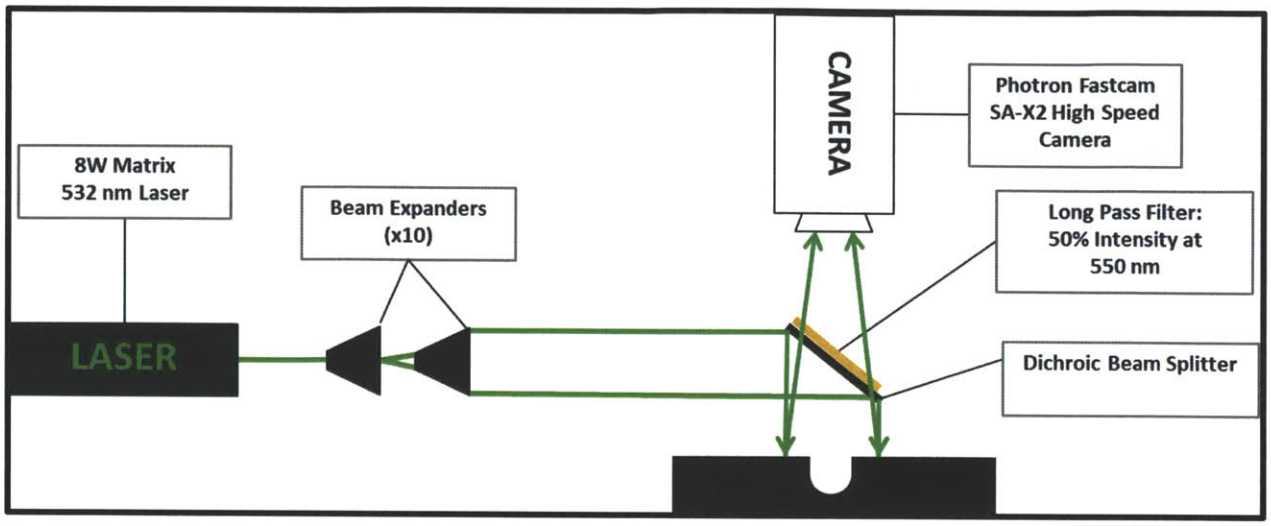

Figure 2-18: Diagram of complete optical setup of New High Speed LIF system.

2.2.6.4 Calibration of High Speed LIF System

With further collaboration between MIT and Daimler, a new calibration device was designed to help measure the temperature dependence of the fluorescent dyes. No quantitative data has been recorded with the device thus far for this thesis, therefore only theory and design will be discussed in this section. The theory behind the device is simple; place an oil sample in between a sapphire window and an aluminum back plate with a set spacer applied in between to create the desired thickness of oil and induce fluorescence as done in the actual setup. These spacers can range from 10 microns to 100 microns to simulate actual oil layer thicknesses. Although actual oil films can become as low as 1-3 microns inside the ring-liner interfaces. These will have to be extrapolated from the measured data. To simulate the engine temperature, three tubular electric heaters are inserted at equidistant positions in the cylinder to heat the oil; no measurements will be heated until steady state is achieved. If temperature can be measured simultaneously with intensity, and assuming a linear temperature dependence as suggested in Equations 2.12 and 2.17, then a psuedo-slope can be calculated using the calibration device which can then be plugged into Equations 2.12 or 2.17 to find the oil film thickness. Possible techniques to measure temperature simultaneously with intensity will be discussed in Chapter 4.

Chapter 3: High Speed Classification of Oil Transport Mechanisms

In this section, oil transport mechanisms observed using the new high speed LIF system will be discussed. The high speed LIF system has brought new understanding into phenomena which were merely just theories prior to this new diagnostic tool. The biggest advantage to this high speed setup is that now instead of one frame per cycle, 15 frames maximum can be captured per crank angle degree at speeds of 800 RPM and for 3500 RPM, 3.43 frames can be captured per crank angle. No other setup has reached this type of time resolution for studying oil transport mechanisms in an IC engine. This section will be broken up in to three sections; the first one will discuss any findings on the oil transport mechanisms found in the piston skirt region; the second will focus on the oil mechanisms that are found to occur in the piston ring pack region and above in the combustion chamber as well, and lastly system optimization will be discussed which will include the qualitative data used in selecting each component of this system. All images in this section were taken at 1500 RPM, ~600 mbar at 50,000 FPS unless otherwise specified.

3.1 Piston Skirt Region Oil Mechanisms

3.1.1 Below the Piston Skirt Region

One of the most prevalent, oil transport, mechanisms that was proposed, but with no hard visual evidence of it occurring, was the oil droplet shedding phenomenon. The hypothesis was that oil droplets created by oil jet were shedding off the backside of the piston, shedding off the skirt at piston velocity and then crashing into the skirt-liner interface. Prior to this study the only evidence of this phenomenon occurring were pictures of these circular spots of oil appearing in the skirt liner interface and small beads of oil accumulated at the bottom of the skirt, see *Figure 3-1*. The first task of the high speed LIF setup was to observe this phenomenon and see if the hypothesis can be confirmed. It should be mentioned that this engine is a "dry-sump" engine meaning that no oil accumulates in the crank case. Some early explanations included that the lobes of the crank shaft were wading in the oil in the sump and thus flinging droplets up toward the piston-skirt interface. With a dry-sump this is impossible, so this new hypothesis had to be explored. Even with the slower speeds of the initial high speed camera, observations were clear enough to confirm that the shedding of oil droplets of the backside of the piston skirt were contributing to the overall oil accumulation of oil in the piston skirt-liner interface.

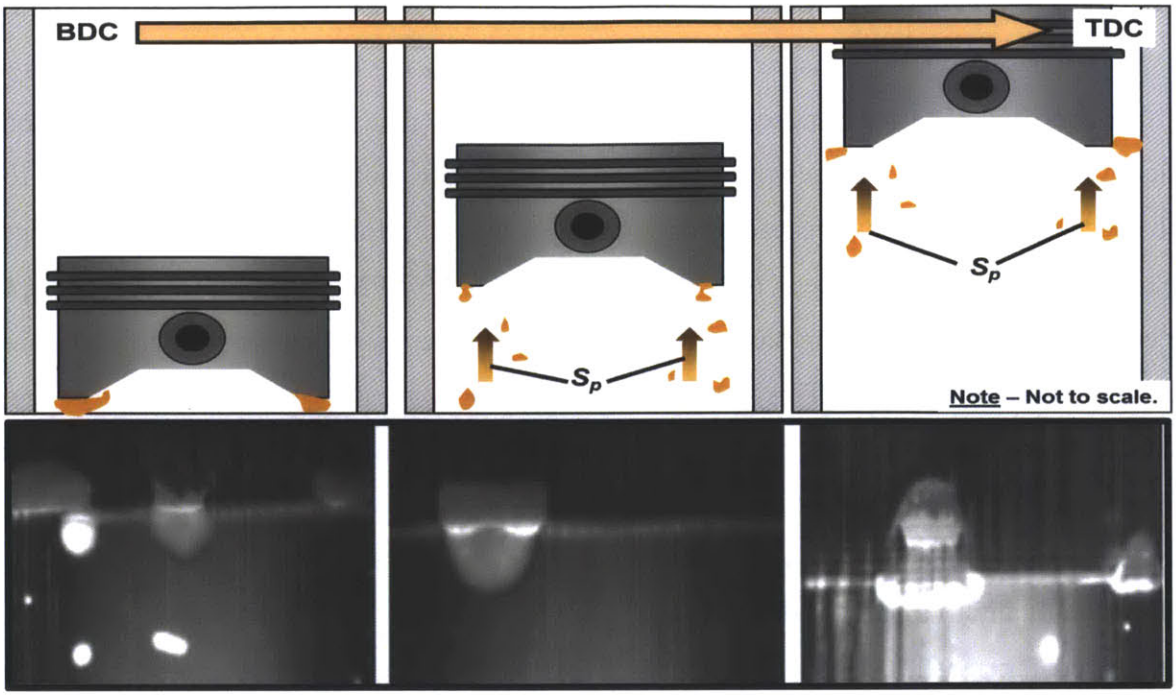

Figure 3-1: Example images showing the droplet shedding phenomenon. Images provided through old Laser Induced Fluorescence (LIF) measurements taken by E. Senzer [5].

Droplets could always be seen entering the skirt liner interface, but there was never a true understanding of where they may have been coming from; what was the true source? As shown in *Figure 3-2* one can make the observation that the origins of the oil droplets come from, in this case, these large strands of oil sliding off the piston, but interestingly enough they are shown not sliding off the front side of the piston skirt. These strands are originating from behind the skirt and giving rise to numerous droplets as shown in the last image of *Figure 3-2*. There are only a couple of different methods for the oil to accumulate behind the piston skirt and each one may very well contribute to the formation of these droplets.

The first and most likely largest source of oil to the backside of the piston skirt is the crank shaft oil jet. This crank shaft oil jet, as discussed in the first chapter of this thesis, has a single purpose and that is to lubricate the piston during all downstrokes. Typical oil jet dynamics follows as such; as the crank shaft rotates, eventually a hole in the connecting rod and a hole in the crank shaft align allowing for the constant pressure inside the crank shaft to force out lubricant at a designated flow rate which then impacts the piston and thrust side of the liner simultaneously. This is one of the largest sources of oil to the control volume being studied in the skirt-liner interface, but what was commonly thought was that only the oil that physically made

contact with the oil was supplying lubricant. As shown in *Figure 3-2* that is not only the case as any oil that comes into contact with the backside of the piston skirt can coalesce into large quantities of oil where surface tension and viscosity cannot keep the oil attached to the piston as the velocity increases.

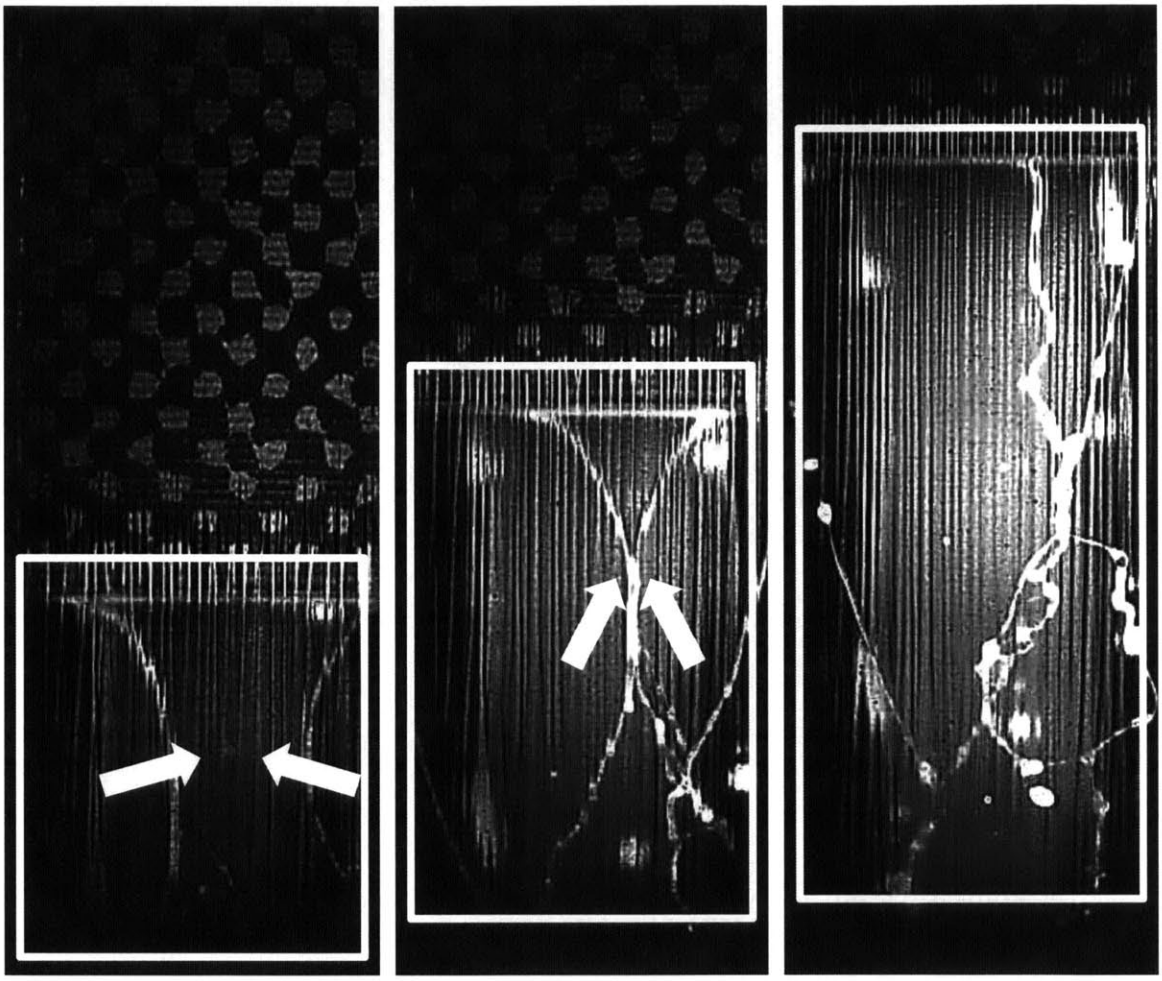

Figure 3-2: Images of droplet shedding taken via the High Speed LIF system. Engine operating conditions were 1,500 RPM and mid-load (~600 mbar). The approximate time scale from the first image to the last is 1.5 ms.

Eventually the velocity becomes too great to which one can see strands of oil and droplets begin to pull away from the piston and become free moving entities in the cylinder. As these droplets are free floating, the piston will begin to decelerate while the droplets continue at the same velocity of the piston when they were shed off allowing them to crash into the edge of the piston skirt region, thus supplying more oil to the skirt-liner interface. For an example of the total process see *Figure 3-3*.

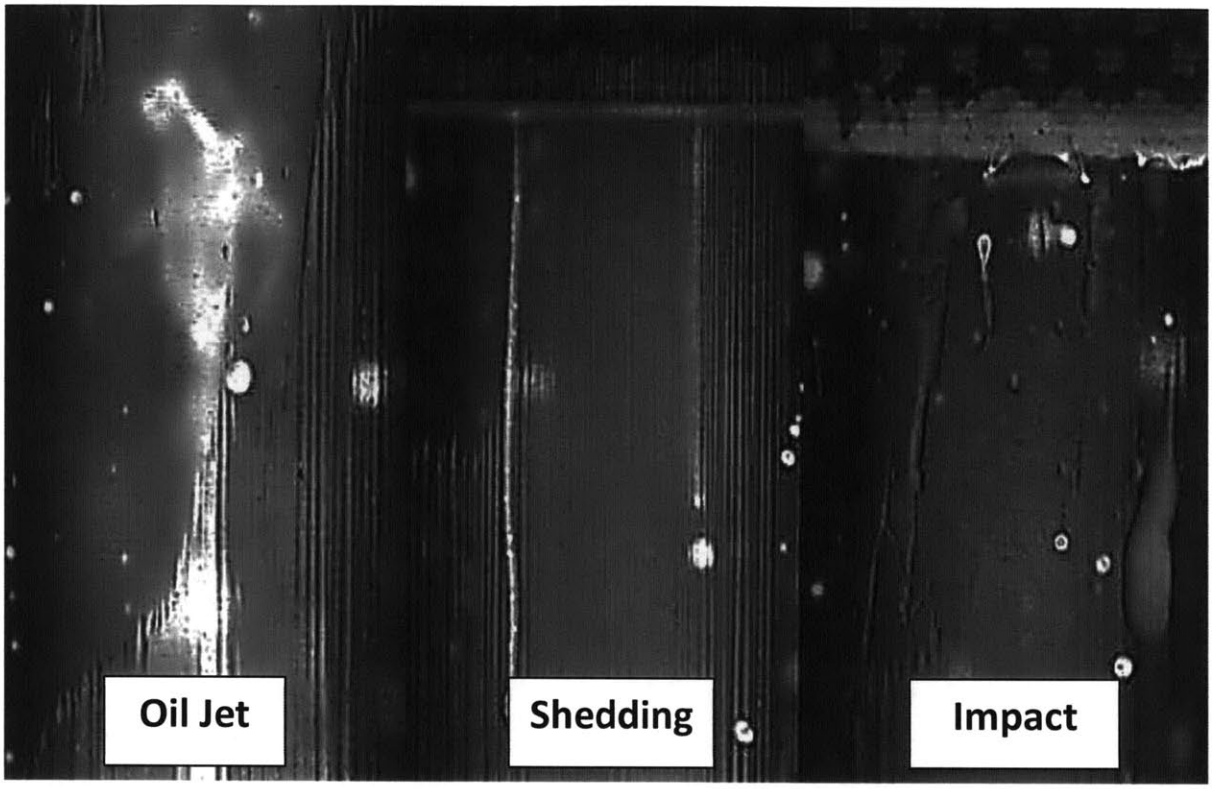

Figure 3-3: Images depicting the flow of events from oil jet to oil droplet shedding to oil droplets crashing into the edge of the skirt. Engine operating at 1,500 RPM and mid-load (~600 mbar)

3.1.2 Mid-Skirt Region

The next phenomenon to be discussed that occurs in the piston skirt region is the streaking/shearing of the oil film due to piston primary motion. This phenomenon is a form of cavitation that occurs at high speeds where these streaks may have the lowest surface energy and thus preferred by the oil [30, 31]. Streaking can occur at any point in the cylinder, previously using the original LIF system streaking was only found during the upstrokes closer to BDC. The logic behind why streaking would occur only toward BDC is that during the end of any downstroke the skirt chamfer will be full with a significant amount of oil. This large volume of oil supplies the skirt-liner interface with enough oil to be sheared by the high speed of the piston during the upstroke. *Figure 3-4* shows some sample images of the streaking of oil films and how it can change based on speed, load, and position. The understanding of streaks is critical due to the fact that seeing if the oil is on the liner or on the skirt is very important. Oil on the skirt will stay with the skirt and continue to lubricate it while oil on the liner is wasted. Streaks are key features that help to determine if oil is on the liner or if it is on the skirt.

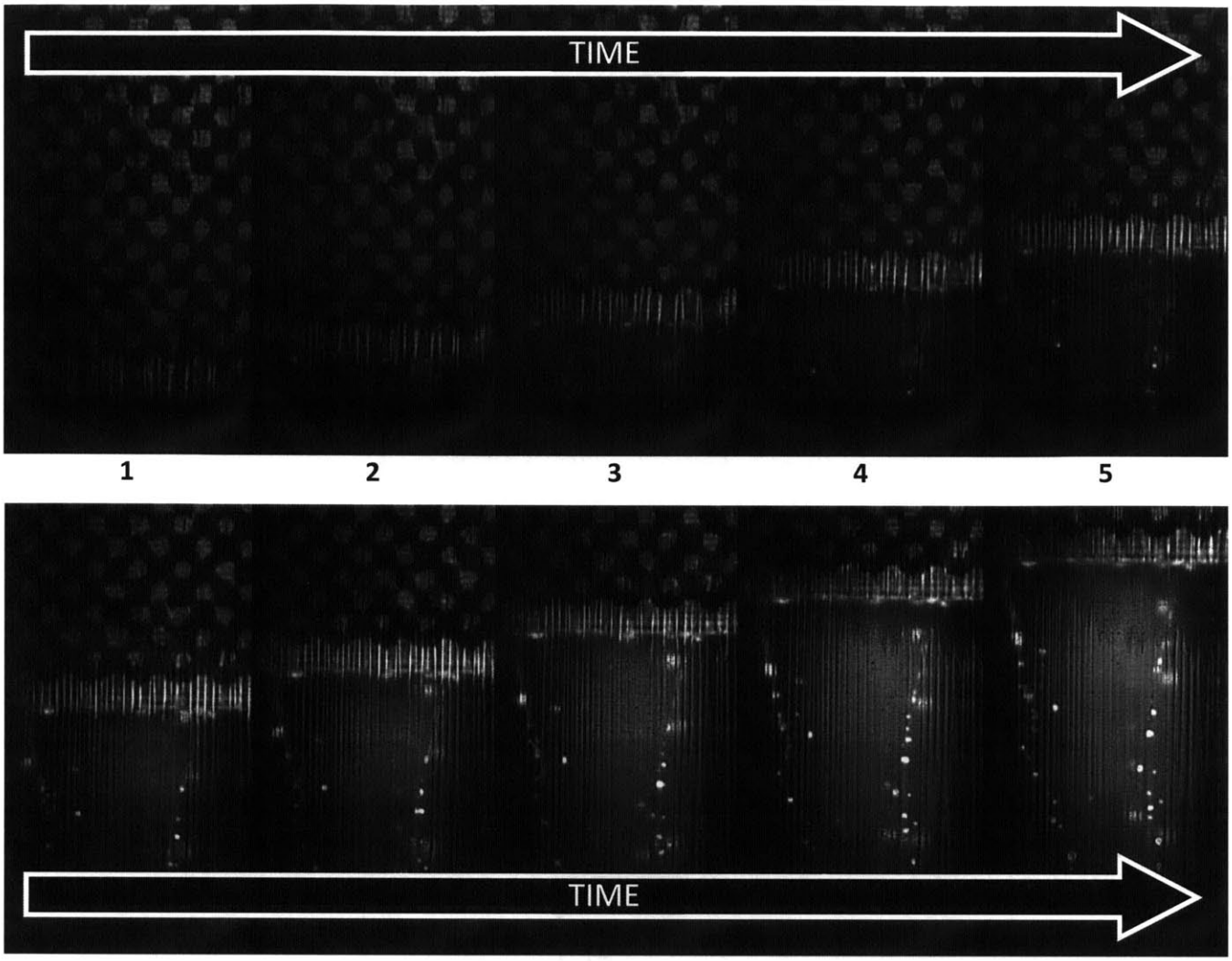

Figure 3-4: A sequence of images showing how streaking develops over time at 2,500 RPM, mid-load, and 72,000 FPS. Streaks can detach from the piston and remain on the liner to be later consumed as shown in the last image. Seeing how these streaks stay on and detach from the piston is critical for modeling.

An excellent opportunity to show off the ability of the high speed LIF system is to attempt to observe the piston "slap" discussed in Chapter 1. This slap, which is a large side force created by combustion occurs in an extremely small amount of time and causes significant influence over the oil film in that short period which can be seen in the diagram in *Figure 3-5*. In *Figure 3-6*, the series of images shows how the piston slap causes the oil film to dissipate very rapidly and studying this behaviour helps validate any models based on piston lubrication. The timing specifically of how the oil film evolves as the piston slams into it is what helps validate these lubrication models.

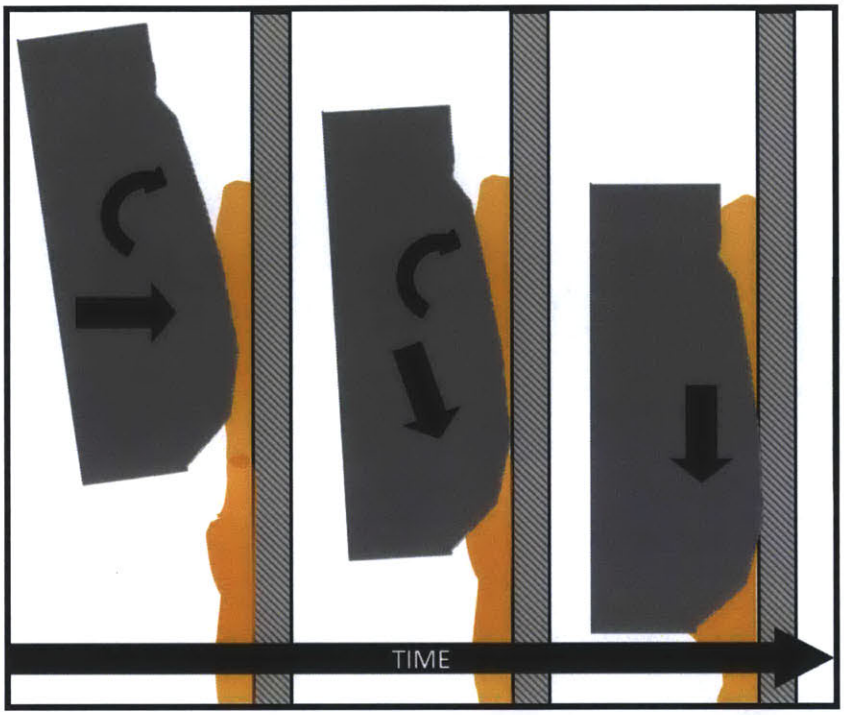

Figure 3-5: A diagram showing how the dynamic piston slap looks in a cross-sectional view.

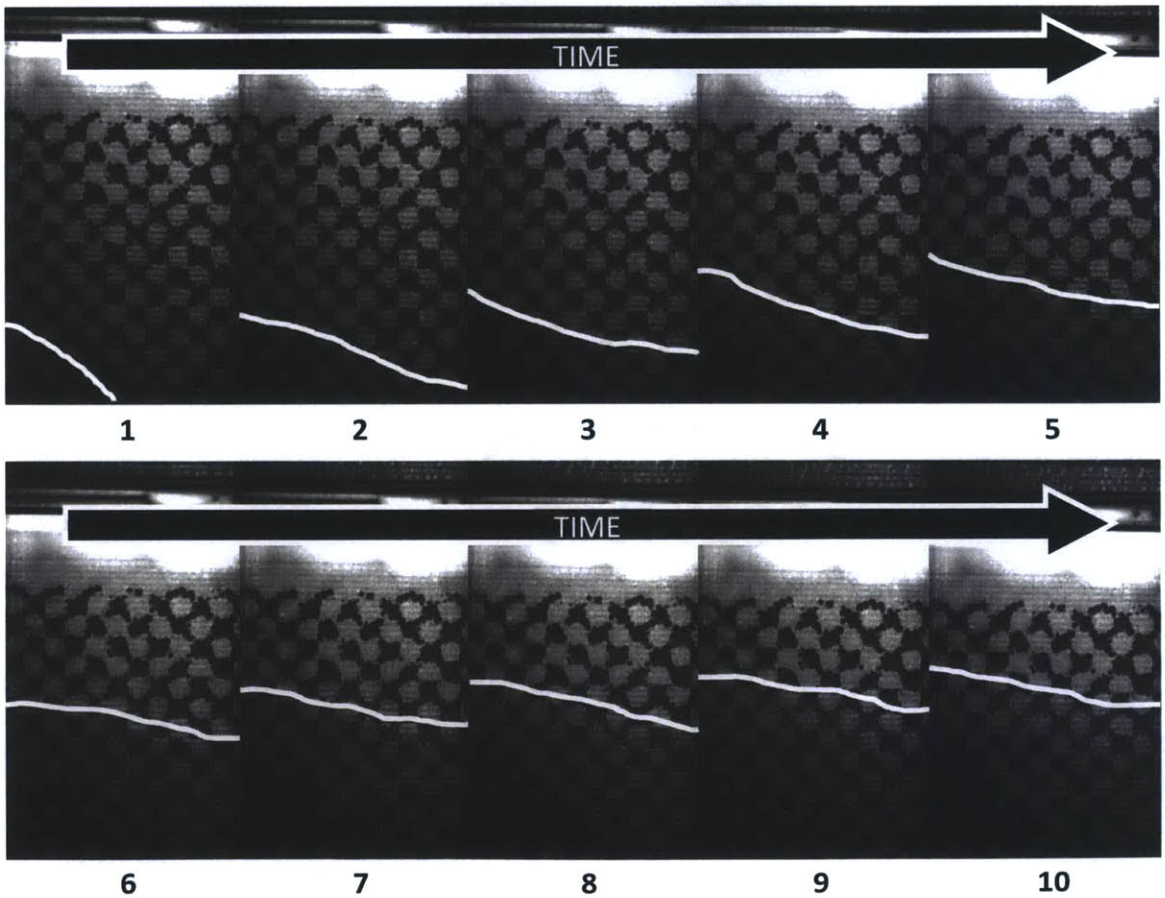

Figure 3-6: A sequence of images showing the rapid piston "slap". Total frames from first image to the last are 90; at 72,000 FPS that is a total time of 1.25 ms. Below the white line indicates contact is being made. (It is quite difficult to see in still images.)

3.1.3 Skirt Chamfer Region

The following oil transport mechanism that will be discussed is the cavitation/separation of the oil film that occurs at much slower speeds than the streaking phenomenon. Slow cavitation of the oil film is a phenomenon that is highly dependent on piston secondary motion. Piston secondary motion as described in Chapter 1 is any motion the piston experiences that is not along the axial direction; lateral motion, piston tilting, etc. An example of secondary motion causing cavitation of the oil film is during the expansion stroke. As combustion occurs, the high pressure causes the piston to slam into the thrust side of the liner which forces the piston skirt to rip itself from the liner on the anti-thrust side which can create intricate patterns shown in *Figure 3-7.* On the thrust side as combustion occurs the oil film undergoes an extremely high pressure slam causing oil to escape from the skirt liner interface. This can cause oil to escape the skirt-liner interface althogether by exiting through the bottom of the skirt or it can accumulate in the skirt chamfer.

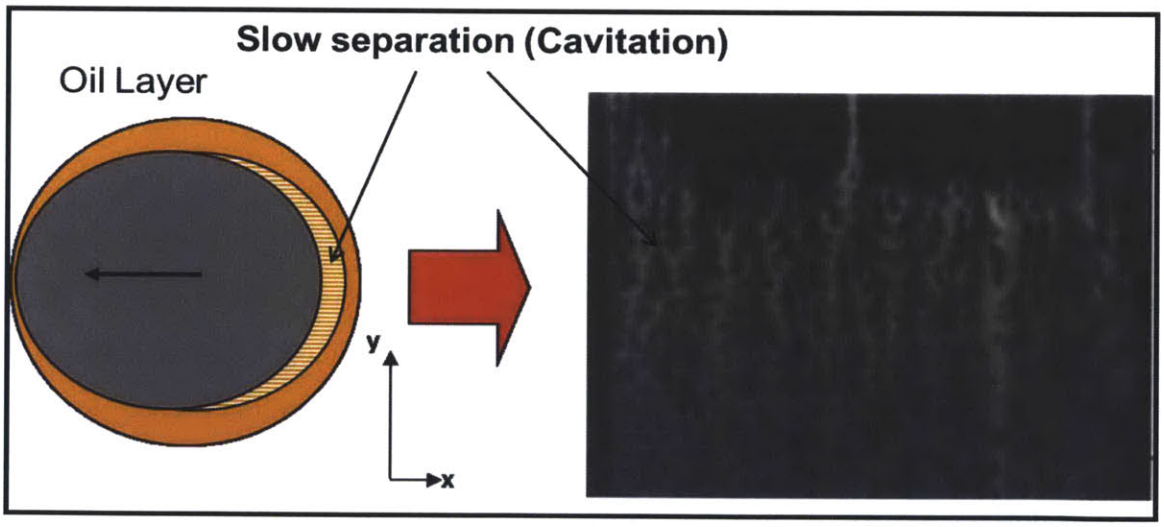

Figure 3-7: Diagram and example image showing the cavitation phenomenon. Images provided through old LIF measurements taken by E. Senzer [5]. Reprinted from *Figure 1-7.*

Using the old LIF system never gave a sense of scale on how fast these phenomena can occur. With the high speed LIF, how these patterns are formed can be seen and what time scales are involved can be determined as well. *Figure 3-8* shows what cavitation can look like using the high speed LIF setup.

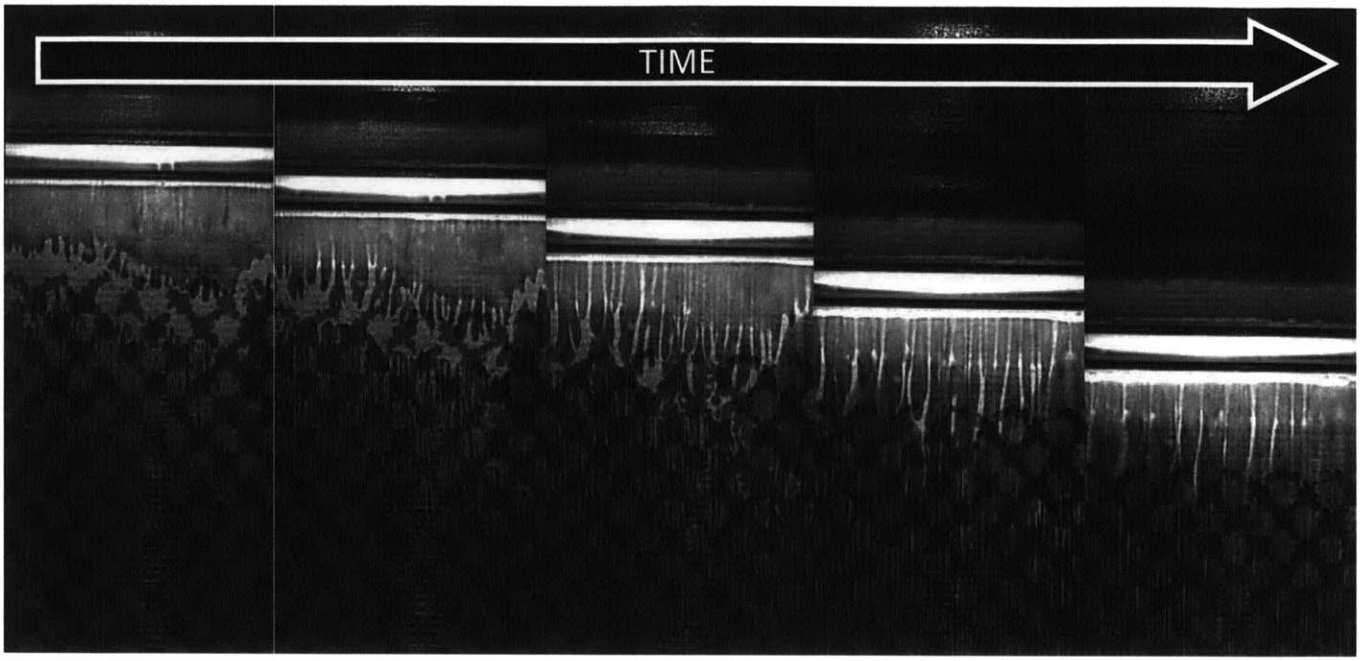

Figure 3-8: A sequence of images showing the evolution of slow-cavitation occuring when piston secondary motion pulls the oil film away from the liner. Taken at 2,500 RPM, mid-load, and 30,000 FPS.

An important understanding of this phenomenon is essential to understanding how the piston skirt itself interacts with the oil film. Seen throughout all figures in this thesis are images of piston skirts with interesting design patterns applied to them. These designs have the possibility to alter the fluid dynamics of the oil and possibly sustain those full oil films. If the oil film begins to shear or cavitate then friction begins to increase to due there being less fluid to build up hydrodynamic pressure to push apart the piston and the liner. A study on different piston skirt designs as well as modeling oil transport mechanisms and piston secondary motion was conducted by P. Totaro [29]. After examining the images in *Figure 3-8*, one can see that as time increases the oil film becomes much less stable as in it becomes a partial film. With partial films the oil can be on the liner and the skirt in a number of different ways and where it ends up can be a large factor when modeling these phenomena. If the oil stays on the skirt it can be used for lubrication later on in the cycle, but if it is on the liner it can end up not being used and possibly even wasted.

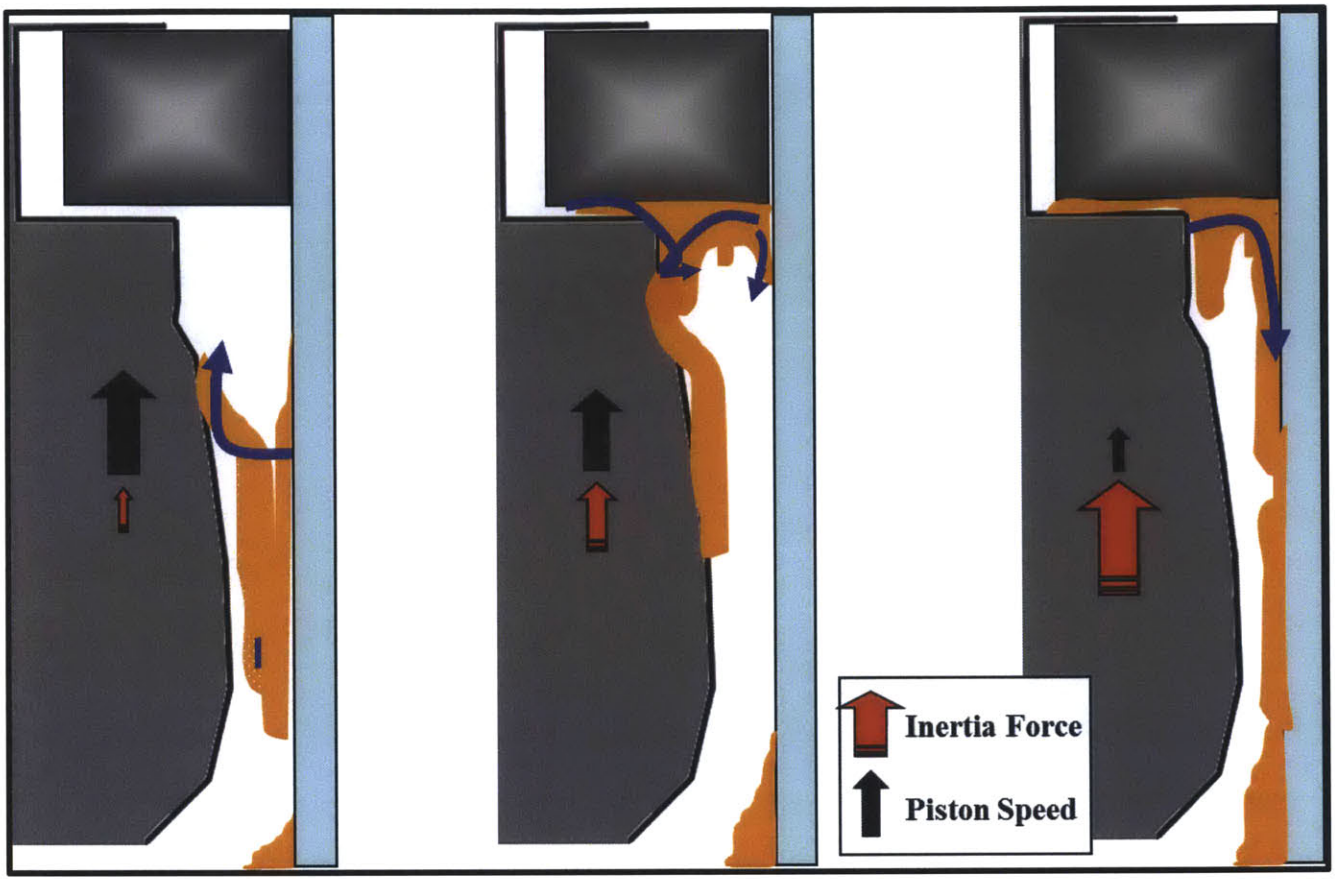

Figure 3-9: Diagram showing the mechanism of how accumulated oil in the skirt chamfer can bridge between the piston skirt and the liner [5].

The final phenomenon that occurs in the piston skirt region to be discussed will be the bridging effect. This effect will also be discussed in the coming section as it occurs in the ring pack region as well. The bridging effect of the oil film is a phenomenon seen quite frequently using the old LIF system. As discussed in Chapter 1, bridging is a phenomenon in which the accumulated oil film can transfer between the skirt and liner when the inertia of said oil film is in the opposite direction of the inertia of the piston. As the piston accelerates from either TDC or BDC, it begins to impart its own inertia to the oil film and drags the film with it. Once the piston reaches mid-stroke it begins to decelerate which causes the oil film to move relative to the piston allowing the oil to crash into any features of the piston that are in its way. In the skirt region oil will crash into the skirt chamfer and begin to accumulate. Bridging in the skirt region occurs earlier than that of bridging in the ring pack due to the chamfer having a substantially larger volume of oil that moves quite chaotically due to the larger clearance between the skirt and the liner. The bridging process is shown by the diagrams in *Figure 3-9.*

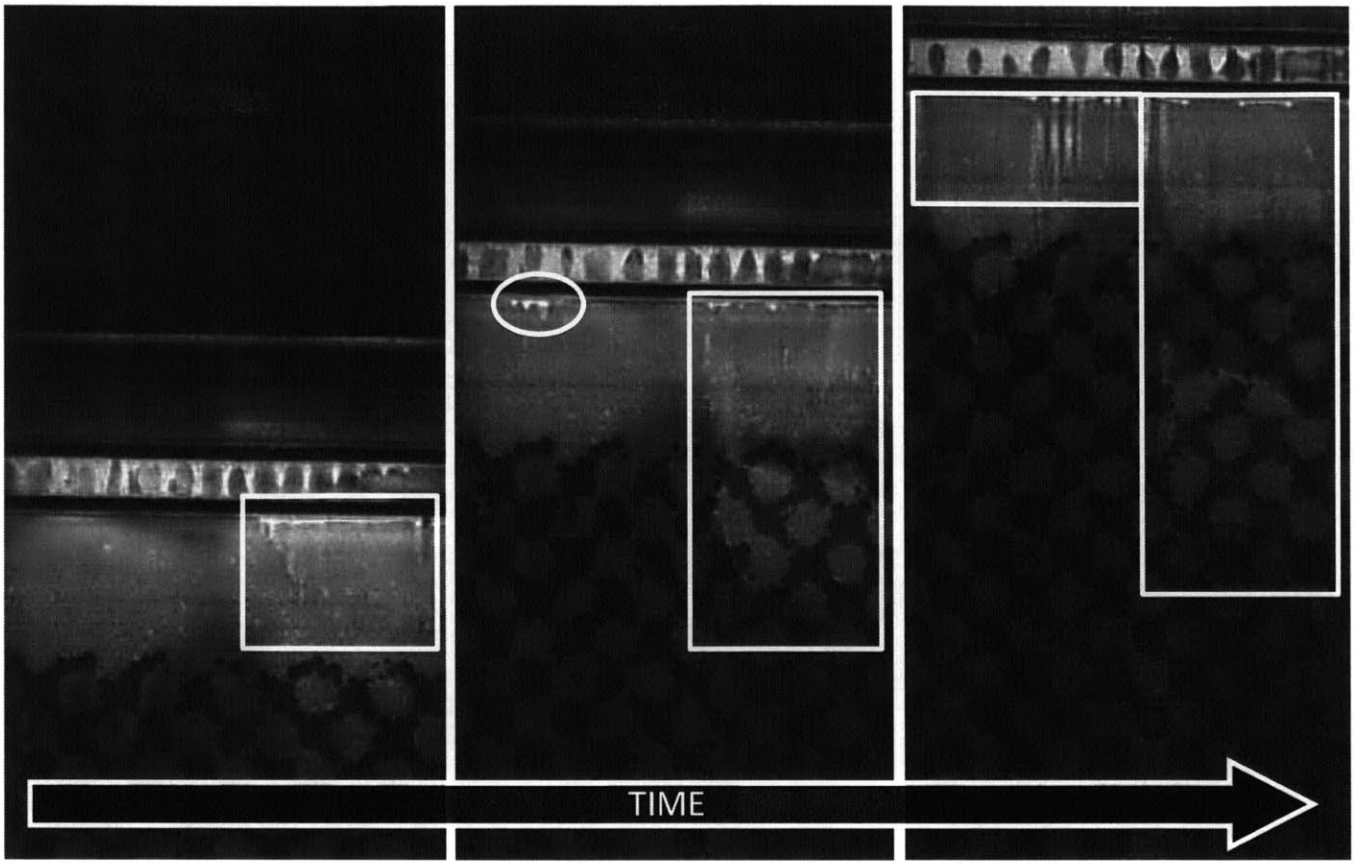

Figure 3-10: Images taken from the high speed LIF videos showing all the different possible ways bridging can occur in a single stroke. Images taken at 1,500 RPM, mid-load (~600 mbar) conditions during compression stroke.

Through the use of the high speed LIF system, one can finally see bridging occur in real-time. In *Figure 3-10*, the process for how bridging occurs can be seen. These images can give a help determine if oil scraped by the OCR reenters the skirt-liner interface to aid in lubrication. The more oil means the more likely it is to bridge, thus in the first image, on the right side of the piston, there may be a relatively larger patch of oil which is starting the bridging process. As time moves forward in each image there is more bridging developing, but only in smaller strands of oil instead of large patches. This may be due to clearance variations, bore distortion, oil distribution, or perhaps piston geometry, it is still unknown, but using high speed imaging will help develop an understanding. As the stroke continues the high speed setup shows how the oil, that has been bridged, is scraped by the oil control ring which may very well play a large part in oil consumption. With the ever growing need to reduce oil consumption, using the high speed LIF system can truly allow an understanding of this bridging effect to be developed. Not only

does the high speed system allow for unprecedented access to this phenomenon, but it can give substantial detail into how oil behaves inside the skirt chamfer.

3.2 Ring Pack Oil Mechanisms

As discussed earlier the ring pack region can be a significant contributor to the overall friction of an IC engine, thus creating significant interest in understanding the oil flow mechanisms of the ring pack. Previous studies of the ring pack using the old LIF system provided a substantial amount of insight into ring pack oil dynamics such as the numerous ways that oil can maneuver around the ring to reach the lands above it. Ring gap dynamics have also previously been studied, but with the high speed LIF system new phenomena have been observed as well as old phenomena.

First to be discussed will be one of the previously studied phenomenon; the bridging effect. Previously, bridging was a significant phenomenon that predominantly occurred in the piston skirt region due to the fact that there was an overabundance of oil in the skirt-liner interface allowing for bridging to occur fairly easily. While bridging was shown to occur in the lands using the old LIF technique, it was rarely shown to occur in the OCR. In the previous figure, *Figure 3-10*, and in *Figure 3-11*, the OCR is visibly experiencing a significant amount of bridging which has never been seen in the original LIF setup.

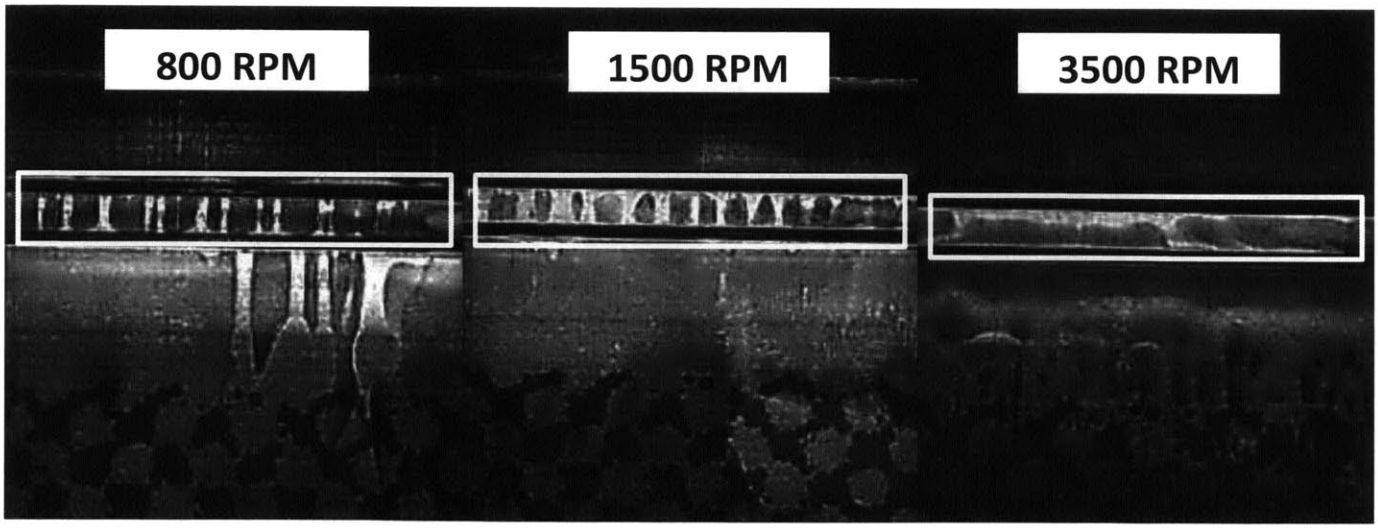

Figure 3-11: Images taken from the high speed LIF videos showing OCR bridging at various engine speeds. Approximate load (~600 mbar).

This does not come as a significant surprise due to the fact that the job of the OCR is to accept and distribute large amounts of oil from the skirt-liner interface. This region is the most chaotic when it comes to oil fluid dynamics in the piston-liner interface.

While examining the images provided in *Figure 3-11*, one can see that engine speed can affect bridging quite significantly. As the engine speed increases, the bridging seems to occur in a more broad fashion where as at lower engine speeds, bridging occurs in more discrete locations, most likely in locations of higher oil concentrations. When the engine is operating at higher speeds, it also is imparting much more of its energy into the oil film allowing more of it to bridge during either TDC or BDC. Bridging in the ring pack occurs significantly in the lands and is a large cause of oil consumption.

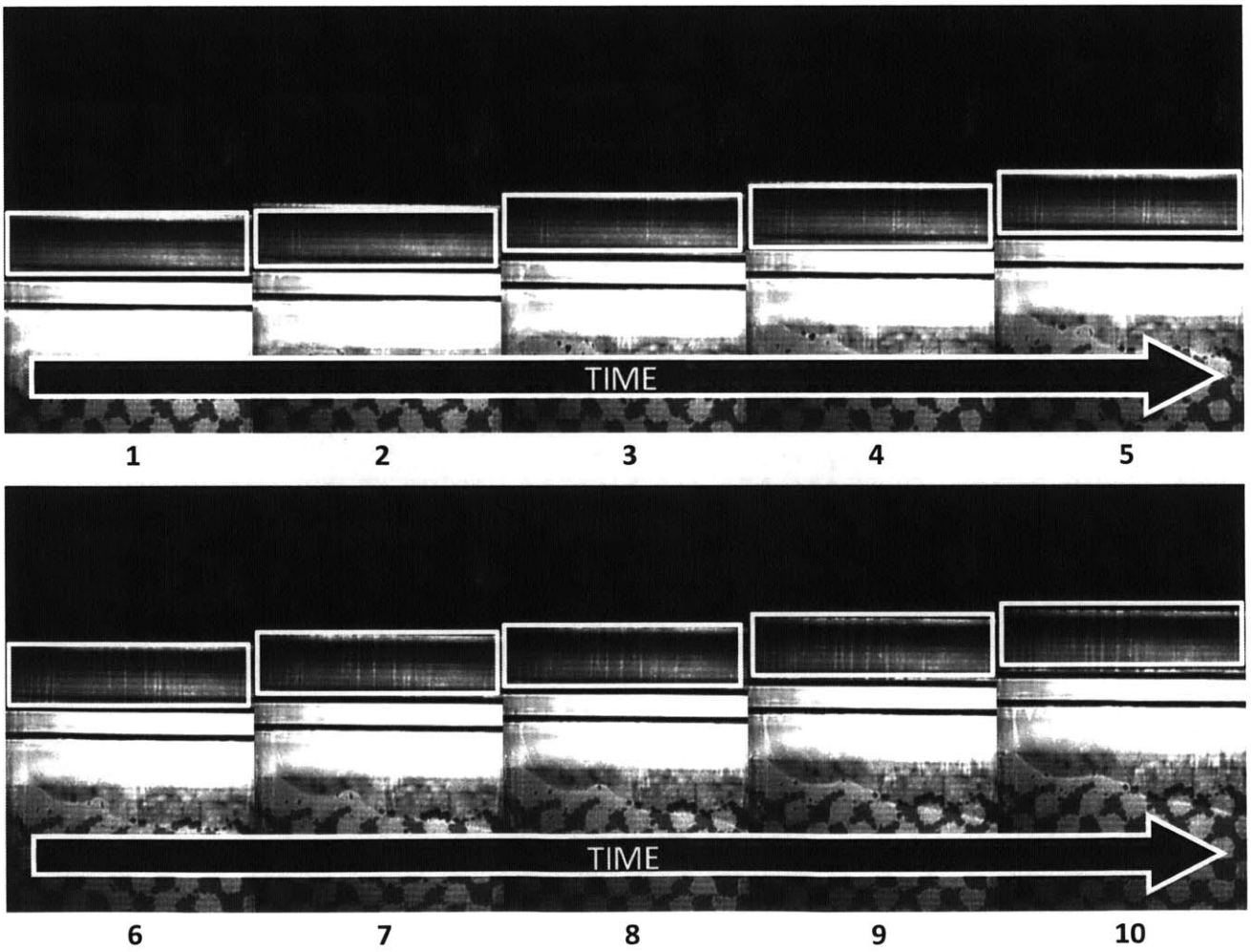

Figure 3-12: A sequence of images showing the thinner ring pack bridging which occurs in the piston lands. Taken at 1,500 RPM, mid-load, and at 72,000 FPS.

Bridging that occurs at TDC has a more detrimental effect on oil consumption because of the fact that lower pressures during exhaust and intake do not allow the top ring to conform to the liner, letting oil pass into the combustion chamber. If oil is left solely on the liner, as is the case with bridging, it becomes harder to scrape using the second ring due to number of reasons, some of which are bore distortion and ring twisting. Bridging in the lands of the ring pack has been documented before [5, 21], but the images only captured large amounts of oil bridging. This may have been due to the lower average power of the original laser. In the high speed LIF system, much finer oil bridging patterns can be seen as such in *Figure 3-12*. Using the high speed camera makes finding the small intricate features significantly easier as well as observing how they change with various engine parameters.

When studying the ring pack in any IC engine, the ring gap is always a prominent area of focus. While building an understanding about oil consumption is no different; the ring gap is an important feature that deserves to be studied constantly. Previous operators of this system, Przesmitzki and Senzer [21, 5] performed a multitude of experiments where the ring gap would be pinned in a manner such that it could be viewed through the optical access for the LIF system. The previous studies on ring gaps used methods to pin the gap to a single location to observe it over many different cycles, in this study no rings were pinned. The biggest reason for why the ring gap is such a large part of research is because it is the largest contributer to oil consumption solely because it is a large passageway for oil to flow through compared to the micron level clearances surrounding the piston otherwise. The ring gap itself does not just have oil flowing through it, combustion gases also flow through and these gases are actually used in an attempt to push back any oil that may be flowing up through the gaps. This makes the ring gap quite the dynamic two-phase region of the ring pack, requiring high speed imaging to analyze it. When using the high speed LIF system, interesting patterns can be seen when the gap comes into view. These patterns created by the combustion gases flowing through the ring gap, shown in *Figure 3-13*, can vary substantially based on speed and load of the engine. Common experiments that are run in the automotive industry are to change the tension on rings to see if friction can be reduced. The effects of ring tension can be seen with the high speed LIF system; changes in tension should relate to changes in flow through the ring gap.

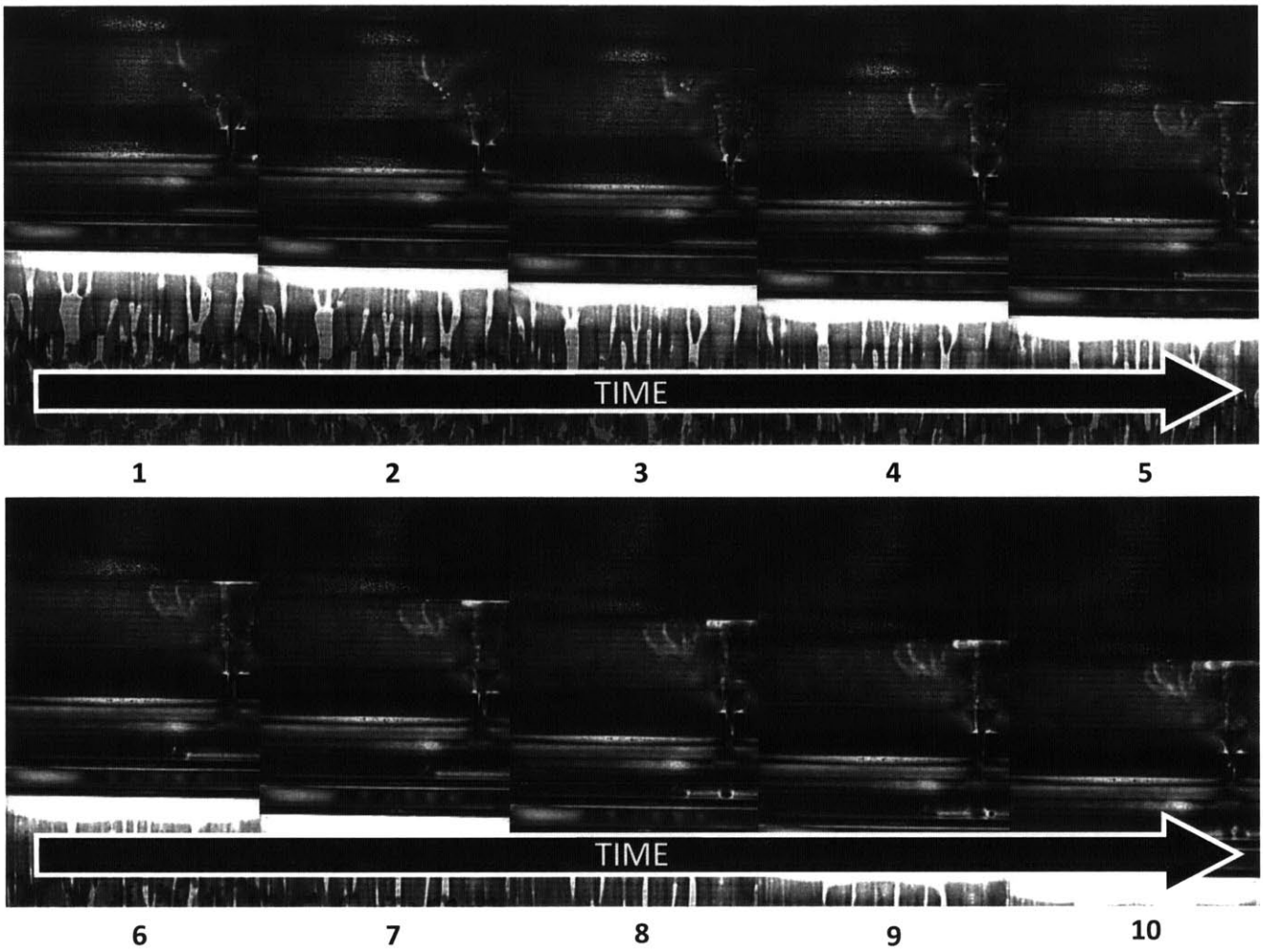

Figure 3-13: A sequence of images showing how oil flows around the ring gap during the intake stroke. Taken at 800 RPM, mid-load, and at 30,000 FPS.

In *Figure 3-13*, the ring gap can be seen affecting oil flow by allowing oil to pass right through the ring and infiltrate the crown land, most likely ending up in the combustion chamber to be consumed. Any oil that reaches the top ring gap is essentially wasted oil; minimizing this should be the best way to reduce oil consumption. It seems that, even at this micron-level scale, it is still very much is a two-dimensional fluid dynamics problem. The oil flow is still a pressure driven flow through a fixed channel and behaves as such with predictable patterns that follow.

The final item to be discussed in regards to oil transport mechanisms that occur in the ring pack region is the presence of oil droplets shedding from the crown land. This phenomenon is the most uncommon of any previously discussed phenomena. Only one video out of the hundreds recorded showed this phenomenon.

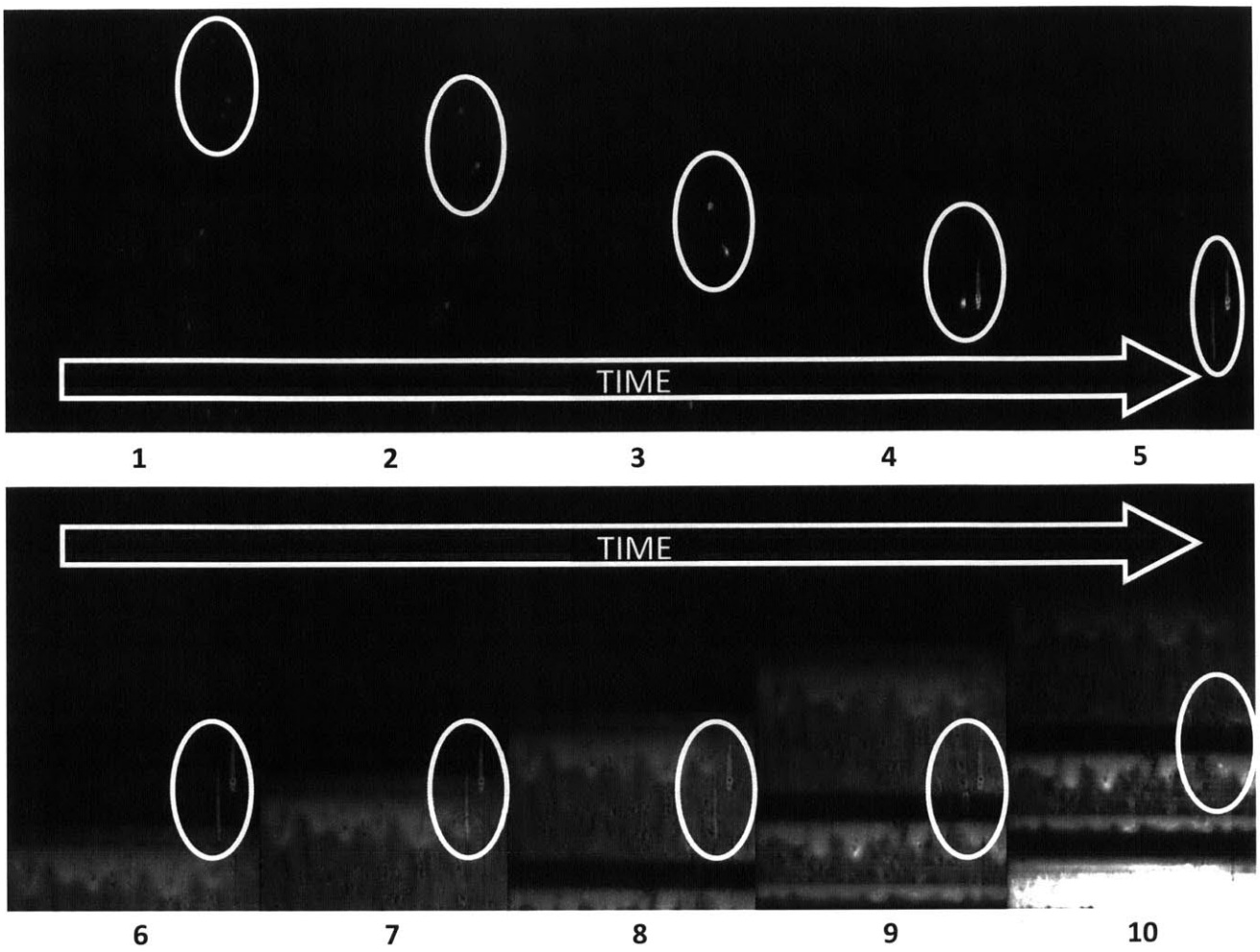

Figure 3-14: A sequence of images showing droplets that have been thrown into the combustion chamber as well as a sequence where the piston scrapes the droplets off the liner. Taken at 3,500 RPM, mid-load, and 72,000 FPS.

It is very possible that it may be a simple outlier in our system, but it is worth the mention. During a motored operation of the engine, droplets can be seen following the piston as it continues its downstroke, seen in *Figure 3-14*. No one denies the fact that oil gets into the combustion chamber, but to be in amounts large enough for the LIF system to view it and in the form of droplets and not just adhering to the liner is somewhat unexpected. One interesting detail about this phenomenon is that it can only be seen in the motored case, no droplets have ever been seen in the fired case. Not to say that droplets do not occur in the fired case, but perhaps too small for the LIF system to capture or maybe the process of combustion affects this phenomenon in some way. It is not a rare occurrence in the video either; consistently almost every downstroke provides images of these droplets falling. The video was taken at 72,000 FPS and the engine was

operating at 3,500 RPM at mid-load (~600 mbar). This may even show possible ways as to how the oil becomes diluted with fuel. If the same droplet shedding phenomenon from the skirt is happening here the droplets may make their way back into the piston-liner interface and possibly into the crank case.

3.3 High Speed Camera Optimization

The optimization of the high speed setup was carried out by performing a number of experiments with various camera settings and optical components including different: camera speeds, shutter speeds, beamsplitters, lenses, filter configurations, diffuser configurations, and lasers. This section should be used to essentially see the process which the author of this thesis went through to attain the most optimal settings for the high speed LIF setup. If anyone were to wish to replicate this setup please use the following components that present the best quality images. In the future the implementation of high speed imaging should be a key component to all automotive diagnostic tools. The value of seeing how such dynamic event occur and evolve over such miniscule timescales is extremely valuable.

3.3.1 Camera Optimization Results

First and one of the most important aspects of the setup, if not the most important element of the setup, is the high speed camera. As discussed previously there were three cameras used in the experiments to create a high speed LIF system. The list of cameras used is as follows: the Phantom V4.6, the Photron Fastcam SA-5, and the Photron Fastcam SA-X2. Images of each of the videos taken by each camera can be found in *Figure 3-15*. Common comparisons of these types of cameras are the speeds at which they run. The Phantom was the oldest model and has since been discontinued and thus had by far the slowest camera frame rates used and was not tested using a laser as the light source, a fiber light source was used instead. The SA-5 and SA-X2 are much more comparable as both could reach speeds of 30,000 FPS at desired resolutions. The SA-X2 being the more advanced model reached speeds of up to 72,000 FPS at the desired resolution and is said to have the most light-sensitive CMOS sensor yet.

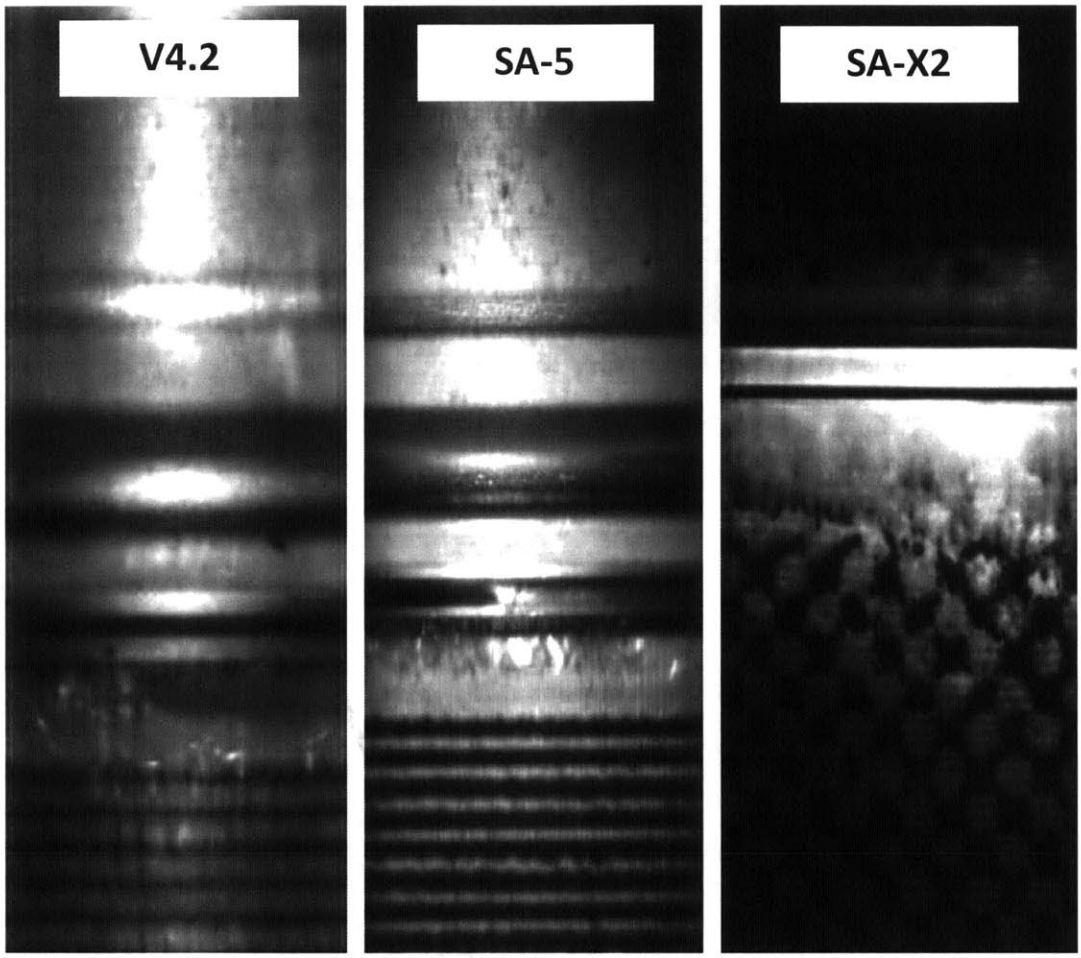

Figure 3-15: Images comparing the three cameras used in this study. Notice the motion blurring that is prevalent in the image captured by the V4.2. Images from V4.2 and SA-5 are continuous white light source whereas the SA-X2 image is using a CW laser.

Looking at the different images in *Figure 3-15*, one can see the differences in the three cameras used in this study. The first high speed camera was only used with a CW laser and therefore motion blur was a significant issue since it cannot reach the frame rates necessary to reduce motion blur. The SA-5 and the SA-X2 both can achieve high speeds without a significant amount of motion blur, although to view higher engine speeds such as 3,500 RPM the SA-X2 is preferred because it is the only one that can achieve fast enough frame rates with a CW laser such that motion blur is insignificant. The maximum speed for the Phantom V4.2, Photron SA-5, and Photron SA-X2 are 3,000 FPS, 30,000 FPS, and 72,000 FPS respectively. The Photron cameras also allow for higher resolutions than the Phantom camera which makes for much better quality videos and improved analysis of oil flow phenomena.

Along the lines of the various frame rates tested with the different cameras, some tests were conducted in changing the shutter speeds of the SA-X2 camera in an attempt to correct for the motion blur problem experienced at higher engine speeds. The default shutter speed for any camera is approximately one divided by the frame rate; for example at 30,000 FPS the shutter speeds is approximately 33 ms. The thinking behind having the shutter speed affect the motion blur problem is that if the camera uses a shorter exposure period (faster shutter speed) then it is capturing less light, but is having images blur together. This is a major reason as to why pulsed lasers are more preferred than any continuous light source. Images from the tests conducted while varying the shutter speeds are found in *Figure 3-16*. As shown in the following figure, the only difference to the images when the shutter speed is changed is the overall brightness and intensity of the image.

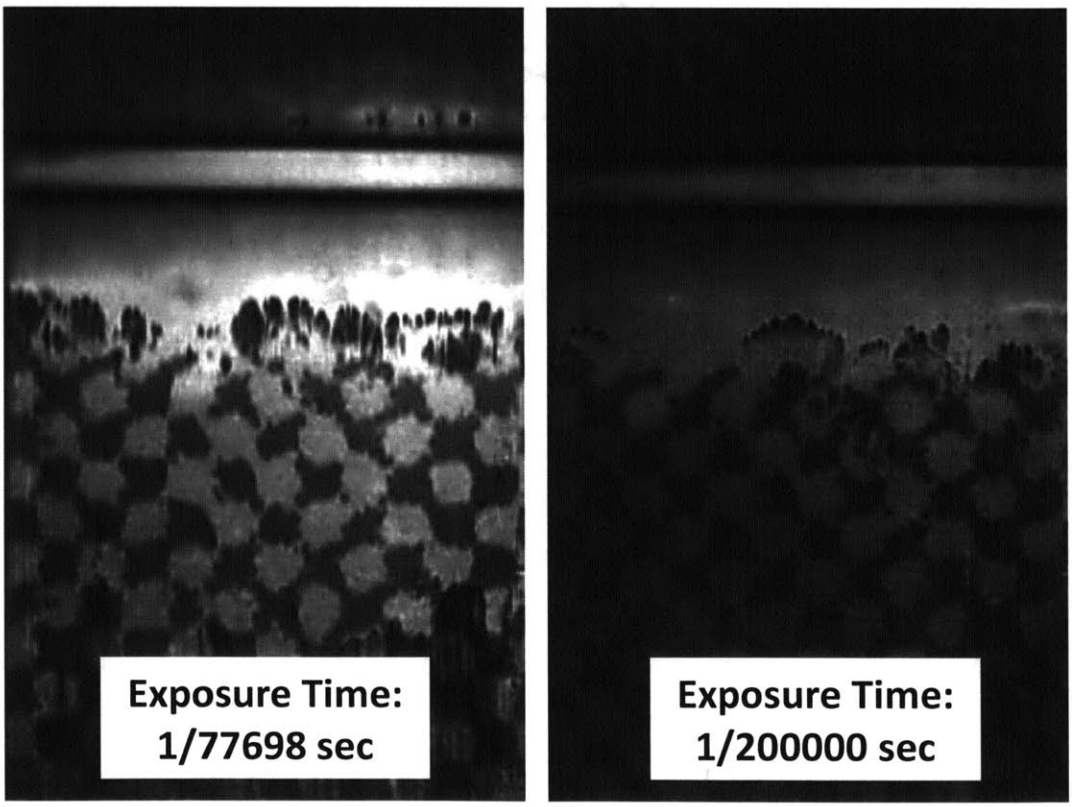

Figure 3-16: Images showing how shutter speed can affect the overall image quality. The shutter speed relates to exposure time where faster shutter speed means shorter exposure time which creates darker images.

This is logical considering that if the shutter speed increases there is a smaller exposure time meaning less time to capture emitted light. The motion blurring effect did not seem to

change significantly, although that is not to say that by increasing the shutter speed motion blur cannot be avoided, the fact is that the increase in shutter speed tested in this thesis was not enough to provide any noticeable effect. If shutter speed were to be taken advantage of it would have to be a significantly high shutter speeds which would then create issues for the illumination for the camera where simply using a pulsed laser circumvents all of this.

3.3.2 Laser Optimization Results

The various cameras used cannot be mentioned without the light sources that they work with and in this study the light sources did vary and may continue to change in the future. In the following paragraph and figure, will be the discussion on how the type and power of a laser affects the quality of the videos and images taken via the high speed LIF system. Initially the laser used in the old setup could not be used in conjunction with any of the new cameras and this was known at the start of this project, for more information on this laser please refer to Chapter 2 Section 2.2.5.3 and Thirouard [20].

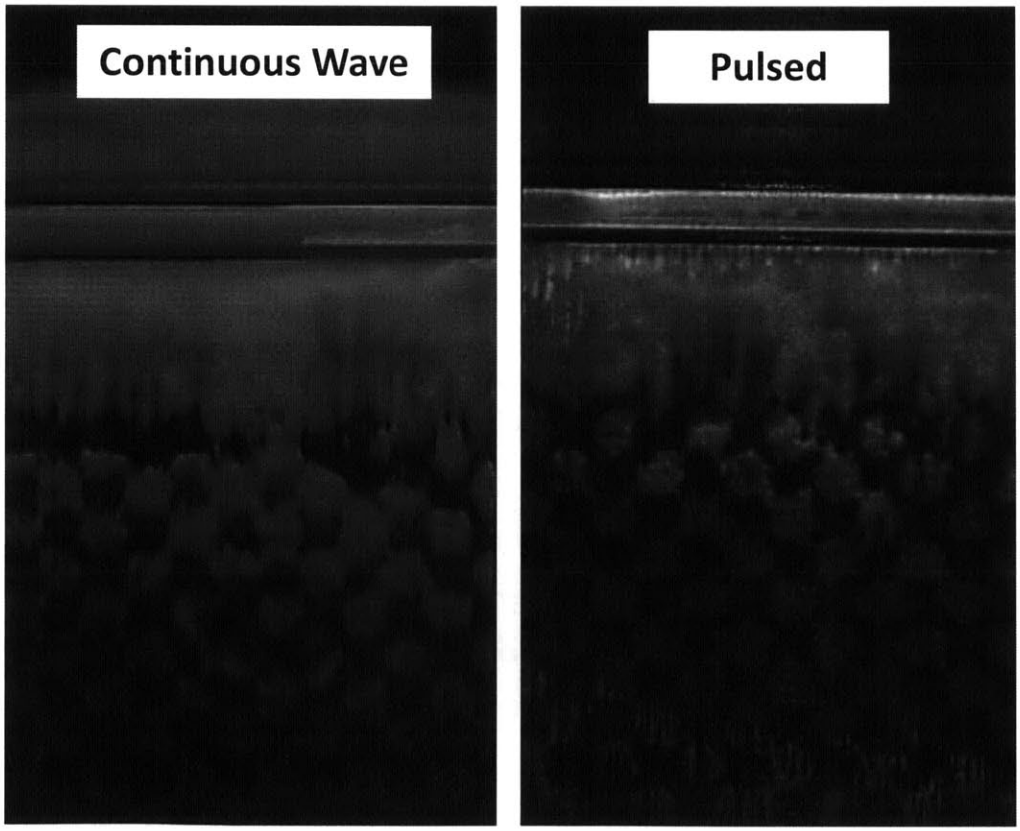

Figure 3-17: Images showing the differences between the CW laser and the pulsed laser that were used in this study. Notice the blurry nature of the CW image whereas the pulsed laser even captured finer details of the piston.

The first laser to be used was the Coherent Verdi G18, which is a Continuous Wave (CW) laser with a maximum power of 18.5 watts. The primary focus of this first laser was to test out to see if a high speed LIF system was even possible. Synchronization between the camera and laser was not a concern initially as it was a proof of concept experiment. Further usage of the CW laser proved that having a continuous light source does have its downsides such as motion blur. *Figure 3-17* contains images showing the differences between the CW laser and the pulsed laser. The lasers themselves do not necessarily have comparable powers; the CW laser was 18.5 W and the pulsed laser was 7 W at a repetition rate of 30 kHz. The intensity of the images is not the key factor to be looked at when observing *Figure 3-17*, what should be noticed is the quality of the image. The image taken using the CW laser is much more blurry than the pulsed one, which would cause errors in any oil film measurements taken.

3.3.3 Optical Components Optimization Results

To keep up with the new lasers and cameras being tested, all previous optics needed to be upgraded and even new components were tested to see if there was a role they could play. The various components that were changed from the original setup were: beam expanders, beamsplitters, lenses, collimators, polarizers, filters, and diffusers. Only a certain few optical components were tested in attempt to optimize the quality of the images captured; these few were beamsplitters, lenses, filters, and diffusers. To see other information on the other optical components please refer back to Section 2.2.6.3.

One of the biggest changes in terms of the optics from the original setup is that instead of using the pre-existing cube beamsplitter, the thought of using a dichroic beamsplitter instead would increase the quality of the image, which means that it may increase the intensity of the images. The problem with the cube beamsplitter is that it transmits 50% and reflects 50% of all incoming light. This reduces the emission intensity significantly and due to the high demand for light while using any high speed camera this causes the images to be very dull if not completely black. Thirouard [20] did think to use a dichroic beamsplitter, but came to the conclusion that the dichroic beamsplitter would cause ghost images. This may have been a problem at the time, but now dichroic beamsplitters have excellent transmission percentages and very steep transition between reflection and transmission allowing for very precise selection of wavelengths to be omitted. The dichroic beamsplitter can be used in place of the cube beamsplitter and the filter,

but complications, to be discussed later, arose where the filter is still necessary. The largest change in image quality when switching to the dichroic beamsplitter was the intensity of the image itself; shown in *Figure 3-18*.

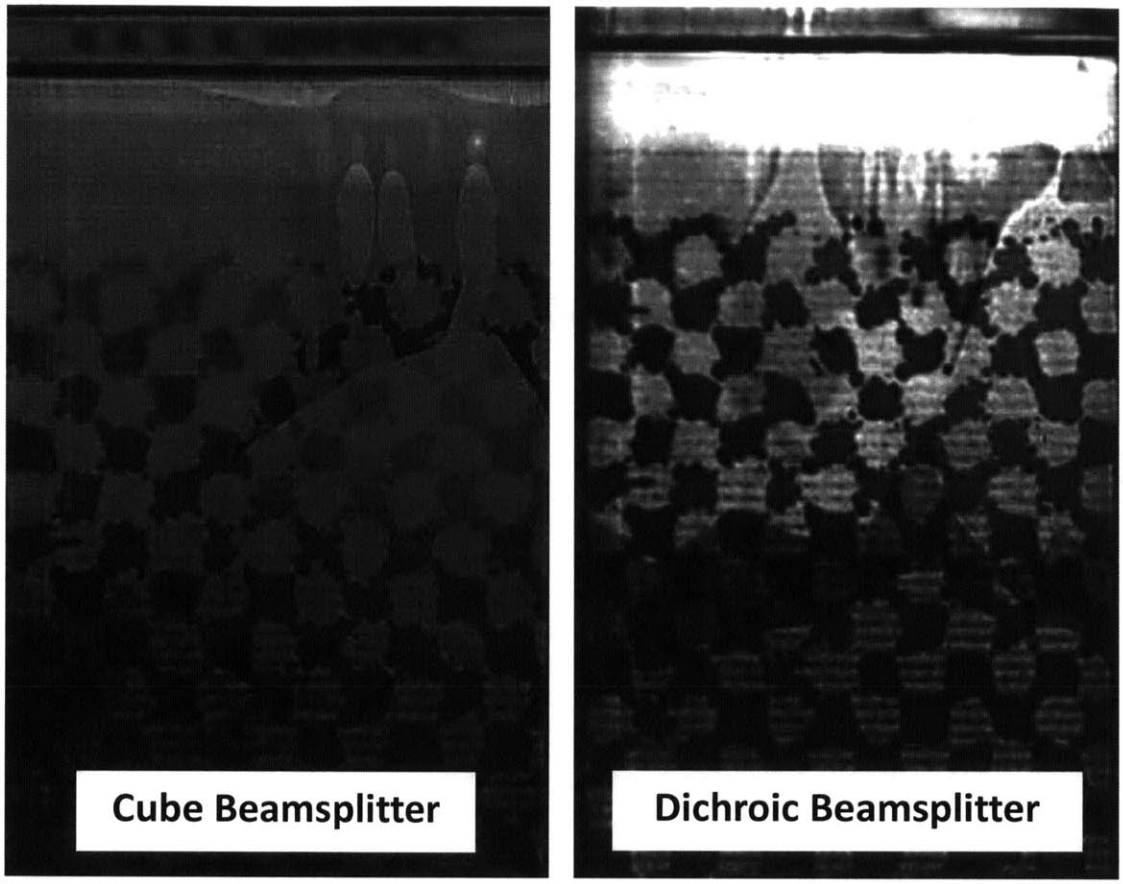

Figure 3-18: Images showing how a dichroic beamsplitter can increase the intensity of an image compared to a cube beamsplitter.

The next optimization made for the high speed LIF system was the choice of which lens would give the best quality of images. Now this selection is still an area of the project that needs to be further be explored. There are too many variables that may change over the course of the project; such as positioning of the camera or what section of the optical access needs to be observed. Currently the optical window is roughly split into three sections, TDC, mid-stroke, and BDC, but one day someone may want to view the whole window which may require a different lens with different parameters.

In this study the lens selection was similar to the setup run by Thirouard [20] and thus only involved a total of three different lenses. One was the original lens used in the LIF setup

and the next two; one was purchased and one was borrowed from a professor. All of them had similar focal lengths, the original was 90 mm while the other two were 105 mm, and all of them had f/#'s of 2.8. In *Figure 3-19*, each image was taken from each lens and it is quite clear that the original lens may have worn considerably due to its severe dull image quality. The other two images are quite similar although the borrowed lens is brighter than the purchased one, which was quite interesting considering it was purchased in an attempt to replace the borrowed lens. Lenses are still an aspect that needs to be explored more if any other requirements are needed of this system.

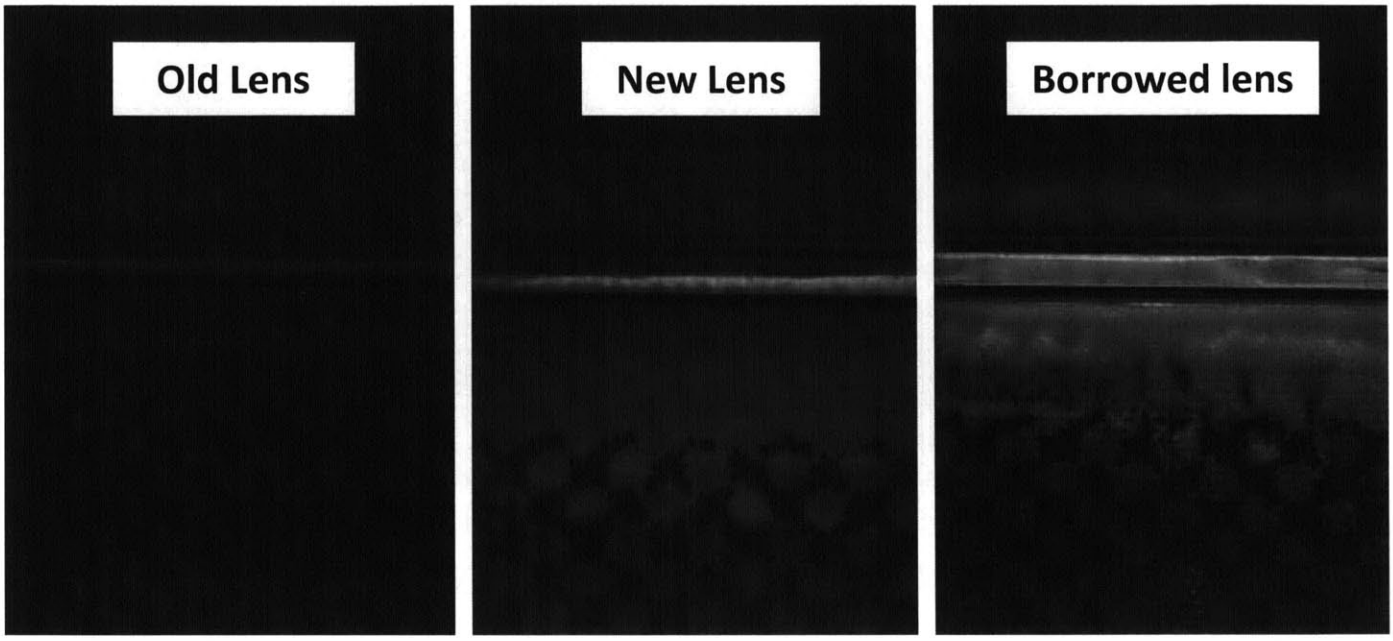

Figure 3-19: Images showing the differences between the three lenses used in this setup. All lense had f/#'s of 2.8, the old lens was 90 mm and the new and borrowed lenses were 105 mm.

Along the lines of lenses was the area of filter where it is crucial that the laser light itself is not captured by the camera, otherwise it will skew the oil film measurements since there is no way for the camera to distinguish between wavelengths of light. Initial planning included the use of the original filter selected by Thirouard, but once the first tests were conducted with the high speed cameras, no images were being captured. The images were all black barely any light was coming through the filter. This was initially mentioned in Section 2.2.6.3 where the filter was in the minimum of emission intensity of each of the dyes and was only visible in the original setup because of the high peak power of the laser. Once the laser was replaced with the CW one, it was not powerful enough to pass through the band-pass filter originally selected. The new filter to

replace the old one was a long-pass filter that has a 50% transmission rating at 550 nm to capture both emission peaks. This will increase the temperature sensitivity of the results, but increase the amount of intensity viewed, which is necessary for the high speed camera. *Figure 3-20* shows not the difference of filters, but what happens when the filter is not used. Initial thoughts were that the dichroic beamsplitter would be enough, but what looks to be thin film interference would be captured in the images. The long-pass filter does create a much cleaner image that can be post-processed much easier.

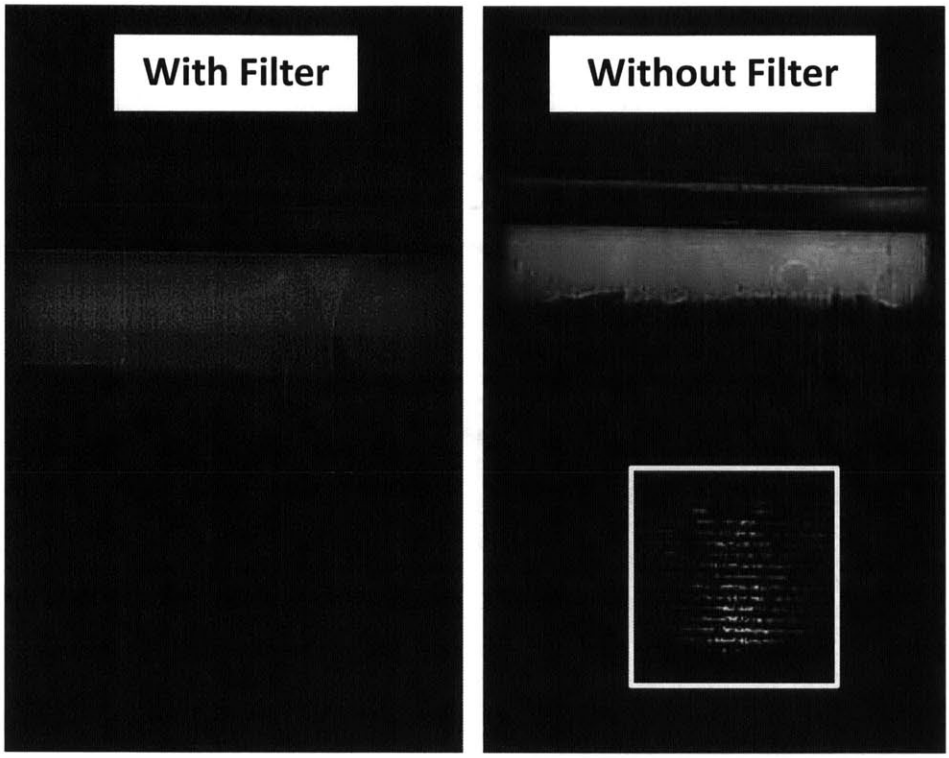

Figure 3-20: Images showing the thin film interference that can occur when the image is not filtered. Focus on the brighter ridges in the image on the right, the dullness of the left image is not significant.

Similar to the experiments with and without the filter, a diffuser was used in some cases to try and create a smoother distribution rather than the normal Gaussian distribution of a laser. The beam actually is slightly less Gaussian once it hits the optical window due to its divergence, but even so in some videos it is possible to see the intensity difference caused by the uneven distribution of light. The diffuser used is an engineered diffuser manufactured by ThorLabs Inc. and is designed to create a uniform square distribution with a 20° divergence angle, a plot provided by the manufacturer of the transmitted intensity can be found in *Figure 3-21* along with

the images comparing the difference when a diffuser is used and when it is not. In this setup the diffuser seems to only dim the images quite substantially with very little gain, which may suggest that the portion of the laser beam that actually contacts the optical window may be closer to a uniform distribution than once thought. The images created by the diffuser appear grainy as well thus creating much more noise any oil film calculations. Whether or not the diffuser has any benefit to the high speed LIF system has yet to be seen.

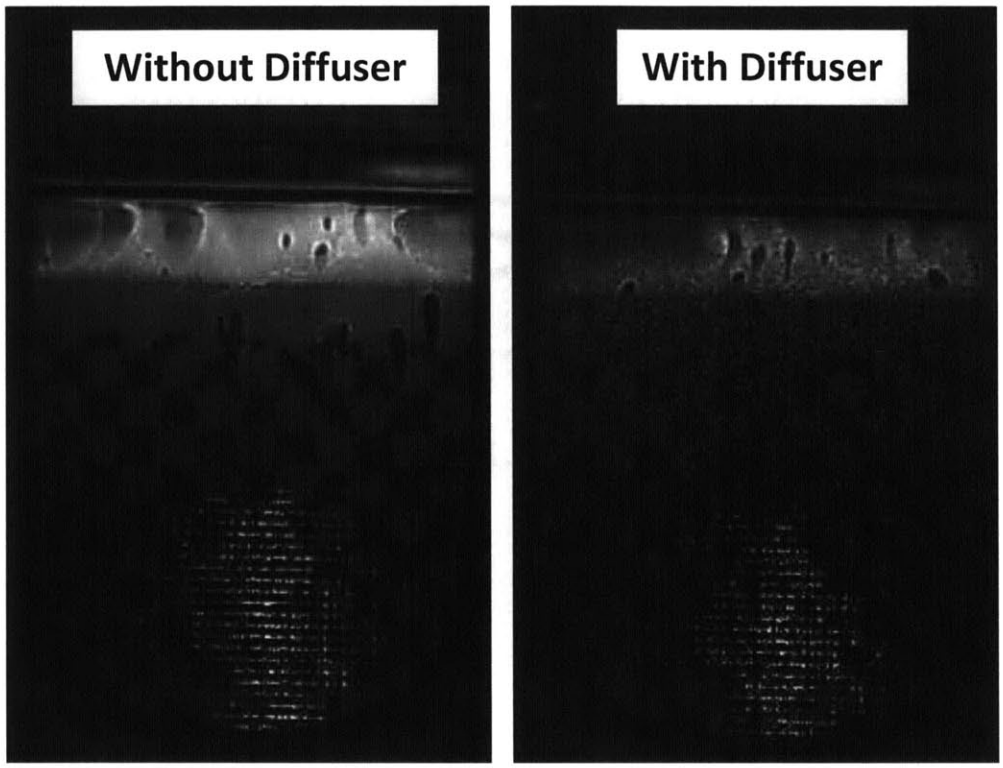

Figure 3-21: Images showing the effects of using a diffuser on the laser beam. The diffused creates a more uniform distribution, but significantly dulls the image and makes the image appear grainy.

Chapter 4: Conclusions and Future Studies

The initial purpose of this study was to integrate a high speed camera into an Internal Combustion (IC) engine being used to study oil transport mechanisms via Laser Induced Fluorescence (LIF). Original operation of the LIF system provided significant data on oil transport behavior that was previously only theory and brought a consensus on topics that were up for debate. Adding the capability of high speed imaging was meant to build upon that developed understanding to hopefully bring new knowledge to the field in attempts to reduce oil consumption and increase fuel economy. These are leading factors in the world of automotive engineering, with the government creating stringent regulations on emissions and consumers wanting more fuel economy due to rising gas prices. Lubrication is an underlying theme for both of these issues and using the high speed LIF system as a diagnostic tool may very well be the key to making those necessary leaps in engine performance.

A high speed LIF system has never been developed and documented prior to the writing of this thesis and it has been a resounding success to confirm that merging high speed imaging with the original LIF system is possible and can provide a wealth of knowledge relevant to the lubrication field. The high speed LIF system has the ability to view oil film transport mechanisms at frame rates of up to 72,000 FPS which translates to the ability to capture a maximum of 15 frames per crank angle at 800 RPM and a minimum of 3.43 frames per crank angle at 3,500 RPM. This is an unprecedented level of resolution when viewing the internal workings of an IC engine. Not only does the system have a high temporal resolution, but it also has a better image resolution due to the improved camera sensor allowing for more spatial information to be observed as well. The camera also had a high intensity resolution due to it being able to record at a bit-depth of 16 bits. This allows the range of intensity to be 0 to 65,536, which seems to correlate well with the range of oil film thickness in the piston-liner interface. Oil films can range from as large as 500 microns in the skirt chamfer to as low as approximately zero microns when there is solid to solid contact between the skirt and the liner. This allows for a resolution of roughly 131 arbitrary intensity units per micron when using the linear approximation of Equation 2.17, further tests will be conducted, however, to validate the linear approximation at 500 microns.

4.1 Oil Transport Mechanisms in an IC Engine

Early use of the system promptly gained traction with its ability to observe many different oil transport mechanisms from new perspectives, allowing for new theories to be developed about the behavior of oil films in an IC engine. As an example, prior to this study not much was understood about how the oil that was released from the primary and secondary jets was contributing to the piston-liner interface. Many believed that only oil that hit the liner was contributing to this control volume, but the high speed LIF system was able to show how droplets of oil on the backside of the piston produced by the primary and secondary jets can shed off the skirt with the same speed as the piston and enter the skirt-liner interface further into the cycle. This understanding allows people to speculate about whether or not these droplets may be contributing to oil consumption and if so what possible engineering modifications can be made in order to reduce the impact of these droplets.

Knowing the inputs and outputs of this oil film control volume is only one part of the equation, knowledge of the how the oil film behavior under certain conditions is absolutely necessary as well. This study was working toward enhancing and creating a much more robust piston secondary motion and skirt lubrication model worked by Totaro [29]. Piston secondary motion affects oil film transport mechanisms substantially as shown throughout Sections 3.1 and 3.2. Phenomena such as streaking or cavitation of the oil film are directly affected by the piston secondary motion. Using the high speed LIF system has allowed for observations in experiments to have the ability to directly affect piston design. With the better temporal resolution provided via the high speed imaging, new piston designs such as the ones seen in the images provided throughout this thesis can be studied easily. The original motive behind this project was to view different patterns designed onto the piston skirt and analyze them to see if there were any added benefits. Unfortunately there were none initially, but work done with the model shows promise of a possible design which may reduce friction of the total piston assembly, which will be tested in the near future. Previous to this system there was never any scale for the speeds of these phenomena, but with the high speed camera approximate speeds can be calculated allowing for a much more quantitative analysis of oil transport mechanisms.

Previous phenomena also benefitted greatly due to the high speed LIF system; the higher temporal resolution of the images captured by the high speed camera allowed for finer details of

the motion to be captured. No processes could truly be observed in the old system, it was a much more discrete observation such as whether or not something happened not how it happened. With the high speed LIF people can now watch and observe how a certain phenomenon occurs such as bridging. This provides a significant step forward into understanding the oil transport mechanisms inside the power cylinder. The individual steps that were proposed for how bridging occurs can be seen in the videos of bridging. One can see the ring scrape and accumulate oil and then trap it and once the inertia of the piston begins to switch directions, the oil begins to bridge to the liner. These individual steps were not visible in the original setup; the only thing observed was the proof of bridging, but no continuous observation to prove hypotheses correct.

4.2 High Speed LIF Optimization

The optimization that was performed on the high speed LIF system has provided a good basis for a system that anyone can recreate if a diagnostic tool that can measure oil film thickness at high frame rates is necessary. Out of all three cameras used, the Photron Fastcam SA-X2 was by far the better choice as it had the highest light sensitivity as well as the highest frame rate at similar resolutions or the largest resolution at similar frame rates. Laser induced fluorescence is impossible without the laser and out of the two lasers used in this study it is clear that the pulsed laser works much better with this setup than the CW laser. Motion blur, a prominent occurrence when CW is used, creates too much error in the film thickness measurements as well as makes analyzing the videos that much more difficult. In an attempt to increase the quality of the images captured by the CW laser, changes in the recording operation were tested. No discernible upgrades in quality were found when increasing the shutter speed, thus still proving the ineffectiveness of the CW laser. Using the pulsed laser with the SA-X2 has created the highest quality sets of images to date in the history of this LIF setup.

To achieve these high quality images, specific optics needed to be determined. All optics from the original LIF setup were either changed or upgraded. The old beam expander had developed artifacts causing poor image quality which can be seen in *Figure 3-18*, in the image for the continuous wave laser; there are rings superimposed over the image. Two new beam expanders were used to compensate for the smaller beam size of the pulsed laser, but were also able to rid the images of the artifacts of the old one. The other pieces of optics of the old system, the polarizer and collimator, were both excluded due to them being unnecessary. The polarizer

may return to help reduce reflections. As mentioned in earlier chapters the filter originally chosen for this setup has no since been thought as a mistake due to its ability to severely reduce the amount of emitted light that transmits through to the camera sensor. To remedy this problem, a long-pass filter was chosen and has provided quite a significant increase in intensity since the change. With the significant amount of intensity there is in these images, the uneven distribution of the laser source is more prevalent than at lower intensities. Therefore, a diffuser was used to try and evenly distribute the incident laser light, but to no avail. The diffuser itself added more noise than it was able to increase the even distribution of the laser profile. The final components that were tested in this study were several lenses with the purpose of giving the best focus and greatest intensity in the images captured. From *Figure 3-20*, the brightest lens was one that was borrowed although it had the same specifications as the purchased lens, which means that more experiments with different lenses should be conducted. Lenses vary significantly depending on what is needed of them; this allows for a significant amount of flexibility with this system that truly shows the promise of what kind of project it can be tailored toward.

4.3 Future Studies

The current setup for the high speed LIF system was a significant step up from its predecessor, but it is far from perfect. Improvements can absolutely be made in the physical setup such as the optics and even the laser itself. The polarizer may return to help reduce reflections caused by thin film interference if the filter ends up wasting too much emitted light. The emitted light may also change by way of switching to a band-pass filter again, but in a region much more aligned with either of the two dyes' emission peaks.

The largest concern for this system is still the same concern that appeared when the original system was developed; the temperature dependence of the dye emission causes errors in the oil film measurements. In the near future calibration experiments will be conducted to understand the true temperature dependence of the doped oil. Once calibration is complete attempts to measure temperature simultaneously will begin. A theory has been proposed the may have the possibility to measure the temperature at any point on the piston based off of a reference to how each point decays. Without the complicated derivations, fluorescent decay is dependent of temperature and if that decay can be measured simultaneously with intensity values then temperature and film thickness can both be measured as well.

Whether or not the temperature dependence is eradicated will not stop the use of this system as a diagnostic tool for understanding oil transport mechanisms. There are still plenty of oil transport phenomena that have been observed, but not explained hence their absence to this thesis. Significant engine operations have not been seen through the eyes of this system either such as transient operation as well as pinning the ring gap. Transient operation is valuable to all automotive manufacturers due to the fact that it is what truly represents what their vehicles go through on a daily basis. Whereas pinning the ring gap is something that is much more fundamental, where knowledge of what is going on at that point is necessary. It is where oil consumption is highest and must be studied further. In the ever growing need to meet the strict regulations on emissions and fuel economy put on the automotive industry, there definitely is a need for a diagnostic tool such as the high speed LIF system which provides unprecedented information about lubrication and oil film transport mechanisms.

References

[1] Tian, T.: "Modeling the performance of the Piston Ring-Pack in Internal Combustion Engines," Ph.D. Thesis, Department of Mechanical Engineering, MIT, June 1997.

[2] Heywood, J.B.: *Internal Combustion Engine Fundamentals*, McGraw-Hill, 1988.

[3] Ruddy, B. L.; and Hildyard: "A Review of Tribological Aspects of Piston Assembly Design," Proc. of the 17th Leeds-Lyon Symposium on Tribology, Leeds, UK, Sept., 1990, pp. 93-112.

[4] Tateishi, Y.: "Tribological Issues in Reducing Piston Ring Friction Losses," Tribology International, Vol. 27, No. 1, pp. 17-23.

[5] Senzer, E.: "Oil Transport Inside the Oil Control Ring Groove and it's Interaction with Surrounding Areas in Internal Combustion Engines," Ph.D. Thesis, Department of Mechanical Engineering, MIT, February 2012.

[6] Ketterer, J. E.: "Soot Formation in Direct Injection Spark Ignition Engines under Cold-Idle Operating Conditions," Ph.D. Thesis, Department of Mechanical Engineering, MIT, September 2013.

[7] Wilkins, A. J. J.; Hannington, N. A.; Matthey, J.: "The Effect of Fuel and Oil Addititves on Automobile Catalyst Performance: The Suitability of Platinum Metals Confirmed," Platinum Metals Rev., Vol. 34, Issue 1, pp. 16-24, 1990.

[8] Sappok, A.; Munnis, S.; Wong, V. W.: "Individual and Synergistic Effects of Lubricant Additive Components on Diesel Particulate Filter Ash Accumulation and Performance," Proc. of the ASME 2012 Internal Combustion Engine Division Spring Technical Conference, ICES2012-81237, Torino, Piemonte, Italy, May, 2012.

[9] Sappok, A.; Wong, V. W., et al.: "Investigation of Ash Formation, Accumulation, and Distribution in Diesel Particulate Filters Using Lubricant Additive Tracers," Proc. of the ASME 2011 Internal Combustion Engine Division Fall Technical Conference, ICEF2011-60072, Morgantown, West Virginia, USA, Oct., 2011.

[10] Drury, C.; and Withehouse, S.: "The Effect of Lubricant Phosphorus Level on Exhaust Emissions in a Field Trial of Gasoline Engine Vehicles," SAE Paper 940233, 1994.

[11] Ueda, F.; Sugiyama, S.; Arimura, K.; Hamagushi, K.; Akiama, K.; "Engine Oil Additive Effects on Deactivation of Monolithic Three-Way Catalysts and Oxygen Sensors," SAE Paper 940746, 1994.

[12] Hill, S. H.; Sytsma, S, J.: "A System Approach to Oil Consumption," SAE Paper 910743, 1991

[13] Burnett, P. J.: "Relationship between Oil Consumption, Deposit Formation and Piston Ring Motion for Single-Cylinder Diesel Engines," SAE Paper 920089, 1992.

[14] Munro, R.: "Emissions Impossible - The Piston and Ring Support System", SAE Paper 900590, 1990.

[15] Mayer, W. J.; Lechman, D. C.; and Hilden, D. L.: "The Contribution of Engine Oil to Diesel Particulate Emissions," SAE 800256, 1980.

[16] Schneider, E. W.; Sell, J. A.; Siekkinen, J., W.: "The Contribution of Lubricating Oil to Exhaust Deposits and Exhaust Particulates from Gasoline Engines - A Radiotracer Medthod," SAE Paper 982580, 1998.

[17] Shaw, B. T.; Hoult, D. P.; Wong, V. W.: "Development of Engine Lubricant Film Thickness Diagnostics Using Fiber Optics and Laser Fluorescence," SAE Paper 920651, 1992.

[18] Casey, S.: "Analysis of Lubricant Film Thickness and Distribution along the Piston/Liner Interface in a Reciprocating Engine," M.S. Thesis, Department of Mechanical Engineering, MIT, Feb., 1998.

[19] Inagaki, H.; Saito, A.; Murakami, M.; Konomi, T.: "Development of the Two Dimensional Oil Film Thickness Distribution Measuring System," SAE Paper 952346, 1995.

[20] Thirouard, B.: "Characterization and Modeling of the Fundamental Aspects of Oil Transport in the Piston Ring Pack of Internal Combustion Engines," Ph.D. Thesis, Department of Mechanical Engineering, MIT, June 2001.

[21] Przesmitzki, S.: "Characterization of Oil Transport in the Power Cylinder of Internal Combustion Engines during Steady State and Transient Operation," Ph.D. Thesis, Department of Mechanical Engineering, MIT, June 2008.

[22] Automobiles Citroën: Direction Export Europe, Documentation Après Vente. January 1998. Moteur: Moteurs XU - Révision, Réf. BRE0384F. Société Anonyme, Inc.

[23] Sauer, M.; Hofkens, J.; Enderlein, J.: *Handbook of Fluorescence Spectroscopy and Iaging*, Wiley-VCH, pp. 1-29, 2011.

[24] Guilbault, G. G.: *Pratical Fluorescence*, Second Edition, Marcel Dekker, Inc., New York.

[25] Pedrotti, F. L.; Pedrotti, L. S.; Pedrotti, L. M.: *Introduction to Optics*, Third Edition, Pearson Prentice Hall, New Jersey, 2007.

[26] Saeki, S.; Hart, D. P.: "Investigation on YAG(532) Laser Dyes for Oil Film Thickness and Temperature Measurement," Proceeding of PSFVIP-3, March 2001, Maui, Hawaii, USA, F3096, 2001.

[27] Schafer, F. P.: *Topics in Applied Physics Volume 1: Dye Lasers*, Springer-Verlag New York/Heidelberg/Berlin 1973, pp. 20 and pp. 147

[28] Mahle, "Mini Piston Manual," Issue 1995, Mahle Gmbh, D-70369 Stuttgart.

[29] Totaro, P.: "Modeling Piston Secondary Motion and Skirt Lubrication with Applications," M.S. Thesis, Department of Mechanical Engineering, MIT, June 2014.

[30] Dowson, D.; Taylor, C. M.: "Cavitation in Bearings," Annual Review of Fluid Mechanics, Vol. 11, pp. 35-36, 1979.

[31] Chen, H.: "Modeling of Liner Finish Effects on Oil Control Ring Lubrication in Internal Combustion Engines Based on Deterministic Method," M.S. Thesis, Department of Mechanical Engineering, MIT, June 2008.

Appendix

A-1: Photron Fastcam SA-5 Specifications

High-Speed Video System
Next generation CMOS sensor technology providing 7,500 fps, 1K x 1K pixels

The Photron FASTCAM SA5 will meet the requirements of the most demanding applications in research and development due to its unrivaled sensitivity, frame rate and resolution.

This high performance will permit the SA5 to be applied to areas of research once dismissed as unsuitable for digital high-speed imaging.

Building on the success of Photron's Emmy award winning high speed cameras our sensor design improves sensitivity, image quality and color reproduction.

The FASTCAM SA5 delivers mega-pixel resolution at 7,500 fps, an impressive maximum frame rate of 775,000 fps and a 1 microsecond exposure time. Optional one million fps and 369 ns shutter capabilities are available subject to export restrictions.

Target applications include:

- Materials research
- Ballistics
- Aerospace
- PIV
- Combustion
- Cavitation
- Fluid dynamics

Benefits

- Performance examples:
  - 1,024 x 1,000 pixels @ 7,500 fps
  - 512 x 512 pixels @ 25,000 fps
  - 256 x 256 pixels @ 87,500 fps
  - 128 x 128 pixels @ 262,500 fps
  - 128 x 24 pixels @ 775,000 fps
- Variable Region of Interest (ROI)
- Capture 12-bit uncompressed data
- 20μm pixels ensure best light sensitivity for demanding high-speed or low light applications
- Equivalent ISO light sensitivity 10,000 (monochrome), 4,000 (color) measured to ISO12232 S sat
- Phase lock to IRIG/GPS
- Composite and SDI video output for real time monitoring during set up, recording and playback
- Optional remote keypad control with integrated viewfinder
- 8GB, 16GB, 32GB or 64GB memory options
- Gigabit Ethernet interface

Photron
www.photron.com

FASTCAM SA5

ULTRA HIGH-SPEED VIDEO SYSTEM

Specifications: Partial Frame Rate / Recording Duration Table

FRAME RATE (fps)	MAXIMUM RESOLUTION Horizontal	Vertical	MAXIMUM SHUTTER SPEED	RECORD DURATION (12-BIT) TIME (Sec.) 8GB	16GB	32GB	64GB	FRAMES 8GB	16GB	32GB	64GB
1,000	1,024	1,024	1 µs 1/1,000,000 sec	5.46	10.92	21.84	43.68	5,457	10,918	21,841	43,686
2,000	1,024	1,024		2.73	5.46	10.92	21.84	5,457	10,918	21,841	43,686
4,000	1,024	1,024		1.36	2.73	5.46	10.92	5,457	10,918	21,841	43,686
5,000	1,024	1,024		1.09	2.18	4.37	8.73	5,457	10,918	21,841	43,686
7,000	1,024	1,024		0.78	1.56	3.12	6.24	5,457	10,918	21,841	43,686
7,500	1,024	1,000		0.75	1.49	2.98	5.96	5,588	11,180	22,365	44,735
9,300	1,024	800		0.75	1.50	3.01	6.01	6,985	13,975	27,956	55,918
10,000	1,024	744		0.75	1.50	3.01	6.01	7,511	15,027	30,061	60,127
15,000	960	528		0.75	1.51	3.01	6.02	11,289	22,587	45,182	90,374
20,000	832	448		0.77	1.54	3.07	6.14	15,352	30,716	61,443	122,898
30,000	768	320		0.78	1.55	3.11	6.21	23,284	46,586	93,189	186,396
50,000	512	272		0.82	1.64	3.29	6.57	41,090	82,211	164,452	328,934
75,000	320	264		0.90	1.81	3.61	7.22	67,737	135,523	271,097	542,244
100,000	320	192		0.93	1.86	3.73	7.45	93,138	186,345	372,758	745,585
150,000	256	144		1.03	2.07	4.14	8.28	155,230	310,575	621,264	1,242,642
300,000	256	64		1.16	2.33	4.66	9.31	349,269	698,794	1,397,845	2,795,946
420,000	128	64		1.66	3.33	6.66	13.31	698,538	1,397,589	2,795,690	5,591,893
525,000	128	48		1.77	3.55	7.10	14.20	931,384	1,863,452	3,727,587	7,455,857
775,000	128	24		2.40	4.81	9.62	19.24	1,862,769	3,726,904	7,455,175	14,911,715
930,000	128	16	369 ns 1/2,712,000 sec	3.00	6.01	12.02	24.05	2,794,154	5,590,357	11,182,762	22,367,573
1,000,000	64	16		5.59	11.18	22.37	44.73	5,588,309	11,180,714	22,365,525	44,735,146

OPTION SUBJECT TO EXPORT LICENSE CONTROL RESTRICTIONS WHERE APPLICABLE

Sensor	12-bit ADC (Bayer system color, single sensor) with 20µm pixel
Shutter	Global electronic shutter from 16.7ms to 1µs independent of frame rate
Lens Mount	Interchangeable F-mount and C-mount using supplied adapters
Extended Dynamic Range	Selectable in twenty steps (0 to 95% in 5% increments) to prevent pixel over-exposure
Memory	8GB (standard: 5,457 frames @ maximum resolution) 16GB (option: 10,913 frames @ maximum resolution) 32GB (option: 21,841 frames @ maximum resolution) 64GB (option: 43,686 frames @ maximum resolution)
Video Output 1	NTSC/PAL composite VBS (BNC). Ability to zoom, pan and tilt within image via keypad. Live video during recording
Video Output 2	HD-SDI: HD-SDI 2 channel (BNC) digital output
Camera Control	Through optional keypad with integrated viewfinder and Gigabit Ethernet or RS-422
User Preset Switches	Four user selectable camera function controls mounted on the camera's rear panel
Low Light Mode	Low light mode drops the frame rate and shutter time to their maximum values, while maintaining other set parameters, to enable users to position and focus the camera
Triggering	Selectable positive or negative TTL 5Vp-p or switch closure
Trigger Delay	Programmable delay on selected input and output triggers, 100ns resolution
Timing	Internal clock or external source
Phase Lock	Enables cameras to be synchronized precisely together to a master camera or external source, such as IRIG/GPS time codes
Event Markers	Ten user entered event markers mark specific events within the image sequence in real time. Immediately accessible through software
Dual Speed Recording	Enables the recording speed to be changed up or down by a factor of 2, 4 or 8 during a recording
Trigger Modes	Start, End, Center, Manual, Random, Random Reset, Random Center, Random Manual and Duals Speed Recording
Saved Image Formats	JPEG, AVI, TIFF, BMP, RAW, PNG, MOV and FTIF. Images can be saved with or without image or comment data
Data Display	Frame Rate, Shutter Speed, Trigger Mode, Date or Time, Status (Playback/Record), Real Time, Frame Count and Resolution
Partitioning	Up to 64 memory segments for multiple recording in memory
Data Acquisition	Supports Photron MCDL and DAQ
Cooling	Actively cooled
Operating Temperature	0 - 40 degrees C (32 - 104 degree F)
Mounting	1 x 1/4 - 20 UNC, 1 x 3/8 - 16 UNC, 6 x M6
Dimensions	165mm (6.50")H×153mm (6.02")W×242.5mm (9.55")D *excluding protrusions
Weight	6.2 kg (13.67 lbs)
Power Requirements	100V-240V AC ~ 1.5A, 50-60Hz DC operation 18-36 V DC, 100VA

Specifications subject to change without notice

PHOTRON USA, INC.
9520 Padgett Street, Suite 110
San Diego, CA 92126-4446
USA
Tel: 858.684.3555 or 800.585.2129
Fax: 858.684.3558
Email: image@photron.com
www.photron.com

PHOTRON (EUROPE) LIMITED
The Barn, Bottom Road
West Wycombe, Bucks, HP14 4BS
United Kingdom
Tel: +44 (0) 1494 481011
Fax: +44 (0) 1494 487011
Email: image@photron.com
www.photron.com

PHOTRON LIMITED
Fujimi 1-1-8
Chiyoda-Ku, Tokyo 102-0071
Japan
Tel: +81 (0) 3.3238 2107
Fax: +81 (0) 3.3238 2109
Email: image@photron.co.jp
www.photron.co.jp

Photron

SLOW MOTION IMAGING SOLUTIONS

A-2: Photron Fastcam SA-X2 Specifications

FASTCAM SA-X2

HIGH PERFORMANCE HIGH-SPEED CAMERA SYSTEM

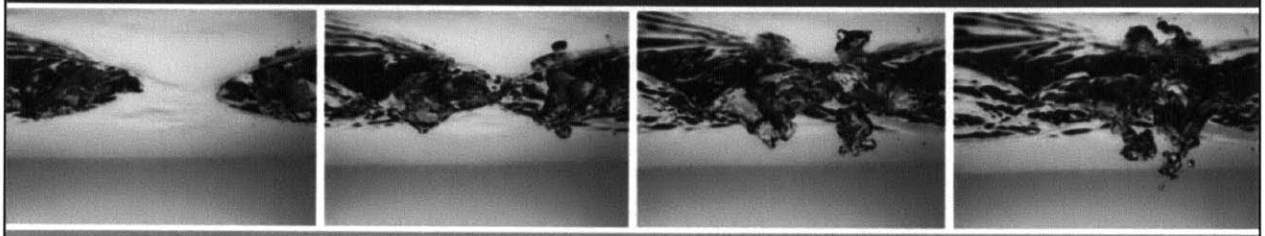

To meet the requirements of the most demanding high-speed imaging applications, a balance of high frame rate, image resolution, dynamic range and light sensitivity is required. The FASTCAM SA-X2 high-speed camera system provides an optimal combination of these critical parameters, with sufficient performance to capture high quality 12-bit megapixel images at up to 13,500 frames per second (fps).

Taking advantage of the very latest CMOS sensor technology, the FASTCAM SA-X2 utilizes large 20 µm square pixels to capture more light than any other high-speed camera. It is rated to ISO 25,000 (against the accredited ISO 12232 Ssat measurement standard) for monochrome 12-bit cameras and ISO 10,000 for 36-bit color (Bayer system, single sensor) cameras. Higher light sensitivity means less additional lighting is required, or higher framing rates or faster shutter speeds can be used with existing lighting conditiors.

The FASTCAM SA-X2 is controlled remotely through Photron's FASTCAM Viewer (PFV) software over a high-speed Gigabit Ethernet network, or locally via an optional handheld keypad. If a PC connection is available, then images can be downloaded via dual industry standard Gig-E ports. Alternatively, two SD card slots allow for the download of recorded image data from the camera without the need for a PC connection.

As with other FASTCAM SA series cameras, the SA-X2 includes both a C-mount and a Nikon G type compatible F-mount, as well as optional support for Canon EF lenses with remote control of aperture and focus, through our PFV software. Wrappers for both LabVIEW™ and MATLAB™ are available with PFV, as is our new automated motion analysis plug-in software — Photron FASTCAM Analysis (PFA).

Target applications include:

- Materials Science
- Combustion Research
- Fluid dynamics (PIV)
- Defense and aerospace research
- Ballistic Imaging
- Shock Waves and Detonations

Photron

www.photron.com

Benefits

- Frame Rate Performance examples:
  - 12,500 fps at 1024x1024 pixel resolution
  - 13,500 fps at 1024x1000 pixel resolution
  - 40,000 fps at 640x488 pixel resolution
  - 100,000 fps at 384x264 pixel resolution
  - 1,000,000 fps at 128x8 pixel resolution (Model 1000K only)
- Market leading light sensitivity (ISO Ssat 12232 standard) ISO 25,000 monochrome / ISO 10,000 color
- High Speed Dual Gigabit Ethernet interface provides reliable system communication and image download rates
- Two SD card slots allow fast image transfer without a PC connection
- Flexible frame synchronization permits synchronization to devices with non-stable external frequencies
- Four Internal Memory Configurations are available to support all application requirements: 8GB, 16GB, 32GB, 64GB
- Integrated mechanical calibration shutter, Nikon F-mount (compatible with Nikon G type lenses), and optional Canon EF mount
- Optional Range Version provides sealed enclosure for electronics, thereby preventing contamination from dust and other materials

FASTCAM SA-X2

HIGH PERFORMANCE HIGH-SPEED CAMERA SYSTEM

Specifications: Partial Frame Rate / Recording Duration Table

FRAME RATE (fps)*	MAXIMUM RESOLUTION Horizontal	Vertical	RECORD DURATION (12-BIT) TIME (Sec.) 8GB	16GB	32GB	64GB	FRAMES 8GB	16GB	32GB	64GB
Model 480K										
1,000	1,024	1,024	5.45	10.91	21.83	43.68	5,455	10,916	21,839	43,684
2,000	1,024	1,024	2.72	5.45	10.91	21.84	5,455	10,916	21,839	43,684
5,000	1,024	1,024	1.09	2.18	4.36	8.73	5,455	10,916	21,839	43,684
10,000	1,024	1,024	0.54	1.09	2.18	4.36	5,455	10,916	21,839	43,684
12,500	1,024	1,024	0.43	0.87	1.74	3.49	5,455	10,916	21,839	43,684
13,500	1,024	1,000	0.41	0.82	1.65	3.31	5,586	11,178	22,363	44,733
18,000	896	848	0.41	0.83	1.67	3.34	7,529	15,066	30,140	60,287
22,500	768	768	0.43	0.86	1.72	3.45	9,699	19,408	38,827	77,663
40,000	640	488	0.45	0.91	1.83	3.66	18,320	36,656	73,327	146,670
45,000	512	512	0.48	0.97	1.94	3.88	21,827	43,672	87,363	174,744
50,000	640	384	0.46	0.93	1.86	3.72	23,282	46,584	93,187	186,394
75,000	512	296	0.50	1.00	2.01	4.03	37,756	75,543	151,116	302,262
100,000	384	264	0.56	1.12	2.25	4.51	56,445	112,934	225,912	451,868
200,000	256	152	0.73	1.47	2.94	5.88	147,058	294,227	588,564	1,177,238
400,000	256	48	1.16	2.32	4.65	9.31	465,690	931,724	1,863,791	3,727,926
480,000	384	24	1.29	2.58	5.17	10.35	62,091	1,242,299	2,485,056	4,970,569
Model 1000K										
720,000	256	8	3.88	7.76	15.53	31.06	2,794,152	5,590,355	11,182,760	22,367,571
900,000	128	8	6.20	12.42	24.85	49.70	5,588,307	11,180,712	22,365,523	44,735,144
1,000,000	128	8	5.58	11.18	22.36	44.73	5,588,307	11,180,712	22,365,523	44,735,144

** FPS = Frame Per Second*

OPTION SUBJECT TO EXPORT LICENSE CONTROL RESTRICTIONS WHERE APPLICABLE
Frequency settings above 900,000 fps require external synchronization
Model 1000K providing frame rates above 480,000 fps subject to export license control

Sensor	20 µm pixel size, 12-bit ADC (Bayer system color, single sensor)
Shutter	Global electronic shutter from 1ms to 1µs independent of frame rate (293ns shutter available subject to export license control)
Lens Mount	Interchangeable Nikon F-mount (compatible with Nikon G type lenses), C-mount using supplied adapters. Optional Canon EF remote control mount
Extended Dynamic Range	Selectable in twenty steps (0 to 95% in 5% increments) to prevent pixel over-exposure
Memory	8GB (standard: 5,455 frames @ maximum resolution) 16GB (option: 10,916 frames @ maximum resolution) 32GB (option: 21,839 frames @ maximum resolution) 64GB (option: 43,684 frames @ maximum resolution)
Recording bit depth	Selectable 8-bit or 12-bit recording
Video Output	Live and playback video through Two HD-SDI or Dual RS-170 (NTSC/PAL) outputs
Nonvolatile Data Storage	Two SD card slots
Camera Control	Remote computer control via high-speed dual port Gigabit Ethernet or optional local control via handheld keypad with LCD monitor
User Preset Switches	Four user selectable camera function controls mounted on the camera's rear panel
Low Light Mode	Low light mode drops the frame rate and shutter time to their maximum values, while maintaining other set parameters, to enable users to position and focus the camera
Triggering	Selectable positive or negative TTL 5Vp-p or switch closure
Trigger Delay	Programmable delay on selected input and output triggers, 100ns resolution
Timing	Internal clock or external source
Phase Lock	Enables cameras to synchronize precisely to a master camera or external signal source, such as IRIG/GPS time code
Event Markers	Ten user specified event markers indicate specific events within an image sequence in real time. Immediately accessible through software
Trigger Modes	Start, End, Center, Manual, Random, Random Reset, Random Center, Random Manual, Image Trigger
Saved Image Formats	JPEG, AVI, TIFF, BMP, RAW, RAWW, MRAW PNG, MOV and FTIF. Images can be saved with or without image or comment data
Data Display	Frame Rate, Shutter Speed, Trigger Mode, Date or Time, Status (Playback/Record), Real Time, Frame Count, Resolution and IRIG time stamp
Partitioning	Up to 64 memory segments for capturing multiple recordings into camera memory
Data Acquisition	Supports Photron and National Instruments™ DAQ options
Operating Temperature	0 - 40 degrees (32 - 104 degree F)
Mounting	1 x 1/4 - 20 UNC, 1 x 3/8 - 16 UNC, 6 x M5
Dimensions	177.7mm (7.0")H×160mm (6.3")W×350mm (13.78")D *excluding protrusions
Weight	9.9 kg (21.3 lbs)
Power Requirements	100V - 240V AC 50-60Hz DC operation 18 - 36 VDC, 210VA

Specifications subject to change without notice

PHOTRON USA, INC.
9520 Padgett Street, Suite 110
San Diego, CA 92126-4446
USA
Tel: 858.684.3555 or 800.585.2129
Fax: 858.684.3558
Email: image@photron.com
www.photron.com

PHOTRON (EUROPE) LIMITED
The Barn, Bottom Road
West Wycombe, Bucks, HP14 4BS
United Kingdom
Tel: +44 (0) 1494 481011
Fax: +44 (0) 1494 487011
Email: image@photron.com
www.photron.com

PHOTRON LIMITED
Fujimi 1-1-8
Chiyoda-Ku, Tokyo 102-0071
Japan
Tel: +81 (0) 3 3238 2107
Fax: +81 (0) 3 3238 2109
Email: image@photron.co.jp
www.photron.co.jp

Photron

SLOW MOTION IMAGING SOLUTIONS

A-3: Coherent Inc. Verdi G18 Data Sheet

Verdi™ G-Series Family

High-Power Optically Pumped Semiconductor Lasers (OPSL)

Optical Specifications[1]	**Verdi**	**G2/G5/G7/G8**	**G10**	**G12/G15/G18/G20**
	Wavelength (nm)		532 ±2	
	Pulse Format		CW	
	Spectral Purity (%)		>99	
	Output Power (W)	2, 5, 7, 8[2]	10[2]	12, 15, 18, 20[2]
	Spatial Mode		TEM_{00}	
	Beam Quality		<1.1	
	Beam Circularity[3]		1.0 ±0.1	
	Beam Waist Diameter (mm)(FW, $1/e^2$)		2.25 ±10%	
	Beam Divergence (mrad)(FW, $1/e^2$)		<0.5	
	Beam Waist Location[4] (m)		±0.5	
	Beam Pointing Stability[5] (µrad/°C)		<2	
	Horizontal Beam Position Tolerance[6] (mm)		±<1.0	
	Vertical Beam Position Tolerance[6] (mm)		±<1.0	
	Polarization Ratio		Linear, >100:1	
	Polarization Direction		Vertical, ±5°	
	Noise (%, rms)(10 Hz to 100 MHz)		<0.02	
	Power Stability[7] (%)(pk-pk)		±<1	
	Warm-Up Time (minutes)		<10	
	CDRH Compliant		Yes	
Electrical Specifications	Operating Voltage (VAC)		100 to 240	
	Frequency (Hz)		50 to 60	
	Power Consumption (W)	500 (2W, 5W), 600 (7W, 8W)	700	1000 (12W), 1250 (15W), 1500 (18W, 20W)
Environmental Conditions	Ambient Temperature (°C)			
	Operating		10 to 40	
	Non-Operating		-10 to 60	
	Relative Humidity (%)		5 to 95[8]	
	CE Marking		IEC 61010-1/EN 61010-1	
	Dimensions (L x W x H)			
	Laser Head[9]	281 x 156 x 85 mm (11.06 x 6.14 x 3.35 in.)		214 x 98 x 68 mm (8.43 x 3.86 x 2.68 in.)
	Benchtop Power Supply	361 x 229 x 160 mm (14.22 x 9.01 x 6.29 in.)		406 x 236 x 171 mm (16.0 x 9.3 x 6.75 in.)
	Cables (laser head to controller)		3m (10 ft.)	

1. Optical parameters measured at the output plane of the laser head, unless noted all parameters valid at the nominal output power and for the lifetime of the unit.
2. This product is offered in several output power versions. The output power can be adjusted down to 250 mW (G2-G10) and 750 mW (G12-G20).
3. Circularity defined as vertical diameter divided by horizontal diameter.
4. Negative value corresponds to a location inside head.
5. After 1 hour warm-up.
6. Measured at the output window.
7. Measured over 8 hrs.
8. Non-condensing.
9. Back connector not included in laser head length dimension.

A-4: Coherent Inc. Matrix 532-7-30 Data Sheet

MATRIX™ 1064 and 532
Solid-State, Q-Switched Laser

		1064-1-LP	1064-7-10[1]	1064-10-30[2]
System Specifications	Average Power (W)	1 at 1.4 kHz	7 at 10 kHz	10 at 30 kHz
	Pulse Repetition Rate (kHz)(single-shot)	up to 10	up to 30	up to 100
	Recommended Power Range (%)	80 to 100	20 to 100	20 to 100
	Pulse Duration (nsec)	>40	<60	<40
	Pulse Energy Stability (%)(rms)	<2	<1.5 at 5 kHz	<1.5
	Beam Parameters[3] (nominal)	0.55 mm and <3 mrad	0.55 mm and <3 mrad	0.55 mm and <3 mrad
	Circularity	>90%		
	Spatial Mode	TEM_{00}		
	Output Power Stability (8h/±3°)	±2%		
	Temperature Range	15 to 50°C (baseplate)		
	Maximum Heat Load (W)	<300	<300	<300
	Static Alignment	±0.2 mm, ±2 mrad		
	Maximum Warm-Up Times	<20 minutes cold start <5 minutes from warm start		
Environmental Specifications	Temperature			
	Operating	15°C to 40°C	15°C to 40°C	15°C to 40°C
	Non-operating	-20°C to 50°C	-20°C to 50°C	-20°C to 50°C
	Altitude			
	Operating	0 to 10,000 ft.		
	Non-operating	0 to 45,000 ft.		
	Relative Humidity (non-condensing)			
	Operating	0 to 90%		
	Non-Operating	0 to 95%		
	Shock			
	Operating	1g/6 ms EN 60068-2-6		
	Non-Operating	25g/6 ms EN 60068-2-6		
Power Supply Specifications	Power Supply Dimensions (H x W x D)	open-frame PCB; can be mounted in 3HE 19 in. rack mount		
	532-14-40	100 x 210 x 325 mm (3.9 x 8.3 x 12.8 in.)		
	All other models	100 x 131 x 335 mm (3.9 x 5.2 x 13.2 in.)		
	External Control	RS-232 interface, TTL QS control		
	Input Power Requirements			
	Input Voltage	90 to 240 VAC, 50 to 60 Hz		
	Input Power			
	532-14-40	1200 VA (max.)/≤500 VA (typ.)		
	All other models	750 VA (max.)/≤350 VA (typ.)		

[1] 1064- Wavelength (nm);7 - Specified Power (W); 10 - Specified Pulse Repetition Rate (kHz).
[2] 1064- Wavelength (nm);10 - Specified Power (W); 30 - Specified Pulse Repetition Rate (kHz).
[3] At waist.

Exciton

PO Box 31126
Dayton, OH 45437
Tel: 937.252.2989 Fax: 937.258.3937
E-mail: info@exciton.com
www.exciton.com

PYRROMETHENE 567

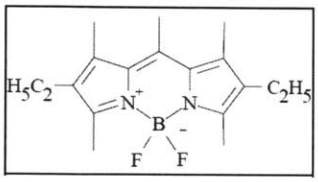

Chemical Name: 1,3,5,7,8-pentamethyl-2,6-diethylpyrromethene-difluoroborate complex
MW: 318.22
CAS Registry Number: 131083-16-4
Synonyms: PMDEP-BF_2, PM-567

Melting Point: 208-209°C
Exciton Catalog No.: 05675

Spectral Information:

$\lambda_{max,abs}$ = 518nm (Ethanol)[198]
ε_{518} = 7.2x10^4 liter mol^{-1} cm^{-1} [198]
$\lambda_{max,fl}$ = 547nm (Ethanol)[195]
Φ_f = 0.83 (Ethanol)[195,198],0.995(Methanol)[213]

Selected Solubility Limits (25°C):		λ_{abs} max:
Methanol	250mg/liter	516
Ethanol	270mg/liter*	518
EG	<90mg/liter	
DMF	5.6g/liter	
NMP	>6.3g/liter	517
EPH	>4.1g/liter	
PPH	>7g/liter	522
PC	>4g/liter	516
DMSO	>2.7g/liter	518
p-Dioxane	>5.5	519

If you received this data sheet prior to 11/06/96, the solubility limit previously listed as 27mg/liter was incorrect.

REPORTED LASER PERFORMANCE DATA

Lasing Wavelength Max. (nm)	Range (nm)	Pump Source (nm)	Solvent	Concentration (molar)	Conversion Efficiency	Stability (1/2- life)
573.4		FL (Triaxial)[227]	Acrylic Copolymer	3.2x10^{-4}	27.4%^{s}	-
540	(537-560)*	FL(Coaxial)[194]	DMA/MeOH,1/10	2x10^{-4}	35%^{s}	-
567		FL[198]	Ethanol	2x10^{-4}	-	-
570		FL[195]	Methanol	-	-	-
580	560-615	N_2(337)[183]	p-Dioxane	40mg/20ml	21%	-
571	552-608	Ar(all-lines)[212]	NMP/PPH	1.5x10^{-3}	36%	460Wh
560	543-584	Ar(514.5)[222]	PPH	3.1x10^{-3}	28%	-
		Nd:YAG(532)[217]	Acrylic Copolymer	3.2x10^{-4}	88.8%^{s}	-
564(bb)		Nd:YAG(532)[216]	ORMOSIL	2.4x10^{-4}	77%^{s}	See note B
566	549-592	Nd:YAG(532,sync,76MHz)[213]	PPH	7.1x10^{-3}	44%	500Wh
567(bb)		Nd:YAG(532)[214]	HTP	1.3x10^{-4}	50%^{s}	See note A
571(bb)		Nd:YAG(532)[215]	Acrylic Copolymer	3.2x10^{-4}	77%^{s}	-

*(FWHM); bb (broad band); s (slope efficiency)
DMA (N,N-Dimethylacetamide); DMF (N,N-Dimethylformamide); DMSO (Dimethylsulfoxide); EG (Ethylene Glycol); EPH (2-Phenoxyethanol); HTP (High Temperature Plastic); MeOH (Methanol); NMP (N-Methyl-2-pyrrolidinone); ORMOSIL (Sol-Gel); PC (Propylene Carbonate); PPH (1-Phenoxy-2-propanol)

PO Box 31126
Dayton, OH 45437
Tel: 937.252.2989 Fax: 937.258.3937
E-mail: info@exciton.com
www.exciton.com

PYRROMETHENE 567

REFERENCES:

183. Thermo Laser Science, Inc., 26 Landsdowne Street, Cambridge, MA 02139
194. S.E. Neister, private communication. [Phase-R Laser System]
195. Pyrromethene-BF_2 Complexes as Laser Dyes: 1, M. Shah, K. Thangaraj, M.-L. Soong, L.T. Wolford, J.H. Boyer, I.R. Politzer, and T.G. Pavlopoulos, *Heteroatom Chem.*, 1(5), 389 (1990). [Non-commercial Dye Laser-details in paper]
196. Efficient Laser Action from 1,3,5,7,8-Pentamethylpyrromethene-BF_2 Complex and its Disodium 2,6-Disulfonate Derivative, T.G. Pavlopoulos, M. Shah, and J.H. Boyer, *Optics Commun.*, 70(5), 425 (1989). [Non-commercial Dye Laser-details in paper]
198. Laser Action from 2,6,8-Position Trisubstituted 1,3,5,7-Tetramethyl-Pyrromethene-BF_2 Complexes: Part 1, T.G. Pavlopoulos, J.H. Boyer, M. Shah, K. Thangaraj, and M.L. Soong, *Appl. Optics*, 29(27), 3885 (1990). [Non-Commercial Dye Laser]
212. Efficient Laser Action from two CW Laser-Pumped Pyrromethene-BF_2 Complexes, S.C. Guggenheimer, J.H. Boyer, K. Thangaraj, M. Shah, M.-L. Soong, and T. Pavlopoulos, *Appl. Optics*, 32(21), 3942 (1993). [Spectra-Physics Model 375B]
213. Synchronously Pumped Visible Laser Dye with Twice the Efficiency of Rhodamine 6G, M.P. O'Neil, *Optics Letters*, 18(1), 37(1993). [Coherent 700 Series]
214. Laser Performance and Material Properties of a High Temperature Plastic Doped with Pyrromethene-BF_2 Dyes, T.H. Allik, S. Chandra, T.R. Robinson, J.A. Hutchinson, G. Sathyamoorthi, and J.H. Boyer, *Mat. Res. Soc. Symp. Proc.*, 329, 291 (1994). [Non-Commercial Dye Laser]
215. High-Efficiency Pyrromethene Doped Solid-State Dye Lasers, R.E. Hermes, T.H. Allik, S. Chandra, J.A. Hutchinson, *Appl. Phys.Lett.*, 63(7), 877 (1993). [Non-Commerical Dye Laser]
216. Advances in Dye-Doped Sol-Gel Lasers, B. Dunn, F. Nishida, R. Toda, J.I. Zink, T.H. Allik, S. Chandra, and J.A. Hutchinson, *Mat.Res. Soc. Symp. Proc.*, 329, 267 (1994). [Non-Commercial Dye Laser]
217. Lasing Performance of Pyrromethene-BF_2 Laser Dyes in a Solid Polymer Host, R.E. Hermes, *SPIE Proceedings: Visible and UV Lasers*, 2115 (1994). [Non-Commercial Dye Laser]
222. M. Benson, Coherent Laser Group, private commun., 1994. [Coherent Model 899-29]
227. Progress in Solid State Dye Laser Development, R.E. Hermes, Proceedings of the Int. Conf. on Lasers '90, STS Press, (1991)

For a current list of biology, biological stain, or biochemistry references for Pyrromethene 567 from PubMed, click on the following link:

Pyrromethene 567

NOTES:

A. The dye maintained over 75% of its original output after <100,000 pulses of 0.16J/cm^2.
B. The laser lifetimes (at 60% relative efficiency) varied from 12,000 pulses (120mJ/cm^2) to 1,000 pulses (460mJ/cm^2).

Pyrromethene 567 is offered by Exciton under U.S. Patent Nos. 4,916,711 and 5,189,029 and other worldwide patents.

Use of EPH and/or PPH as a laser dye solvent is subject to U.S. Patent No. 4,896,329 (Exciton).

A-6: Rhodamine 640 Data sheet

PO Box 31126
Dayton, OH 45437
Tel: 937.252.2989 Fax: 937.258.3937
E-mail: info@exciton.com
www.exciton.com

RHODAMINE 640 PERCHOLRATE

Synonym: 9-(2-carboxyphenyl)-2,3,6,7,12,13,16,17-octahydro-1H,5H,11H,15H,-xantheno[2,3,4-ij:5,6,7-i'j']-diquinolizin-4-ium perchlorate; Rhodamine 101
Catalog No.: 06400
CAS No.: 72102-91-1 **MW:** 591.05
Chemical Formula: $C_{32}H_{31}N_2O_3.ClO_4$
Appearance: Dark green crystals with bronze sheen
Structure:

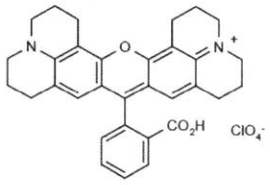

Lasing Wavelength Max. (nm)	Range (nm)	Pump Source (nm)	Solvent	Concentration (molar)	Abs λ-max	Fl λ-max
630		FL[27]	Ethanol(basic)		575(a)[m]	594[m]
635	610-670	FL[69]	Methanol	4×10^{-5}		
640		FL[27]	Ethanol(acidic)			
642	627-657	FL[69]	Methanol			
643	623-657	FL[3]	Ethanol	1×10^{-4}		
650		FL[63]	Methanol	1.2×10^{-4}		
652	620-687	FL[12]	MeOH/H_2O,3/2	1.1×10^{-4}		
618	608-668	XeCl(308)[114]	Ethanol	1.3×10^{-3}		
623	613-672	XeCl(308)[118]	Ethanol	1.2×10^{-3}(osc)		
625	610-673	XeCl(308)[204]	Methanol	1.25×10^{-3}(osc), 7×10^{-4}(amp)		
602	589-623	Nd:YAG(532)[55]				
603	598-626	Nd:YAG(532)[57]	Methanol	2.4×10^{-4}(osc), 3.2×10^{-5}(amp)		
605	594-629	Nd:YAG(532)[53]	Methanol	R640(3.6×10^{-5}) + R610(7.9×10^{-5})(osc), R640(1.8×10^{-5}) + R610(3.9×10^{-5})(amp)		
611		Nd:YAG(532)[54]	Methanol	5×10^{-4}		
612	598-640	Nd:YAG(532)[58]				
613	605-630	Nd:YAG(532)[53]	Methanol	3.6×10^{-4}(osc), 1.9×10^{-4}(amp)		
619	607-640	Nd:YAG(532)[110]	Methanol	2.5×10^{-4}		
620	608-668	Nd:YAG(532)[116]	Ethanol	5×10^{-4}		
624	614-662	Nd:YAG(532)[239]	Ethanol	4.2×10^{-4}		
630	621-674	Nd:YAG(355)[239]	Ethanol	8.5×10^{-4}		
650	620-680	Nd:YAG(355)[109]	MeOH/H_2O,3/2	3.5×10^{-3}		
640	620-680	N_2(337)[30]	Ethanol	5×10^{-3}		
644	620-673	N_2(337)[50]	Ethanol	5.7×10^{-3}		
652	620-678	N_2(337)[114]	Ethanol	5.1×10^{-3}		
653	625-680	N_2(337)[183]	Methanol	60mg/20ml		

PO Box 31126
Dayton, OH 45437
Tel: 937.252.2989 Fax: 937.258.3937
E-mail: info@exciton.com
www.exciton.com

RHODAMINE 640 PERCHOLRATE

Lasing Wavelength Max. (nm)	Range (nm)	Pump Source (nm)	Solvent	Concentration (molar)	Abs λ-max	Fl λ-max
659	626-700	N_2(337)[90]	Ethanol	5×10^{-3}		
671	634-704	N_2(337)[73]	DMSO + HCl			
645	620-690	Ar(458-514)[17]	EG	1.5×10^{-3}(R640), 1.5×10^{-3}(R590)		
648	608-710	Ar or Kr(568)[68]	MeOH/EG,1/7.5	80% pump absorption		
652	624-675	Ar(vis)[87]	EG	2×10^{-3}(R640), 1×10^{-3}(R590)		
616	605-633	Cu(511,578)[153]	Methanol	1×10^{-3}		
630	607-659	Cu(511,578)[175]	Methanol			

DMSO = Dimethylsulfoxide; EG = Ethylene glycol; HCl = Hydrochloric acid; MeOH/H_2O = Methanol/water; m = methanol

REFERENCES:

3. Phase-R Corporation, Box G-2 Old Bay Rd., New Durham, NH 03855
12. Chromatix, 560 Oak Meade Parkway, Sunnyvale, CA 94086
17. Spectra-Physics, 1250 W. Middlefield Road, Mountain View, CA 94039
27. What's Ahead in Laser Dyes, K.H. Drexhage, *Laser Focus*, 9(3), 35 (1973)
30. S. Woodruff and D. Ahlgren, private commun., 1977
50. G. Holtom, private commun., 1978
53. Continuum, 3150 Central Expressway, Santa Clara, CA 95051, formerly, Quantel International
54. W. R. Green, private commun., 1977
55. A High-Power Dye-Laser Pumped by the Second Harmonic of a Nd-YAG Laser, W. Hartig, *Optics Commun.*, 27(3), 447 (1978)
57. Quanta-Ray, Note: Quanta-Ray is now incorporated as a part of Spectra-Physics, 1250 W. Middlefield Road, Mountain View, CA 94039
58. J.K. Lasers Ltd., Somers Road, Rugby, Warwickshire, U. K.
63. High Energy Pulsed Dye Lasers for Atmospheric Sounding, J.Y. Allain, *Appl. Optics*, 18(3), 287 (1979)
68. Coherent Inc., 3210 Porter Dr., Palo Alto, CA 94304
69. Candela Laser Corporation, 530 Boston Post Road, Wayland, MA 01778-1833
73. Laser Dye DCM, Spectral Properties, Synthesis and Comparison with other Dyes in the Red, P.R. Hammond, *Optics Commun.*, 29(3), 331 (1979)
87. The Selective Excitation of Lithium Isotopes by Intracavity Nonlinear Absorption in a CW Dye Laser, M. Yamashita, M. Kasamatsu, H. Kashiwagi and K. Mashida, *Optics Commun.*, 26(3), 343 (1978)
90. Jobin Yvon, 16-18 rue du Canal B.P. 118, 91163 Longjumeau Cedex France
109. Tuning Ranges of 355 nm Pumped Dyes from 410-715 nm, D.M. Guthals and J.W. Nibler, *Optics Commun.*, 29(3), 322 (1979)
114. Optimization of Spectral Coverage in an Eight-Cell Oscillator-Amplifier Dye Laser Pumped at 308nm, F. Bos, *Appl. Optics*, 20, 3553 (1981)
116. Versatile High-Power Single-Longitudinal-Mode Pulsed Dye Laser, F. Bos, *Appl. Optics*, 20(10), 1886 (1981)
118. The XeCl Excimer Laser: A Powerful and Efficient UV Pumping Source for Tunable Dye Lasers, H. Telle, W. Huffer and D. Basting, *Optics Commun.*, 38(5,6), 402 (1981)
153. Cooper LaserSonics, Inc. 5674 Sonoma Drive, Pleasanton, CA 94566
175. CVL-Pumped Dye Laser For Spectroscopic Application, M. Broyer, J. Chevaleyre, G. Delacretaz and L. Wöste, *App. Phys. B*, 35, 31 (1984)
183. Laser Science, Inc., 26 Landsdowne Street, Cambridge, MA 02139
204. Questek, Inc., 44 Manning Road, Billerica, MA 01821 (Tuning Curves for Model 5200B Dye Laser, PDL-3)
239. P. Jauernik, private commun., Sirah Laser- und Plasmatechnik, 2003.

For a current list of biology, biological stain, or biochemistry references for Rhodamine 640 from PubMed, click on the following link:

Rhodamine 640 or Rhodamine 101 (all references are listed under Rhodamine 101 in PubMed as of May 2006)